**Title**
CHARACTERIZATION OF BRITTLE CRACK INITIATION IN WELDED A-36 AND A-537 STEELS



**Author**
Offer, Henry Peter.

**Publication Date**
1974-06-01

LBL-2251
c.1



# CHARACTERIZATION OF BRITTLE CRACK INITIATION IN WELDED A-36 AND A-537 STEELS

Henry Peter Offer
(M. S. thesis)

June 1974

Prepared for the U. S. Atomic Energy Commission
under Contract W-7405-ENG-48



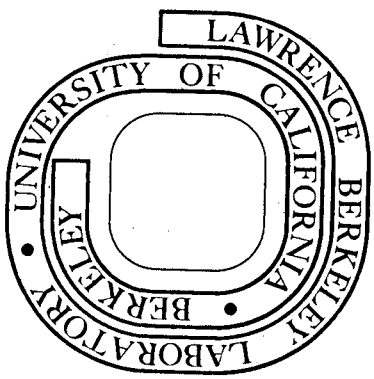


LBL-2251
c.1

## DISCLAIMER

CHARACTERIZATION OF BRITTLE CRACK INITIATION
IN WELDED A-36 AND A-537 STEELS

Contents

# CHARACTERIZATION OF BRITTLE CRACK INITIATION IN WELDED A-36 AND A-537 STEELS

Henry Peter Offer

Inorganic Materials Research Division, Lawrence Berkeley Laboratory and Department of Materials Science and Engineering, College of Engineering; University of California, Berkeley, California 94720

## ABSTRACT

An investigation has been made of the fracture toughness of the microstructures in the fusion and heat affected zones and in the normalized plate microstructure of two welded low strength structural steels. Wedge opening loading (WOL) specimens were machined from 1 in. thick A-36 steel plate and 2 in. thick A-537 steel plate in the transverse direction. These specimens were tungsten-inert gas (TIG) welded in the crack tip area, and were then fatigue cracked to depths corresponding to the three predominant microstructural regions.

Testing of each steel was performed at 23, 0, -40 and -75°C for the welded, side grooved specimens and at the same temperatures for two thicknesses of unwelded specimens with and without deep side grooves. Vickers microhardness measurements were made for a strength correlation in all microstructural regions tested. Charpy V-notch and uniaxial tensile tests were performed for the normalized microstructures at all temperatures investigated.

The results show that altering microstructure, testing temperature, toughness level, and degree of mechanical constraint has a significant effect on the corresponding fracture characteristics. The most important effect of altering these variables is on the amount of slow, ductile crack propagation before catastrophic, brittle crack propagation.

# I. INTRODUCTION

Numerous brittle fractures of engineering structures fabricated from low yield strength steels have occurred over the past three decades[1-3] and continue to occur despite the existence of several analytical and experimental performance criteria for fracture resistance.[4-12] The use of linear elastic fracture mechanics (LEFM) criteria for fracture prediction of low strength steels is limited by the very large and, therefore, expensive test specimens required in generating data for fracture before general yielding of the net section, by the high testing machine capacity necessary to fracture such large specimens, and by the limit transition temperature range (LTTR), a metallurgical barrier to plane-strain fracture in these steels.[9] The use of the generalized fracture analysis diagram (FAD), although correlated with many service failures, is limited by the lack of an analytical relationship between nominal stress and critical flaw size.[10] The J integral approach to fracture mechanics may prove very useful in extending a failure criterion into the elastic-plastic and fully plastic behavior ranges.[7] To establish the general validity of this approach, much more testing is needed. Critical crack opening displacement (COD) analyses show experimental justification under conditions of small plastic deformation.[11,12] Critical COD values, however, show dependence on specimen thickness as plastic deformation increases. The general usefulness of this approach will depend on verification of the assumption that fracture occurs at a critical value of local strain at the crack tip. Near crack tip strain has also been proposed as an engineering ductile fracture criterion,[13] but has not been substantiated with a wide variety of

materials, specimen geometries and types of loading. Thus, there has been much interest in obtaining a fundamental understanding of fracture from both engineering and metallurgical viewpoints.

A major problem with the existing performance criteria is that engineering structures are often subjected to microstructural, design, fabrication and environmental conditions all of which cannot be accounted for in the performance criteria or in existing test specimens. Some of these conditions which frequently promote brittle fracture are low ductility microstructures, regions of triaxial stress, residual stresses, high strain rates, low temperatures, chemical environments and sharp cracks. Each of these conditions can lead independently to brittle, low energy fracture, and in combination often lead to brittle fracture at average stresses well below material yield strengths.

The purpose of this investigation was to characterize, for use in engineering design, the individual and combined enbrittling effects of temperature, microstructure, toughness level and triaxial stress as determined by testing relatively small size sharply cracked fracture toughness specimens of low strength steels. The effect of temperature was determined by varying the test environment from 23°C to -75°C. Microstructural effects were determined by locating sharp cracks in the various microstructures existing near a welded region, and in normalized plate microstructures. The effect of triaxial stress was determined by varying the thickness of smooth faced test specimens, and also by deep side grooving test specimens. The presence of sharp cracks was simulated by fatigue precracking the specimens through the thickness. The effect of toughness level was investigated by testing steels with different rates of change of toughness with temperature.

## II. EXPERIMENTAL PROCEDURE

### A. Materials Tested

The materials used in this investigation were A-36 and A-537 steel, which are commonly used in engineering structures with low strength-to-weight ratio requirements. Table I lists the thickness, heat number and chemical composition (provided by the Grove Value and Regulator Company) for these steels. Specimens were machined from the plate material in the as-received condition, which was a ferrite-pearlite microstructure with slight banding in the A-36 steel and pronounced banding in the A-537 steel (Fig. 1).

### B. Mechanical Testing

#### 1. Hardness Testing

In order to obtain a qualitative measure of the tensile strength of the microstructures existing in the heat affected zone, Vickers microhardness measurements were made. The test was performed with a Leitz Wetzlar testing unit with an applied load of 2000 grams. For each material three separate measurements were made at each position tested below the fused surface, and the average value at each position was reported. Measurements were taken every 0.025 in. starting 0.025 in. from the surface until no change in average hardness occurred.

#### 2. Tensile Testing

Uniaxial tensile stress-strain properties were determined using a 1 in. gage length, 0.250 in. diameter round specimens shown in Fig. 2. These specimens were ground from the normalized plate material parallel to the rolling direction, and tested according to ASTM standard E8-69.[14]

A 300,000 lb capacity electrohydraulic closed-loop MTS testing machine was used to test the specimens in stroke control. A displacement rate of 0.030 in./min was maintained for all tests. The yield strength reported is the lower yield value. Strain was measured using an Instron strain gage extensometer with a 1 in. gage length, which was calibrated with a micrometer for a total displacement range of 0.30 in. The tensile tests were conducted at 23°C in air and at 0°C, -40°C and -75°C in a bath of dry ice and ethanol.

3. Charpy V-Notch Testing

The longitudinal impact properties were determined using the standard ASTM Charpy V-notch specimen shown in Fig. 2. The tests were performed on a pendulum impact testing machine with a 225 ft lb capacity and a hammer velocity of 16.9 ft/sec.

The impact tests were conducted at 23°C, and at 0°C, -20°C, -40°C, -60°C and -75°C within 5 sec of removal from a crushed dry ice-ethanol bath. Duplicate tests were made following ASTM E23-72[15] for each steel at all temperatures tested, and the two values were averaged.

4. Fracture Toughness Testing

Wedge opening loading (WOL) fracture toughness specimens were machined according to Fig. 3 from normalized plate. The crack plane was oriented perpendicular to the direction of rooling in all specimens.

The A-36 steel specimens were machined to three geometries: (1) 1.000 in. thick without side grooves, (2) 1.000 in. thick with side grooves 0.015 in. wide and 0.125 in. deep, and (3) 0.750 in. thick without side grooves. The A-537 steel specimens were machined also to

three geometries: (1) 1.500 in. thick without side grooves, (2) 1.500 in. thick with side grooves 0.015 in. wide and 0.250 in. deep, and (3) 1.000 in. thick without side grooves. The side grooves were cut after fatigue precracking.

After machining the specimens were fused in the crack tip area across the thickness of the specimen. A Miller welder model 330 PLA-SCM was used with 230 DC amperes current, 20 volts straight polarity potential, and 35 cfh argon gas cover. The 1/8 in. diameter tungsten electrode, spaced 1/8 in. from the specimen surface, was shrouded with the fabricated alumina cup shown in Fig. 4. Weld passes were controlled with a Heliweld Automatic Control Panel model HMC-F at a speed of 2.0 in./min. The specimens were mounted on an Airline model FAL 1/308 longitudinal weld fixture. The welding equipment is shown in operation in Fig. 5. A welded specimen side view is shown in Fig. 4.

After one fusion pass a fatigue crack starter slot 0.008 in. wide and a minimum of 0.050 in. deep was made with an abrasive slitting wheel. The specimens were then fatigue cracked according to ASTM E399-72[16] a minimum of 0.050 in. The overall crack average length was controlled in order that the fatigue crack edge would be in microstructural region A, B or C.

Microstructural regions A, B and C were tested with side grooves for both steels. The specimens of both steels without side grooves were tested only in region A in order to isolate the effects of plastic constraint in the thickness direction.

Each specimen geometry and microstructural region was tested at 23°C in air and at 0°C, -40°C and -75°C in a dry ice-ethanol bath.

The testing was performed on a 300,000 lb capacity electrohydraulic closed-loop MTS testing machine in stroke control,[17] shown in Fig. 6. The loading pin displacement rate was maintained at 0.030 in./min for all tests. Crack growth was monitored with a double-cantilever-beam displacement gage,[16] shown in Fig. 7, and was autographically recorded.

For each specimen geometry tested, an experimental compliance calibration curve was determined.[18] The 0.008 in. wide fatigue crack starter slot was successively increased in 0.025 in. increments and the specimen compliance corresponding to the total crack length was measured in the linear elastic load range. The double-cantilever-beam displacement gage, calibrated with a micrometer for a total displacement range of 0.150 in., was used to determine specimen compliance. The compliance curves are plotted in Fig. 8. Values of compliance calculated at incremental crack lengths are presented in Table II.

## C. Microscopy

### 1. Optical Microscopy

Metallographic specimens were cut from the welded WOL toughness specimens after testing with the plane of polish immediately below and parallel to the fracture surface. After mounting in Bakelite, the specimens were ground on silicon carbide paper to 600 grit, polished on a 1μ diamond abrasive wheel, and given a final polish with 0.05 gamma alumina micropolish. Specimens were then etched with a 2% nital solution for 10 to 30 sec.

Observations were made with a Carl Zeies Ultraphot II metallograph, mounted with Nomarski interference-contrast and reflected light polarizer equipment for bright field illumination. Micrographs were made of the welded specimens at positions 3mm, 2mm and 1mm into the heat affected zone and at the surface of the fusion zone. These positions will be referred to as microstructural regions A, B, C and D as shown in Figs. 9 and 10 for A-36 steel and Figs. 11 and 12 for A-537 steel. Micrographs were also made of the normalized microstructures of both materials, shown in Fig. 1.

### 2. Scanning Electron Microscopy

The Joelco model JSM-U3 scanning electron microscope was used to study the Charpy V-notch and WOL toughness specimen fracture surfaces. The accelerating potential was set at 25 kV for the secondary electron emission mode of operation. The examined surfaces were protected with acetate tape during specimen sectioning. Prior to observation the acetate tap was removed and the specimen was ultrasonically cleaned in acetone.

Observations were made of the central region of the Charpy fracture surfaces at 100X and 1000X magnification to determine fracture modes, and at the center of the fatigue crack edge region of the WOL specimens at 1000X to determine any crack tip plasticity before catastrophic crack propagation.

## III. EXPERIMENTAL RESULTS AND DISCUSSION

### A. General

A complete solution of the three dimensional stress distribution for triaxial stresses at a crack tip does not exist at present. Analytical and empirical attempts to characterize the triaxial state of stress existing at a crack tip in relatively small fracture toughness specimens by the modification of analytical biaxial stress fracture criteria have resulted in limited success.[19-21] An experimental approach is therefore adopted.

The approach of this investigation is based on the Griffith theory for critical strain-energy release rate, $G_c$, determined by experimental fracture mechanics analysis.[4] When external loading causes the stress field at an existing crack tip to become large enough for the crack to propagate catastrophically, then an energy balance exists between reductions in the strain energy of the cracked body plus the potential energy of the external forces and increases in the surface energy, plastic deformation energy, or kinetic energy of the body. The rate at which the strain and potential energies are reduced depends on the applied load and the change of compliance with crack length. Compliance is given by $C = X/P$ where X is the displacement between the points of application of load P. The incremental change of compliance with incremental crack extension, $dC/da$, is obtained experimentally by measurement of the compliance corresponding to successively longer simulated cracks. The rate of energy reduction per unit of crack width B is given by[4]

$$G_c = \frac{P^2}{2B} \frac{dC}{da} \quad .$$

When the external loads are such that a crack of a given length will not propagate catastrophically, then the strain-energy release rate G is less than the critical value $G_c$.

A plastic stress zone always exists at the tip of a sharp crack in engineering materials under elastic stress. Under plane strain conditions, the radius of this zone $r_y$ is given by[22]

$$r_y = \frac{GE}{6\pi S_y^2 (1 - \nu^2)}$$

where $S_y$ is the material yield strength in uniaxial tension, E is Young's modulus and $\nu$ is Poisson's ratio. The value of $r_y$ is generally added to the actual crack length as an adjustment for plasticity. As plane strain conditions are approached, $r_y$ becomes an increasingly smaller fraction of B until at "valid" plane strain[16]

$$B \geq \frac{2.5\, r_y}{6\pi} \quad .$$

Linear elastic behavior between load P and displacement X occurs under plane strain when the crack length and plastic zone size are both small relative to specimen thickness and width. Under these conditions the net section stress is less than $S_y$. Deviations from linearity between P and X represent slow crack growth and a small amount of crack tip blunting, and invalidate the use of LEFM.

The use of side grooves in relatively thin specimens to simulate the triaxial stress at a crack tip in thick specimens (where $r_y$ is a small fraction of B) makes the resulting measured value of $G_c$ an average

of G along the crack front. The value of G decreases to $G_{1c}$ from the specimen surface to midsection for both side grooved and ungrooved specimens; however, this rate of decrease corresponding to the rate of triaxial stress increase is much higher near the root of side grooves than near the face of ungrooved specimens. The result is a much more uniform value of G in the midsection of side grooved specimens.

Numerous combinations of side groove geometries were tested, and the slit groove was chosen for providing the most plastic constraint. Maximum plastic constraint is obtained for a rigid-plastic material in plane strain when

$$\ln\left(\frac{\omega + 1}{2}\right) = \frac{\pi}{2} - \alpha$$

where $\omega$ is the ratio of specimen width to root width and $2\alpha$ is the groove angle.[23,24] For $\alpha = 0°$, $\omega = 8.62$, which is impractical for small specimens. For the strain-hardening materials tested the values of $\omega$ chosen were 1.33 and 1.50 for $\alpha = 0°$.

## B. Mechanical Testing

### 1. Hardness, Tensile and Charpy V-Notch Behavior

The variation of average Vickers microhardness with distance from the fused region surface, in the plane of the fatigue precrack, is shown in Fig. 13. Hardness values are listed in Table III. The A-537 steel exhibits a higher hardness at all positions than the A-36 steel. This difference in hardness decreases with distance from the fused region surface.

The uniaxial tensile properties at 23°C, 0°C, -40°C and -75°C are given in Table IV. The engineering stress-strain curves for the A-36

and A-537 steels at the four test temperatures are shown in Figs. 14 and 15. The variation of yield and ultimate strength and of reduction in area is presented in Figs. 16 and 17 for both steels. All of the tensile data were taken for the normalized plate microstructures with the loading direction parallel to the plate rolling direction.

Charpy V-notch impact energy for the normalized plate microstructures is plotted for both steels tested as a function of temperature in Fig. 18. The plane of fracture in all of the Charpy tests was oriented perpendicular to the rolling direction. The values of energy absorbed are presented in Table V, and the fracture surfaces are shown in Fig. 19. The higher Charpy fracture toughness of the A-537 steel relative to the A-36 steel is primarily due to its finer grain size and higher alloy content. The ASTM grain sizes of the A-36 and A-537 steels are No. 6 and No. 8, respectively, as shown in Fig. 1 at 100X magnification. The greater increase in toughness with increasing temperature makes the A-537 steel have a larger plastic zone size than the A-36 steel, since the yield strengths of each material decrease with increasing temperature. The change in fracture mode from predominately dimpled rupture to mixed fracture to predominately quasi-cleavage with reduction in test temperature occurs for both the A-36 steel, shown in Figs. 20 and 21, and the A-537 steel, shown in Figs. 22 and 23. The flat facets characteristic of quasi-cleavage appear at higher temperatures for the A-36 steel than for the A-537 steel, which correlates with the higher temperature transition of Charpy energy of the A-537 steel.

2. Fracture Toughness Behavior

a. Normalized plate microstructures--no side grooves. The autographic record of load and double cantilever beam strain gage displacement for the WOL fracture toughness specimens without side grooves are shown in Figs. 24 and 25 for the A-36 steel normalized plate microstructure. Extensive slow crack growth occurred before fast crack propagation for both the 0.750 in. and 1.000 in. thick specimens at 23°C and 0°C. A small amount of slow crack growth occurred for both thicknesses at -40°C, and only crack tip blunting occurred before fast crack propagation for both thicknesses at -75°C, which failed in plane strain conditions.[16] The critical strain energy release rate variation with temperature is plotted in Fig. 26 for these specimens. The very low value of $G_c$ for the 0.750 in. thick specimens tested at 23°C is due to the extensive slow crack growth and corresponding low load at catastrophic failure. Optical macrophotographs of the fracture surfaces for the 0.750 in. and 1.000 in. thick specimens are shown in Figs. 27 and 28, respectively. Shear lip formation is apparent and indicates the decrease in plastic zone size with decreasing temperature.

The A-537 steel normalized plate microstructure load-gage displacement plots for the 1.000 in. and 1.500 in. thick WOL fracture toughness specimens without side grooves are shown in Figs. 29 and 30, respectively. Slow crack growth across the full width of the specimen occurred for both specimen thicknesses at test temperatures of 23°C and 0°C. The $G_c$ values obtained for these specimens are given in Fig. 31, and the fracture surfaces are shown in Figs. 32 and 33. A-537 steel exhibits a higher fracture toughness than the A-36 steel, which

is evident from a comparison of $G_c$ values from the 1.000 in. thick WOL specimens of these materials (Figs. 26 and 31). Figure 32(A) and (B) and Fig. 33(A) and (B) show delamination perpendicular to the fracture surface in the direction of plate rolling. The delamination occurred only during slow crack growth and is due to the banded microstructure (Fig. 1).

A summary of the fracture toughness properties is given in Table VI for A-36 steel and Table VII for A-537 steel.

b. Normalized plate microstructures--with side grooves. The amount of slow crack growth before catastrophic fracture was not substantially reduced with the addition of side grooves for A-36 steel, which is evident from a comparison of load-gage displacement records of WOL specimens without and with side grooves having the same ligament thickness (Figs. 24 and 34). Poisson contraction is substantially reduced with side grooves for A-36 steel normalized plate microstructure (Figs. 27 and 35).

A-537 steel load-gage displacement records (Fig. 36) showed the same trends with side grooves in the normalized plate microstructure as the A-36 steel. The use of side grooves did, however, raise the values of $G_c$ at all temperatures tested (Figs. 31 and 37). The fracture surfaces of the A-537 steel side grooved specimens are shown in Fig. 38 for the four test temperatures.

Scanning electron fractographs of A-36 steel in the fatigue crack tip area (Fig. 39) show the reduction with temperature in the amount of stretching at the crack tip before crack growth. Essentially, no stretching occurred at -75°C, as evidenced by the abrupt fracture mode change. These fractographs are typical of the four test temperatures for both steels.

c. Heat affected zone microstructures--with side grooves. Microstructural region B is shown in Fig. 9(B) at 100X and in Fig. 10(B) at 1000X magnification for A-36 steel, and in Fig. 11(B) at 100X and in Fig. 12(B) at 1000X magnification for A-537 steel. This region consists primarily of fine grain size ferrite and pearlite in the A-36 steel and fine grain size ferrite and acicular bainite in the A-537 steel.

The load-gage displacement records (Fig. 40) for the side grooved A-36 steel WOL specimens tested in region B show a substantial decrease in slow crack growth existed compared to microstructural region A. This behavior also existed for A-537 steel except at 23°C, where slow crack growth occurred across the full width of the specimen in region B (Fig. 41). Plane strain conditions existed for the side grooved geometries of both steels in region B at -75°C and -40°C. The fracture surfaces of the A-36 and A-537 steels are shown for region B in Figs. 42 and 43, respectively, for each temperature tested. Crack arrest occurred in A-36 steel at 23°C and 0°C and in A-537 steel at 0°C, and is indicated by the darker grey fracture surface typical of ductile tearing. Microstructural region C is shown in Fig. 9(C) at 100X and in Fig. 10(C) at 1000X magnification for A-36 steel, and in Fig. 11(C) at 100X and in Fig. 12(C) at 1000X magnification for A-537 steel. The microstructure in this region is large grained proeutectoid ferrite and acicular bainite in the A-36 steel and large grained feathery bainite in the A-537 steel.

The critical strain energy release rate for region C is plotted in Fig. 44 for A-36 steel and in Fig. 37 for A-537 steel. $G_c$ for A-36

steel shows a slight decrease with decreasing temperature, whereas $G_c$ for A-537 steel shows a much larger decrease with decreasing temperature for both microstructural regions B and C. The fracture surfaces of region C for both steels are shown in Figs. 45 and 46. At 23°C the plastic zone size is large enough relative to the heat affected zone size to prevent fast crack propagation in A-537 steel, but not in A-36 steel. This effect can be seen by comparing the load-gage displacement curves for the two materials (Figs. 47 and 48).

## IV. SUMMARY AND CONCLUSIONS

The results of this investigation show that the testing of relatively small specimens in which brittle fracture has been induced can be a valuable aid for the prevention of such fracture in engineering structures. Due to the lack of an adequate stress analysis for elastic-plastic and fully plastic behavior, and due to the lack of an empirical criterion for fracture prediction in these regimes which has general validity, it is necessary to rely on extensive testing under simulated service conditions for engineering design data. The lack of quantitative relationships between the factors controlling brittle crack initiation also necessitates extensive testing for rational engineering design.

To make full use of the available data, tests must be carried out at full plate thickness on the embrittled microstructures of any structure. Conclusions regarding the method of testing for the assessment of the quantitative relationships and the results of the test method are listed below.

1. Slow crack growth is not necessarily reduced in WOL specimens of A-537 steel and A-36 steel by the addition of deep side grooves, despite the corresponding elimination of large shear lips.

2. A-537 steel shows a higher fracture toughness than A-36 steel as measured by Charpy V-notch and WOL specimens for the temperature range 23°C to -75°C in the normalized plate microstructural condition.

3. Microstructures existing in the HAZ promote brittle crack initiation compared to normalized plate microstructures, if the HAZ size is large relative to the plastic zone size at a crack tip.

4. The use of deep grooves improves the resulting value of $G_c$ for specimens of the same ligament thickness by increasing crack tip triaxiality of stress and the corresponding nominal stress required for fast crack initiation.

5. Brittle microstructures at a crack tip are more effective in promoting brittle crack initiation than triaxial stresses produced by deep side grooves in small specimens, especially at low temperatures where the plastic zone size is small.

6. For the ranges of the variables tested, temperature has the strongest effect on brittle crack initiation. At 23°C and 0°C slow crack growth occurred across the full width of several A-537 steel specimens, whereas at -75°C no slow crack growth occurred. At 23°C extensive slow crack growth occurred in A-36 steel specimens, but at -75°C only limited crack tip blunting occurred.

7. Increasing the thickness of WOL specimens without side grooves in the thickness range investigated inproves the resulting value of $G_c$. This effect is attributed to the increase in triaxiality of stress at the crack tip and the corresponding average stress at fast crack initiation.

8. Every combination of the variables tested resulted in a mixed state of stress except those combinations including the lowest temperatures investigated. Most of the tests at -40°C and all of the tests at -75°C were under plane strain conditions.

9. The amount of slow crack propagation before catastrophic fracture was the most important result associated with altering the variables in the ranges investigated in this study.

ACKNOWLEDGEMENTS

The author wishes to thank Professor Earl R. Parker and Professor Victor F. Zackay for their guidance and encouragement during the course of this investigation.

The author also wishes to express his gratitude to Gloria Pelatowski for her help with line drawings and to Jean Wolslegel for her help with typing the manuscript.

This research was performed under the auspices of the U. S. Atomic Energy Commission through the Inorganic Materials Research Division of the Lawrence Berkeley Laboratory.

REFERENCES

1. E. R. Parker, Brittle Behavior of Engineering Structures (John Wiley, New York, 1957).
2. M. E. Shank, Control of Steel Construction of Avoid Brittle Failure (Welding Research Council, New York, 1957).
3. W. H. Munse, Brittle Fracture in Weldments in Fracture, H. Liebowitz, ed. (Academic Press, 1969), Vol. 4, p. 371.
4. G. R. Irwin and P. D. Paris, Fundamental Aspects of Crack Growth and Fracture in Fracture, H. Liebowitz, ed. (Academic Press, New York, 1971), Vol. 3, p. 1.
5. G. C. Sih, Handbood of Stress Intensity Factors, Institute of Fracture and Solid Mechanics, Lehigh University, Bethlehem, Penn., 1973.
6. G. C. Sih, J. of Engineering Fracture Mechanics 5(2), 365 (1973).
7. G. C. Sih, A Special Theory of Crack Propagation in Methods of Analysis and Solutions to Crack Problems, G. C. Sih, ed. (Noordhoff International Publishing, Holland, 1973).
8. R. W. Nichols and A. Cowan, Selection of Material and Other Aspects of Design Against Brittle Fracture in Large Steel Structures in Fracture, H. Liebowitz, ed. (Academic Press, New York, 1969), Vol. 5, p. 233.
9. F. A. McClintock, Plasticity Aspects of Fracture in Fracture, H. Leibowitz, ed. (Academic Press, New York, 1971), Vol. 3, p. 47.
10. A. S. Tetelman and A. J. McEvily, Jr., Fracture of Structural Materials (John Wiley, New York, 1967).
11. J. R. Rice, Mathematical Analysis in the Mechanics of Fracture in Fracture, H. Liebowitz, ed. (Academic Press, New York, 1968), Vol. 2, p. 191.

12. H. W. Liu, W. J. Gavigan and J. S. Ke, Intern. J. of Fracture Mechanics 6(1), 1970.

13. E. A. Lange, Fracture Toughness of Structural Metals, NRL Report 7046, Washington, D. C. (1970).

14. W. S. Pellini and P. P. Puzak, Fracture Analysis Diagram Procedures for the Fracture-Safe Engineering Design of Steel Structures, NRL Report 5920, Washington, D. C. (1963).

15. A. A. Wells, Proceedings of the Crack Propagation Symposium, Cranfield, Royal College of Aeronautics, England, Vol. 1, p. 210 (1962).

16. R. E. Dolby, G. R. Egan, M. Pawes, G. G. Saunders and G. L. Archer, Brittle Fracture Initiation in Welded Low Strength Steels in Practical Fracture Mechanics for Structural Steel, M. O. Dobson, ed. (U. K. Atomic Energy Authority, 1969).

17. J. S. Ke and H. W. Liu, Engineering Fracture Mechanics 5, 182 (1973).

18. ASTM Standards E8-69, Tension Testing of Metallic Materials in Book of ASTM Standards, p. 194, part 31 (1972).

19. ASTM Standards E23-72, Notched Bar Impact Testing of Metallic Materials in Book of ASTM Standards, p. 276, part 31 (1972).

20. ASTM Standards E399-72, Plane Strain Fracture Toughness Testing of Metallic Materials in Book of ASTM Standards, p. 955, part 31 (1972).

21. S. R. Swanson, Testing Systems and Associated Instrumentation in Experimental Techniques in Fracture Mechanics, A. S. Kobayashi, ed. (Society for Experimental Stress Analysis, Connecticut, 1973), p. 76.

22. R. T. Bubsey, D. M. Fisher, M. H. Jones and J. E. Srawley, Compliance Measurements in Experimental Techniques in Fracture Mechanics, A. S. Kobayashi, ed. (Society for Experimental Stress Analysis, Connecticut, 1973), p. 76.

23. G. C. Sih and R. J. Hartranft, International Journal of Fracture 9(1), 75 (1973).

24. C. N. Freed, Application of Side Grooves in the Determination of $K_{IC}$ for High-Strength Metals in Fracture Toughness of High Strength Materials: Theory and Practice (The Iron and Steel Institute, London, 1970), p. 29.

25. C. N. Freed and J. M. Krafft, J. of Materials 1(4), 770 (1966).

26. G. R. Irwin, Proceedings of the 7th Sagamore Ordinance Materials Research Conference (Syracuse University Press, New York, 1961).

27. J. E. Neimark, J. Appl. Mech. 90, 115 (1967).

28. D. J. F. Ewing and R. Hull, J. of Mechanics and Physics of Solids 15, 115 (1967).

Table I. Material composition wt%.

| Plate Thickness* | Alloy Grade | Heat Number† | C | Mn | P | S | Si | Cu | Ni | Cr | Mo |
|---|---|---|---|---|---|---|---|---|---|---|---|
| 1 in. | A-36 | 93985 | 0.20 | 1.01 | 0.013 | 0.025 | 0.04 | | | | |
| 2 in. | A-537 | 93995 | 0.20 | 1.29 | 0.011 | 0.025 | 0.38 | 0.07 | 0.16 | 0.18 | 0.05 |

*Normalized at 1700°F for one hour per in. of thickness.

†Manufactured by Kaiser Steel Mill.

Table II. Fracture toughness specimen compliance, in./lb×$10^{-6}$.

| Crack Length in. | Specimen Thickness Ratio in./in. | | | | |
|---|---|---|---|---|---|
| | 0.750/0.750 | 1.000/0.750 | 1.000/1.000 | 1.500/1.000 | 1.500/1.500 |
| 0.900 | 4.72 | 3.88 | 3.69 | 2.60 | 2.58 |
| 0.925 | 4.94 | 4.06 | 3.86 | 2.75 | 2.70 |
| 0.950 | 5.22 | 4.22 | 4.06 | 2.90 | 2.81 |
| 0.975 | 5.56 | 4.44 | 4.28 | 3.08 | 2.95 |
| 1.000 | 5.92 | 4.67 | 4.53 | 3.21 | 3.10 |
| 1.025 | 6.30 | 5.00 | 4.81 | 3.45 | 3.32 |
| 1.050 | 6.56 | 5.33 | 5.00 | 3.65 | 3.55 |
| 1.075 | 6.94 | 5.56 | 5.33 | 3.89 | 3.70 |
| 1.100 | 7.26 | 5.94 | 5.59 | 4.23 | 3.95 |

Table III. Average Vickers microhardness 2000 gram load.

| Distance From Weld Edge (in.) | A-36 Steel | A-537 Steel |
|---|---|---|
| 0.025 | 371 | 446 |
| 0.050 | 360 | 430 |
| 0.075 | 315 | 402 |
| 0.100 | 245 | 372 |
| 0.125 | 203 | 335 |
| 0.150 | 181 | 275 |
| 0.175 | 154 | 214 |
| 0.200 | 148 | 179 |
| 0.225 | 140 | 170 |
| 0.250 | 136 | 159 |
| 0.275 | 135 | 152 |
| 0.300 | 135 | 150 |

Table IV. Tensile data.

| Material | Temperature (°C) | R.A. (%) | $\sigma_y$ (ksi) | $\sigma_u$ (ksi) | $\varepsilon_f$ (%) |
|---|---|---|---|---|---|
| A-36 | 23 | 41.6 | 33.6 | 67.3 | 25.5 |
| A-537 | 23 | 47.6 | 48.9 | 78.9 | 25.0 |
| A-36 | 0 | 42.0 | 35.6 | 69.7 | 25.9 |
| A-537 | 0 | 46.0 | 50.1 | 82.6 | 25.7 |
| A-36 | -40 | 40.8 | 40.4 | 75.2 | 25.2 |
| A-537 | -40 | 45.6 | 55.0 | 88.1 | 26.2 |
| A-36 | -75 | 39.2 | 47.1 | 79.5 | 26.1 |
| A-537 | -75 | 42.0 | 63.1 | 100.3 | 24.3 |

Table V. Charpy V-notch energy.

| Material | Testing Temp. (°C) | CVN (ft-lbs) | Average CVN (ft-lbs) |
|---|---|---|---|
| A-36 | 23 | 39.3 | |
| A-36 | 23 | 37.7 | 38.5 |
| A-537 | 23 | 81.5 | |
| A-537 | 23 | 79.6 | 80.6 |
| A-36 | 0 | 14.4 | |
| A-36 | 0 | 12.1 | 13.3 |
| A-537 | 0 | 49.2 | |
| A-537 | 0 | 36.3 | 42.8 |
| A-36 | -20 | 7.4 | |
| A-36 | -20 | 7.4 | 7.4 |
| A-537 | -20 | 24.5 | |
| A-537 | -20 | 31.6 | 28.1 |
| A-36 | -40 | 3.4 | |
| A-36 | -40 | 3.9 | 3.7 |
| A-537 | -40 | 16.6 | |
| A-537 | -40 | 18.6 | 17.6 |
| A-36 | -60 | 2.6 | |
| A-36 | -60 | 3.4 | 3.0 |
| A-537 | -60 | 6.0 | |
| A-537 | -60 | 6.5 | 6.3 |
| A-36 | -75 | 2.9 | |
| A-36 | -75 | 2.9 | 2.9 |
| A-537 | -75 | 4.1 | |
| A-537 | -75 | 9.6 | 6.9 |

Table VI. Fracture toughness data.
A-36 Steel

| Microstructural Region | Test Temp.,°C | Specimen Thickness Ratio, in./in. | Critical Load, lbs | Maximum Load, lbs | Strain Energy Release Rate, lb/in. |
|---|---|---|---|---|---|
| A | 23 | 1.000/0.750 | 6000 | 7150 | 330 |
| A | 0 | 1.000/0.750 | 7430 | 7430 | 515 |
| A | -40 | 1.000/0.750 | 6080 | 6080 | 345 |
| A | -75 | 1.000/0.750 | 5860 | 5860 | 320 |
| B | 23 | 1.000/0.750 | 8040 | 8040 | 603 |
| B | 0 | 1.000/0.750 | 7870 | 7870 | 578 |
| B | -40 | 1.000/0.750 | 6660 | 6660 | 406 |
| B | -75 | 1.000/0.750 | 6410 | 6410 | 383 |
| C | 23 | 1.000/0.750 | 7650 | 7650 | 546 |
| C | 0 | 1.000/0.750 | 7570 | 7570 | 525 |
| C | -40 | 1.000/0.750 | 7350 | 7350 | 504 |
| C | -75 | 1.000/0.750 | 6370 | 6370 | 378 |
| A | 23 | 0.750/0.750 | 1650 | 1650 | 25.4 |
| A | 0 | 0.750/0.750 | 6600 | 6600 | 406 |
| A | -40 | 0.750/0.750 | 6300 | 6300 | 370 |
| A | -75 | 0.750/0.750 | 6150 | 6150 | 353 |

Table VI. Continued.

| Microstructural Region | Test Temp., °C | Specimen Thickness Ratio, in./in. | Critical Load, lbs | Maximum Load, lbs | Strain Energy Release Rate, lb/in. |
|---|---|---|---|---|---|
| A | 23 | 1.000/1.000 | 10,650 | 10,650 | 794 |
| A | 0 | 1.000/1.000 | 10,130 | 10,130 | 718 |
| A | -40 | 1.000/1.000 | 9,220 | 9,220 | 595 |
| A | -75 | 1.000/1.000 | 8,400 | 8,400 | 494 |

Table VII. Fracture toughness data.
A-537 Steel

| Microstructural Region | Test Temp.,°C | Specimen Thickness Ratio, in./in. | Critical Load, lbs | Maximum Load, lbs | Strain Energy Release Rate, lb/in. |
|---|---|---|---|---|---|
| A | 23 | 1.500/1.000 | | 17,930 | |
| A | 0 | 1.500/1.000 | | 17,480 | |
| A | -40 | 1.500/1.000 | 16,575 | 16,580 | 960 |
| A | -75 | 1.500/1.000 | 16,350 | 16,350 | 935 |
| B | 23 | 1.500/1.000 | | 18,600 | |
| B | 0 | 1.500/1.000 | 18,000 | 18,000 | 1140 |
| B | -40 | 1.500/1.000 | 17,250 | 17,250 | 1040 |
| B | -75 | 1.500/1.000 | 12,000 | 9,080 | 504 |
| C | 23 | 1.500/1.000 | | 18,960 | |
| C | 0 | 1.500/1.000 | 18,150 | 18,300 | 1160 |
| C | -40 | 1.500/1.000 | 16,500 | 16,500 | 955 |
| C | -75 | 1.500/1.000 | 10,800 | 10,800 | 408 |
| A | 23 | 1.000/1.000 | | 13,130 | |
| A | 0 | 1.000/1.000 | | 14,930 | |
| A | -40 | 1.000/1.000 | 14,550 | 14,550 | 740 |
| A | -75 | 1.000/1.000 | 12,600 | 12,600 | 555 |

Table VII. Continued.

| Microstructural Region | Test Temp.,°C | Specimen Thickness Ratio, in./in. | Critical Load, lbs | Maximum Load, lbs | Strain Energy Release Rate, lb/in. |
|---|---|---|---|---|---|
| A | 23 | 1.500/1.500 | | 14,100 | |
| A | 0 | 1.500/1.500 | | 17,850 | |
| A | -40 | 1.500/1.500 | 21,000 | 21,000 | 1030 |
| A | -75 | 1.500/1.500 | 21,750 | 21,750 | 1110 |

FIGURE CAPTIONS

Fig. 1. Normalized plate microstructures, 100×. (A) A-36 steel, (B) A-537 steel.

Fig. 2. Geometry of Charpy V-notch and tensile specimens.

Fig. 3. Geometry of WOL specimens without side grooves.

Fig. 4. (A) Fabricated gas shroud for fracture toughness specimen welding, (B) WOL specimen showing heat affected zone.

Fig. 5. Equipment for welding fracture toughness specimens.

Fig. 6. Equipment for WOL fracture toughness specimen testing.

Fig. 7. Strain gage mounting on double cantilever beams and strain gage bridge circuit.

Fig. 8. Variation of fracture toughness specimen compliance with crack length, experimentally determined for five specimen geometries.

Fig. 9. Microstructures produced along crack plane in A-36 steel. (A) 3 mm from fused surface, (B) 2 mm from fused surface, (C) 1 mm from fused surface, (D) at fused zone surface.

Fig. 10. Microstructures produced along crack plane in A-36 steel. (A) 3 mm from fused surface, (B) 2 mm from fused surface, (C) 1 mm from fused surface, (D) at fused zone surface.

Fig. 11. Microstructures produced along crack plane in A-537 steel. (A) 3 mm from fused surface, (B) 2 mm from fused surface, (C) 1 mm from fused surface, (D) at fused zone surface.

Fig. 12. Microstructures produced along crack plane in A-537 steel. (A) 3 mm from fused surface, (B) 2 mm from fused surface, (C) 1 mm from fused surface, (D) at fused zone surface.

Fig. 13. Variations of average Vickers microhardness with distance from the fused region surface for A-36 and A-537 steels.

Fig. 14. Variation of engineering stress with engineering strain at 23°C, 0°C, -40°C and -75°C for A-36 steel in the normalized microstructural condition.

Fig. 15. Variation of engineering stress with engineering strain at 23°C, 0°C, -40°C and -75°C for A-537 steel in the normalized microstructural condition.

Fig. 16. Variation of yield strength and ultimate strength with temperature for A-36 and A-537 steel.

Fig. 17. Variation of reduction in area with temperature for A-36 and A-537 steel.

Fig. 18. Variation of Charpy V-notch energy absorbed with test temperature for A-36 and A-537 steels in the normalized microstructural condition.

Fig. 19. Fracture surfaces of Charpy V-notch specimens at 23°C, 0°C, -40°C and -75°C test temperatures (left to right). (A) A-36 steel, (B) A-537 steel.

Fig. 20. Scanning electron fractographs of the central region of Charpy V-notch specimens of A-36 steel. (A) 23°C test temperature, (B) 0°C test temperature, (C) -40°C test temperature, (D) -75°C test temperature.

Fig. 21. Scanning electron fractographs of the central region of Charpy V-notch specimens of A-36 steel. (A) 23°C test temperature, (B) 0°C test temperature, (C) -40°C test temperature, (D) -75°C test temperature.

Fig. 22. Scanning electron fractographs of the central region of Charpy V-notch specimens of A-537 steel. (A) 23°C test temperature, (B) 0°C test temperature, (C) -40°C test temperature, (D) -75°C test temperature.

Fig. 23. Scanning electron fractographs of the central region of Charpy V-notch specimens of A-537 steel. (A) 23°C test temperature, (B) 0°C test temperature, (C) -40°C test temperature, (D) -75°C test temperature.

Fig. 24. Variation of load with gage displacement at 23°C, 0°C, -40°C and -75°C for A-36 steel, microstructural region A. WOL specimen thickness is 0.750 in.

Fig. 25. Variation of load with gage displacement at 23°C, 0°C, -40°C and -75°C for A-36 steel, microstructural region A. WOL specimen thickness is 1.000 in.

Fig. 26. Variation of critical strain energy release rate with test temperature for 0.750 in. and 1.000 in. thick WOL fracture toughness specimens of A-36 steel in the normalized microstructural condition.

Fig. 27. WOL fracture toughness specimen, 0.750 in. thick, A-36 steel, microstructural region A. (A) 23°C test temperature, (B) 0°C test temperature, (C) -40°C test temperature, (D) -75°C test temperature.

Fig. 28. WOL fracture toughness specimen, 1.000 in. thick, A-36 steel, microstructural region A. (A) 23°C test temperature, (B) 0°C test temperature, (C) -40°C test temperature, (D) -75°C test temperature.

Fig. 29. Variation of load with gage displacement at 23°C, 0°C, -40°C and -75°C for A-537 steel, microstructural region A. WOL specimen thickness is 1.000 in.

Fig. 30. Variation of load with gage displacement at 23°C, 0°C, -40°C and -75°C for A-537 steel, microstructural region A. WOL specimen thickness is 1.500 in.

Fig. 31. Variation of critical strain energy release rate with test temperature for 1.000 in and 1.500 in. thick WOL fracture toughness specimens of A-537 steel in the normalized microstructural condition.

Fig. 32. WOL fracture toughness specimen, 1.000 in. thick, A-537 steel, microstructural region A. (A) 23°C test temperature, (B) 0°C test temperature, (C) -40°C test temperature, (D) -75°C test temperature.

Fig. 33. WOL fracture toughness specimen, 1.500 in. thick, A-537 steel, microstructural region A. (A) 23°C test temperature, (B) 0°C test temperature, (C) -40°C test temperature, (D) -75°C test temperature.

Fig. 34. Variation of load with gage displacement at 23°C, 0°C, -40°C and -75°C for A-36 steel, microstructural region A. WOL specimen thickness ratio is 1.000 in./0.750 in.

Fig. 35. WOL fracture toughness specimen, 1.000 in./0.750 in. thickness ratio, A-36 steel, microstructural region A. (A) 23°C test temperature, (B) 0°C test temperature, (C) -40°C test temperature, (D) -75°C test temperature.

Fig. 36. Variation of load with gage displacement at 23°C, 0°C, -40°C and -75°C for A-537 steel, microstructural region A. WOL specimen thickness ratio is 1.500 in./1.000 in.

Fig. 37. Variation of critical strain energy release rate with test temperature for 1.500 in. thick WOL fracture toughness specimens with side grooves 0.015 in. wide and 0.250 in. deep in microstructural regions A, B and C of A-537 steel.

Fig. 38. WOL fracture toughness specimen, 1.500 in./1.000 in. thickness ratio, A-537 steel, microstructural region A. (A) 23°C test temperature, (B) 0°C test temperature, (C) -40°C test temperature, (D) -75°C test temperature.

Fig. 39. WOL fracture toughness specimen scanning electron fractograph of fatigue crack edge, indicated by arrow, A-36 steel, microstructural region A. (A) 23°C test temperature, (B) 0°C test temperature, (C) -40°C test temperature, (D) -75°C test temperature.

Fig. 40. Variation of load with gage displacement at 23°C, 0°C, -40°C and -75°C for A-36 steel, microstructural region B. WOL specimen thickness ratio is 1.000 in./0.750 in.

Fig. 41. Variation of load with gage displacement at 23°C, 0°C, -40°C and -75°C for A-537 steel, microstructural region B. WOL specimen thickness ratio is 1.500 in./0.750 in.

Fig. 42. WOL fracture toughness specimen, 1.000 in./0.750 in. thickness ratio, A-36 steel, microstructural region B. (A) 23°C test temperature, (B) 0°C test temperature, (C) -40°C test temperature, (D) -75°C test temperature.

Fig. 43. WOL fracture toughness specimen, 1.500 in./1.000 in. thickness ratio, A-537 steel, microstructural region B. (A) 23°C test temperature, (B) 0°C test temperature, (C) -40°C test temperature, (D) -75°C test temperature.

Fig. 44. Variation of critical strain energy release rate with test temperature for 1.000 in. thick WOL fracture toughness specimens with side grooves 0.015 in. wide and 0.125 in. deep in microstructural regions A, B and C of A-36 steel.

Fig. 45. WOL fracture toughness specimen, 1.000 in./0.750 in. thickness ratio, A-36 steel, microstructural region C. (A) 23°C test temperature, (B) 0°C test temperature, (C) -40°C test temperature, (D) -75°C test temperature.

Fig. 46. WOL fracture toughness specimen, 1.500 in./1.000 in. thickness ratio, A-537 steel, microstructural region C. (A) 23°C test temperature, (B) 0°C test temperature, (C) -40°C test temperature, (D) -75°C test temperature.

Fig. 47. Variation of load with gage displacement at 23°C, 0°C, -40°C and -75°C for A-36 steel, microstructural region C. WOL specimen thickness ratio is 1.000 in./0.750 in.

Fig. 48. Variation of load with gage displacement at 23°C, 0°C, -40°C and -75°C for A-537 steel, microstructural region C. WOL specimen thickness ratio is 1.500 in./1.000 in.

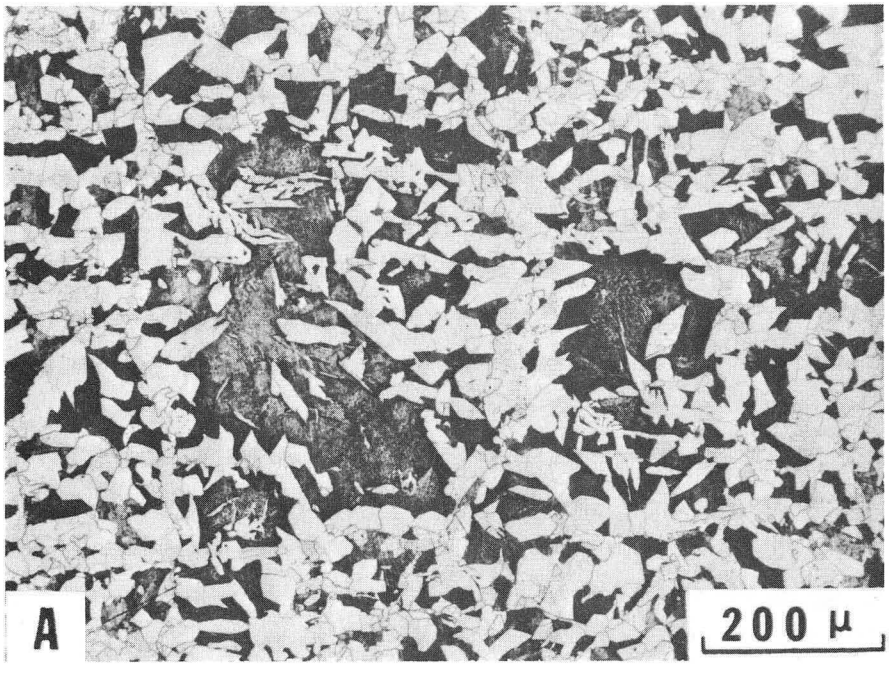


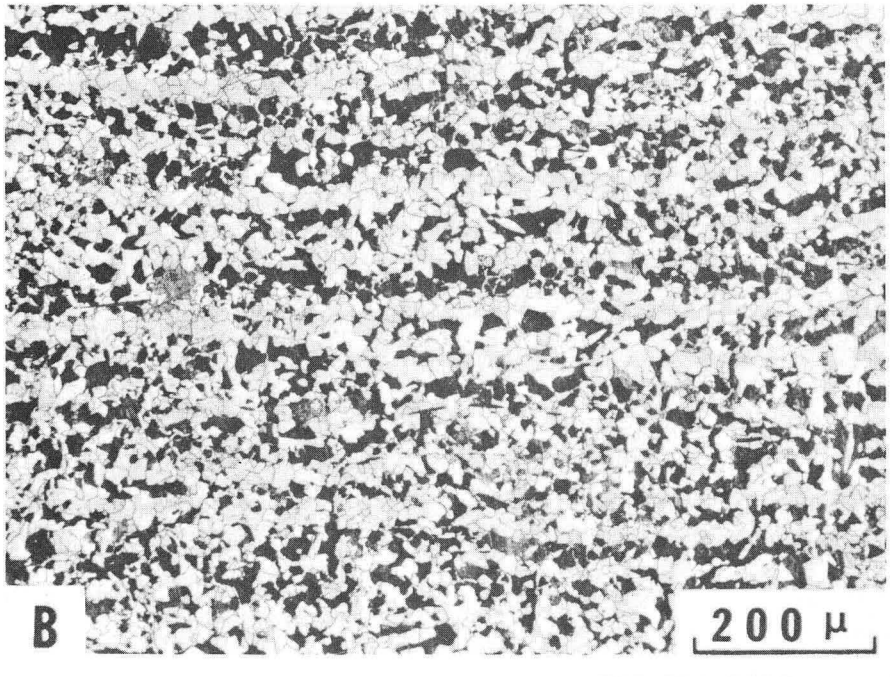


XBB 744-2305

Fig. 1

Standard Charpy V-Notch Specimen

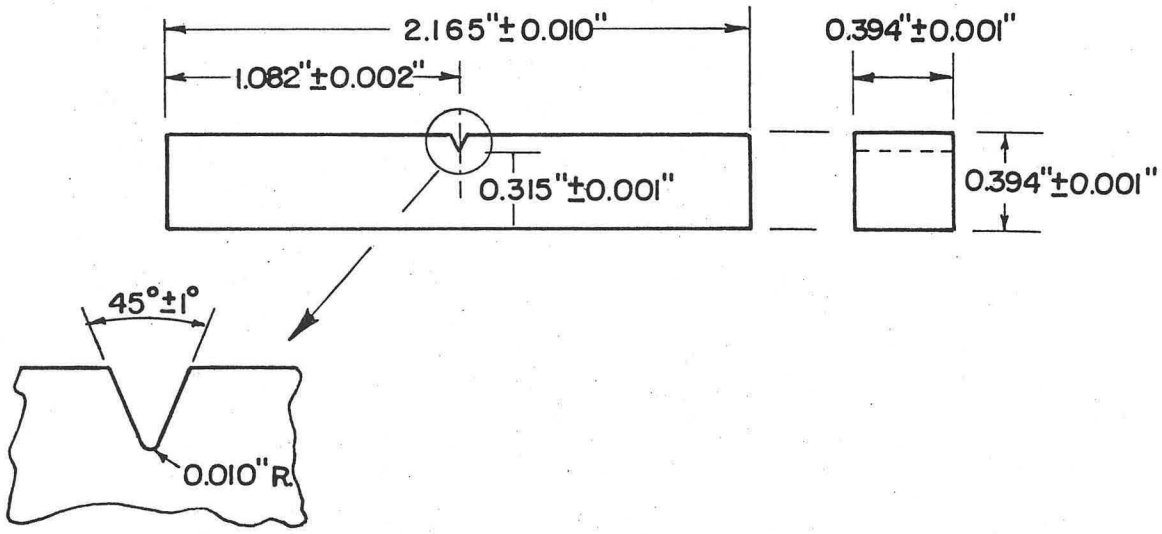


Tensile Specimen

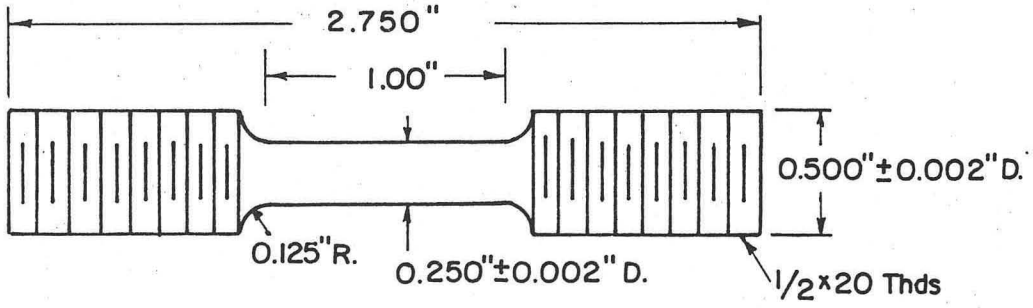


XBL729-6982

Fig. 2

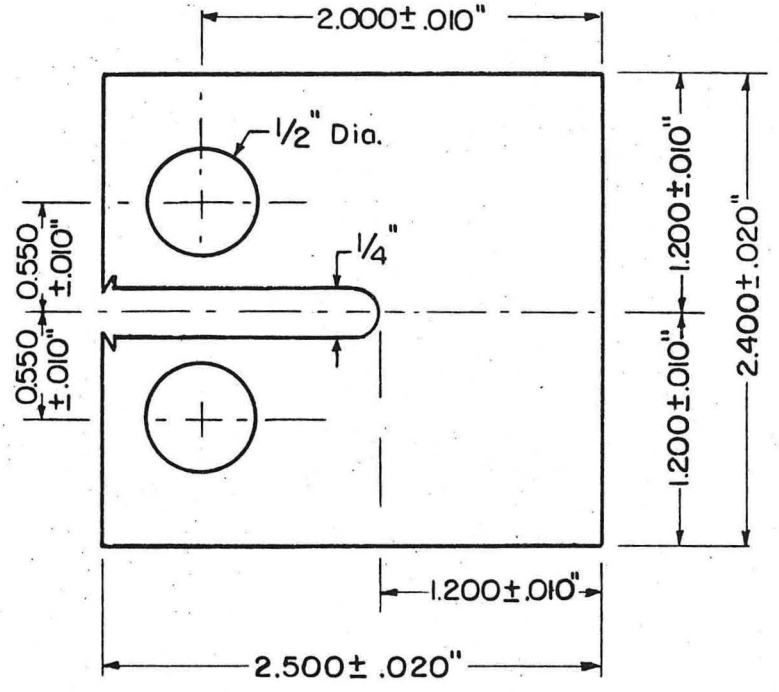


XBL 734-5986A

Fig. 3

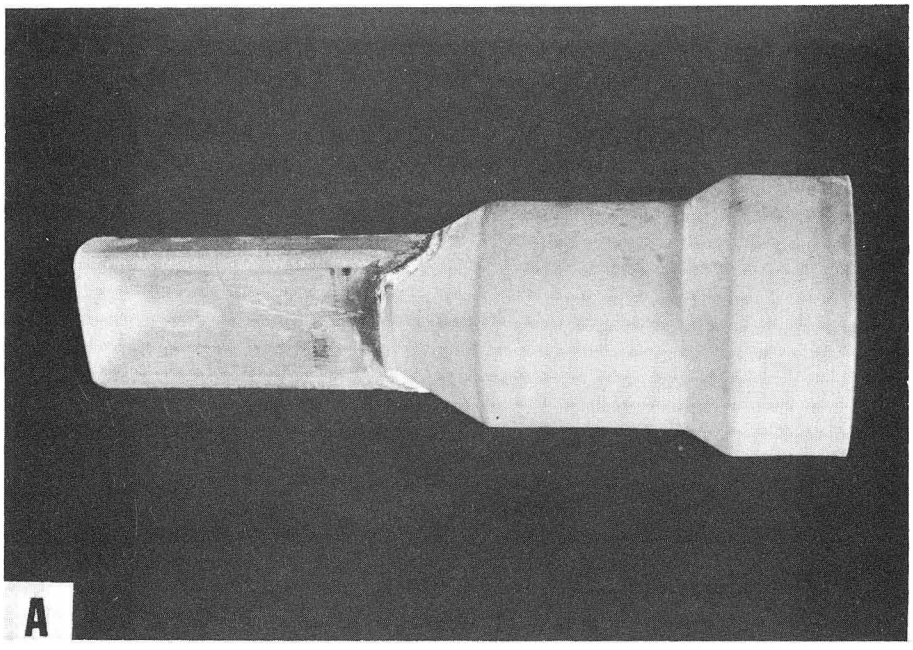


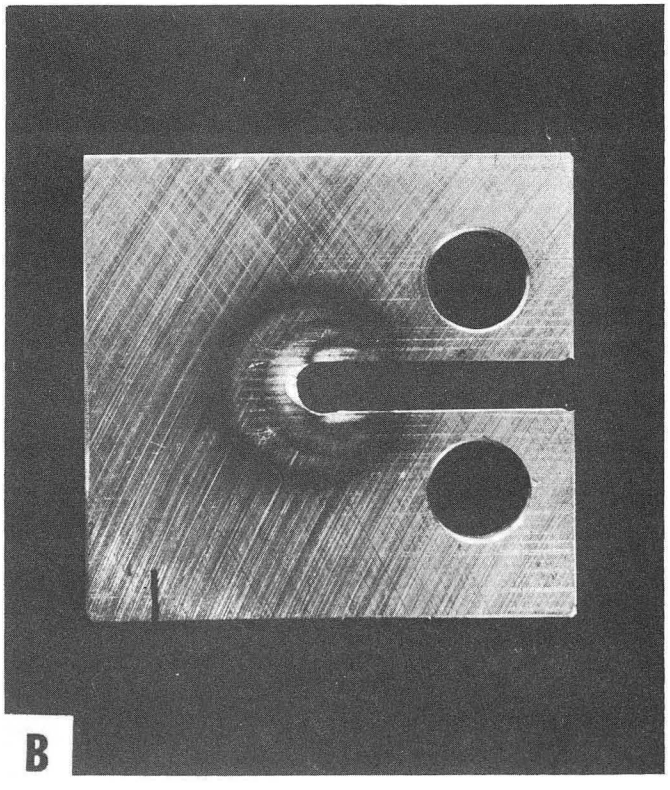


XBB 744-2293

Fig. 4

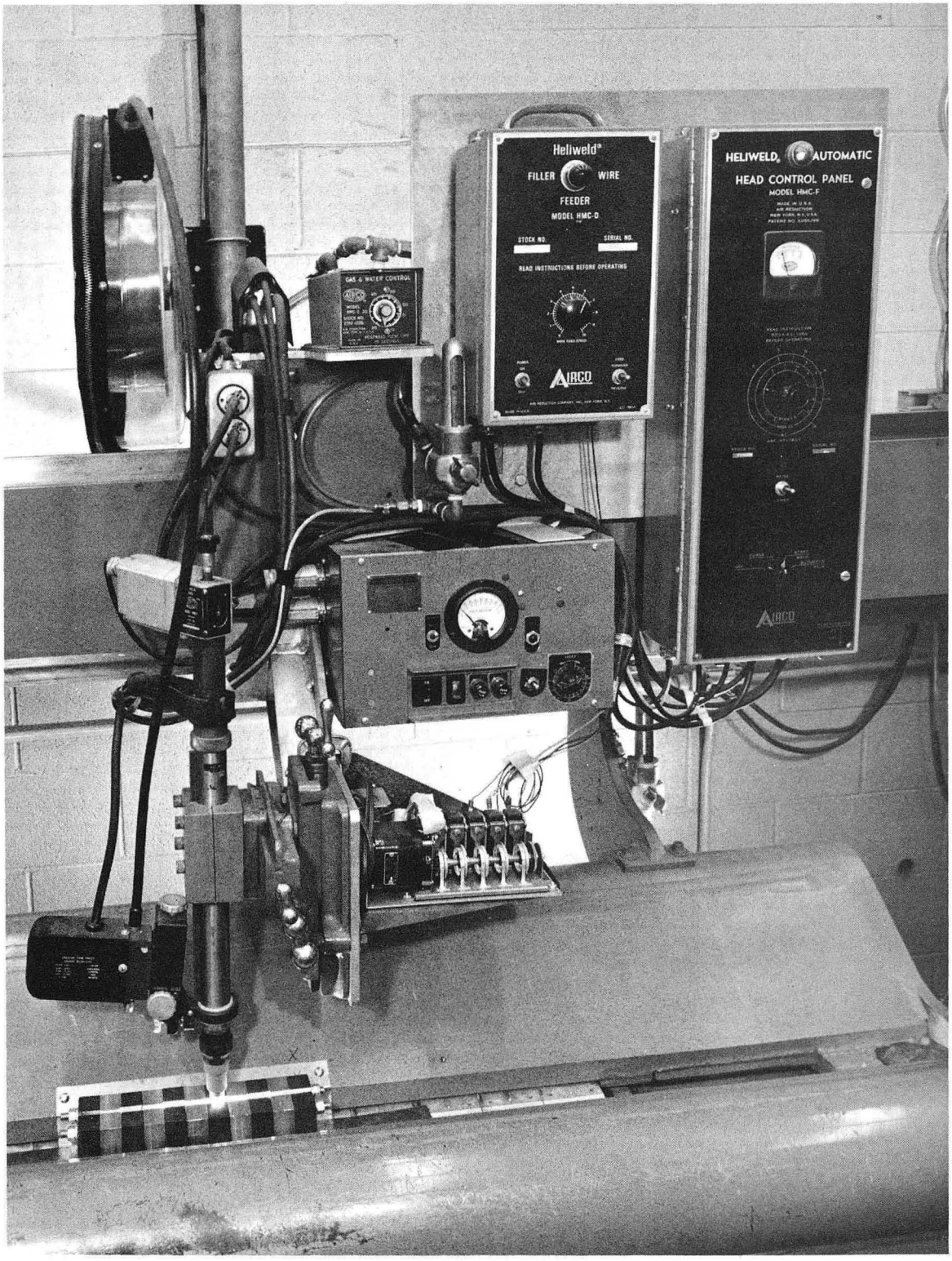


XBB 742-1142

Fig. 5

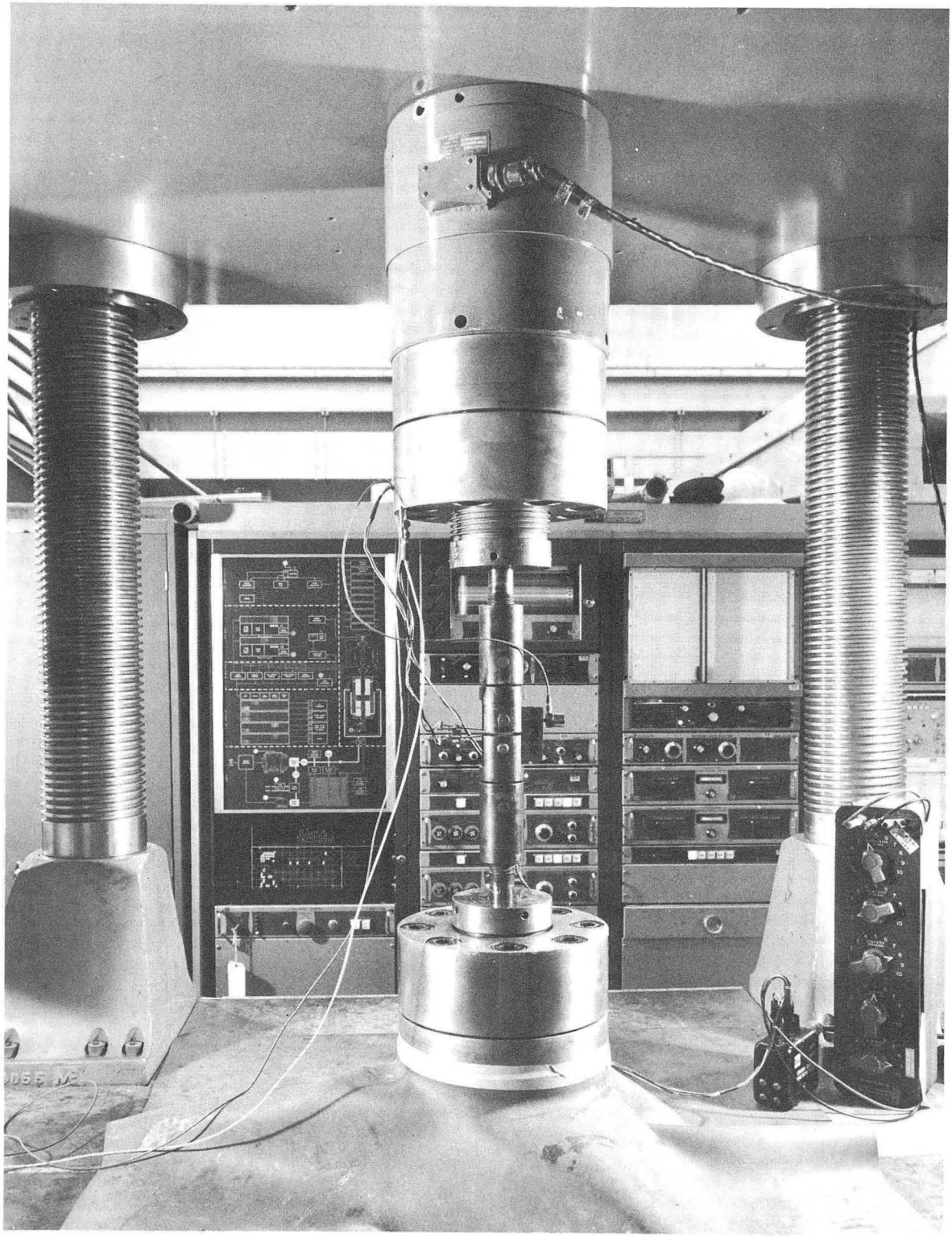

XBB 692-1024

Fig. 6

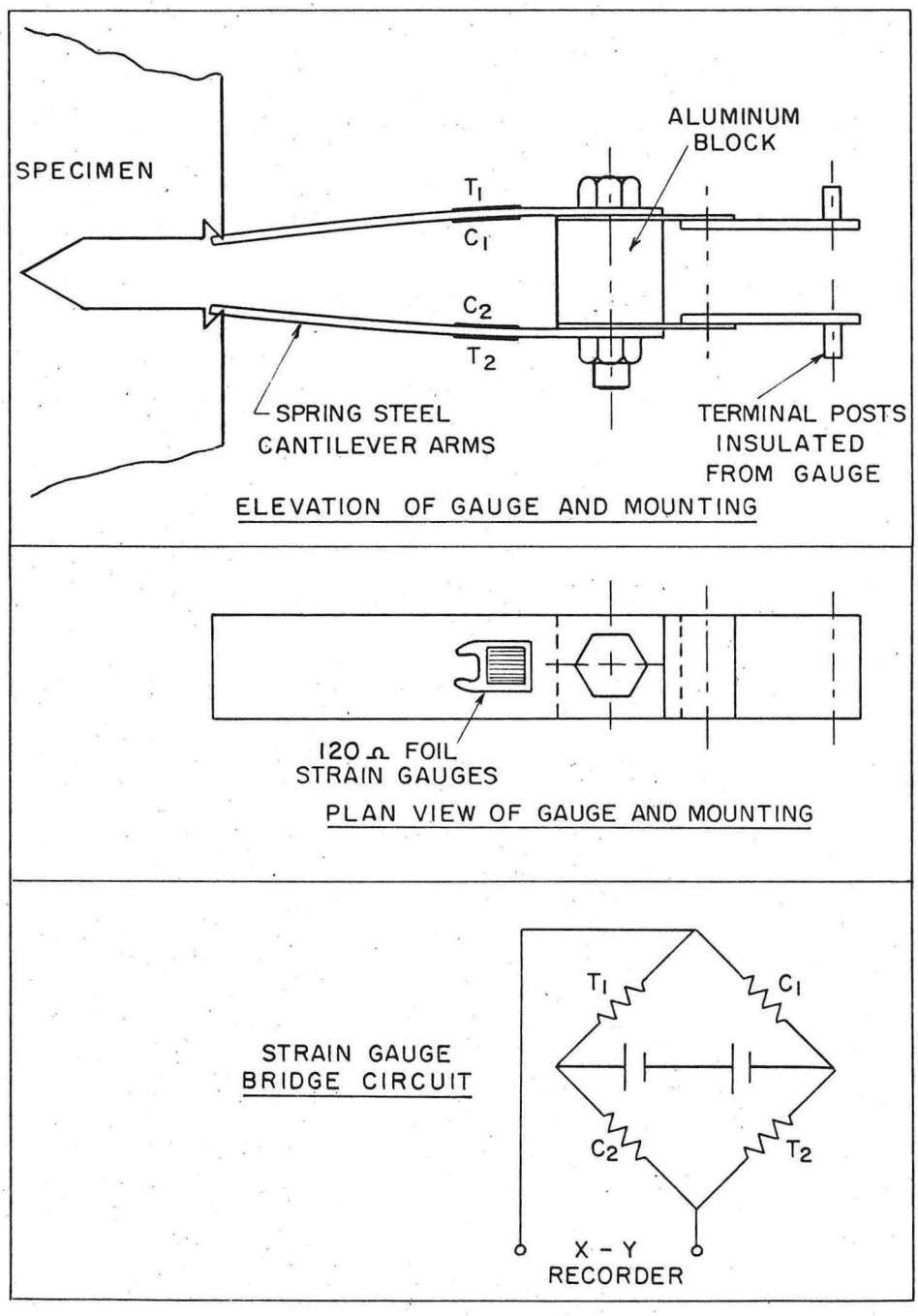


XBL 679-4971

Fig. 7

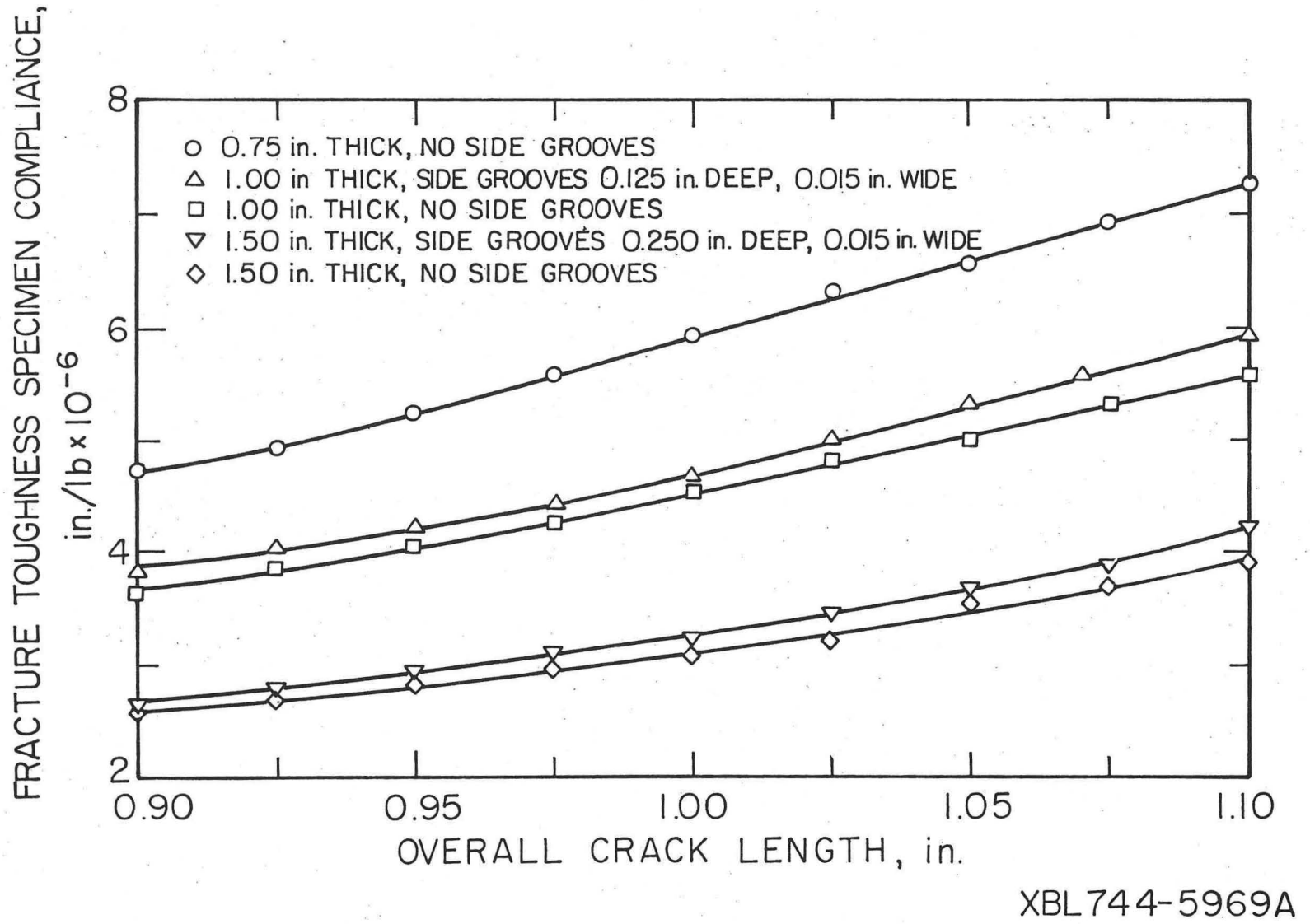
FRACTURE TOUGHNESS SPECIMEN COMPLIANCE, in./lb x 10⁻⁶
8
6
4
2
0.90
0.95
1.00
1.05
1.10
OVERALL CRACK LENGTH, in.
○ 0.75 in. THICK, NO SIDE GROOVES
△ 1.00 in THICK, SIDE GROOVES 0.125 in. DEEP, 0.015 in. WIDE
□ 1.00 in. THICK, NO SIDE GROOVES
▽ 1.50 in. THICK, SIDE GROOVES 0.250 in. DEEP, 0.015 in. WIDE
◇ 1.50 in. THICK, NO SIDE GROOVES
XBL744-5969A

Fig. 8

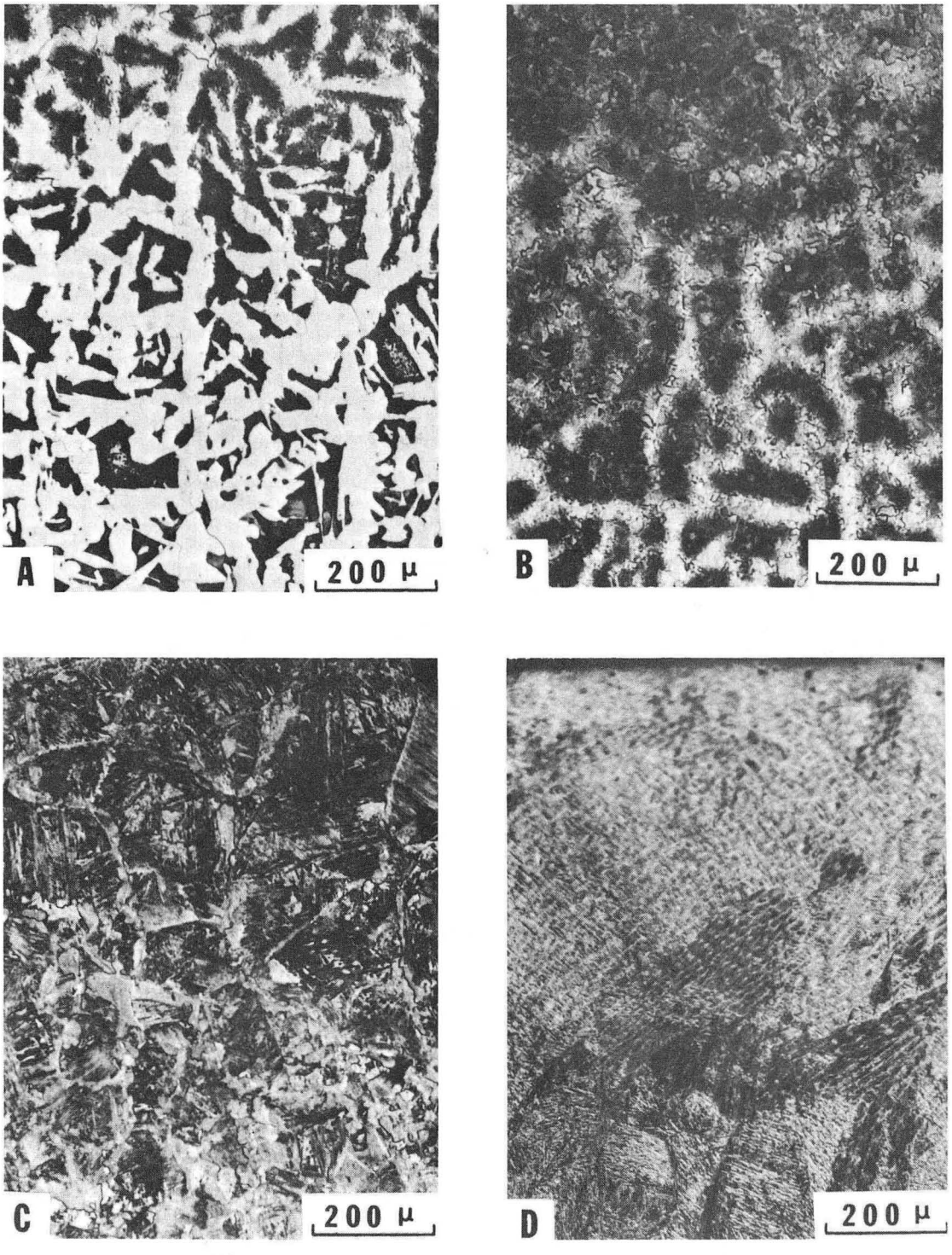


XBB 745-3469

Fig. 9

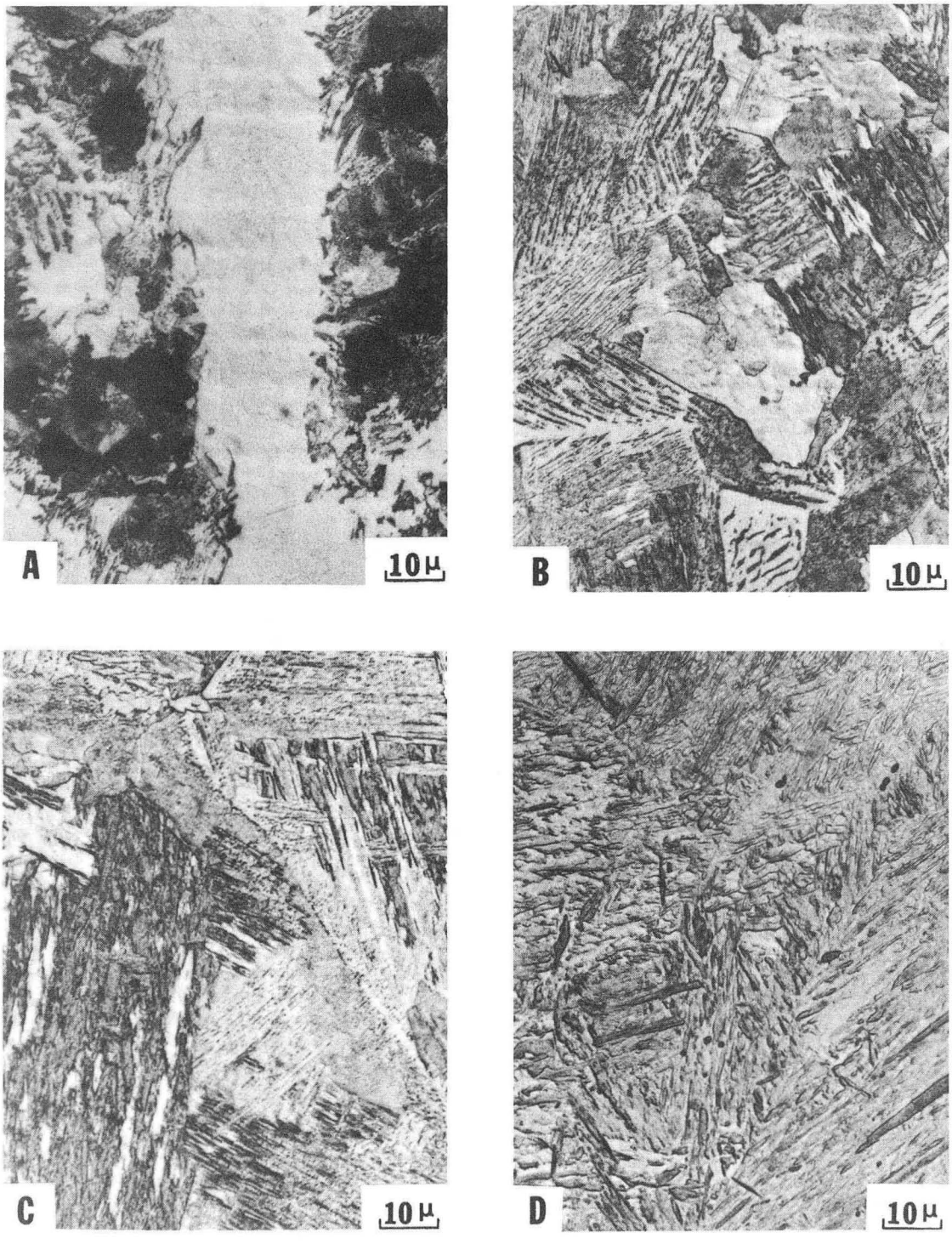


XBB 745-3470

Fig. 10

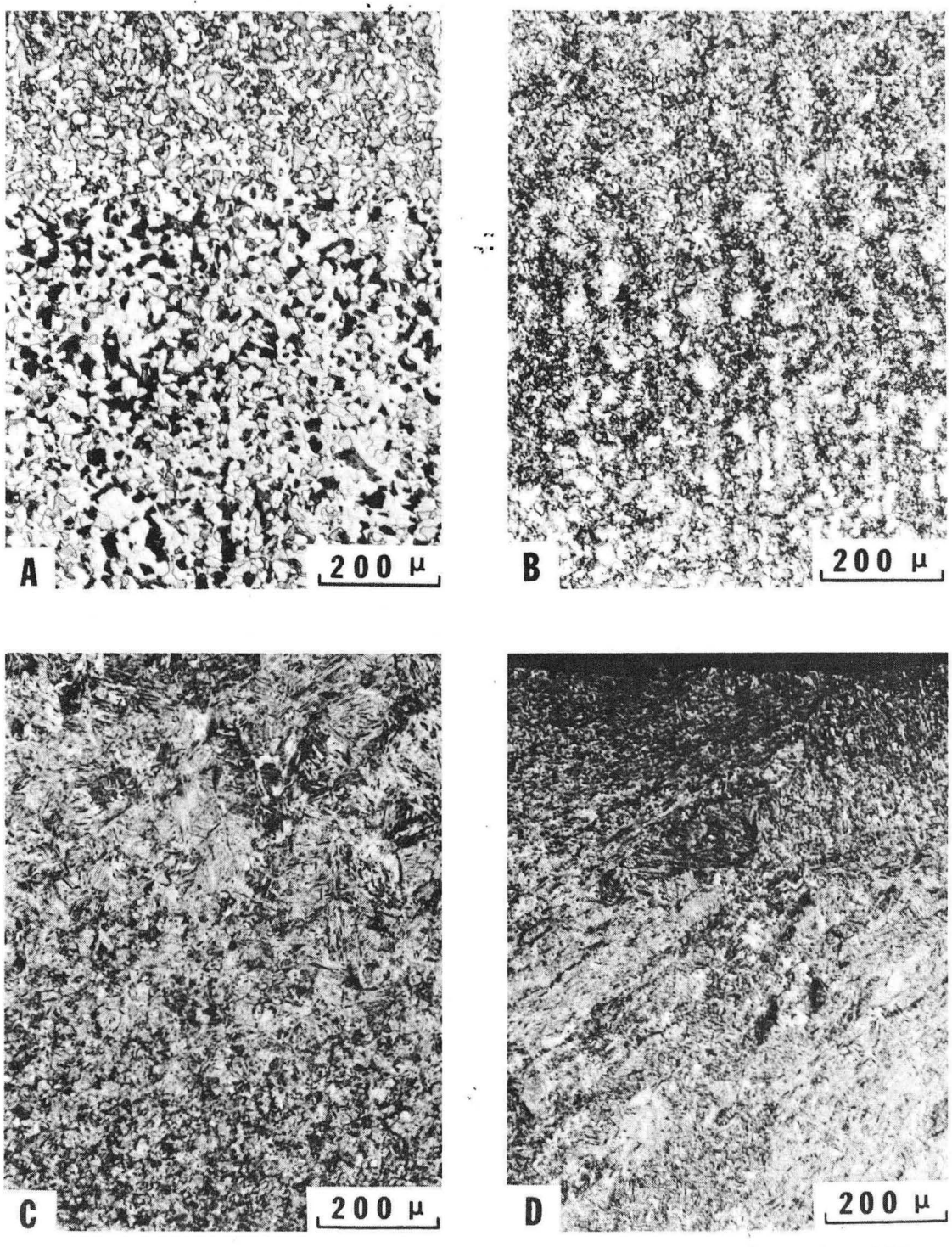


XBB 745-3468

Fig. 11

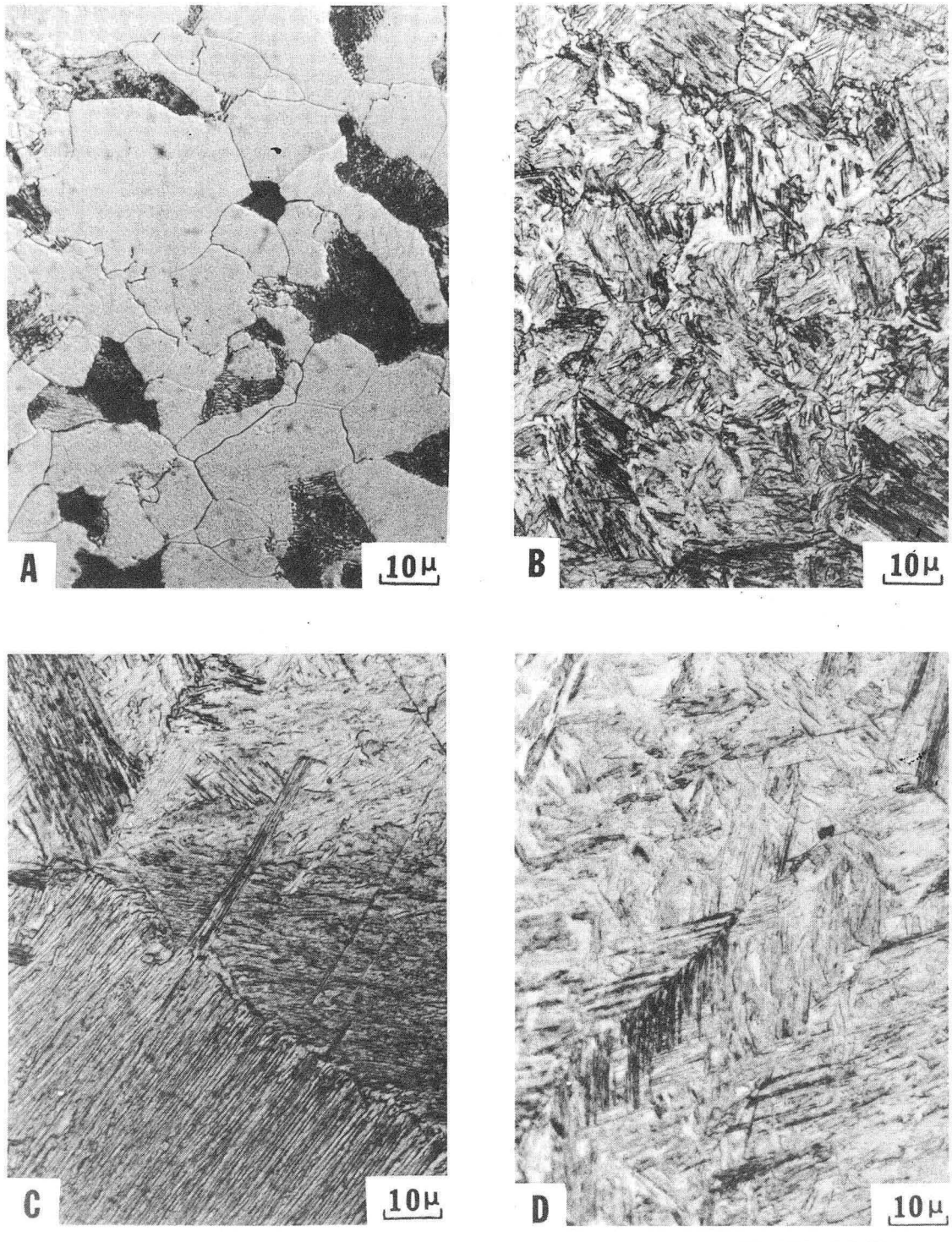


XBB 745-3467

Fig. 12

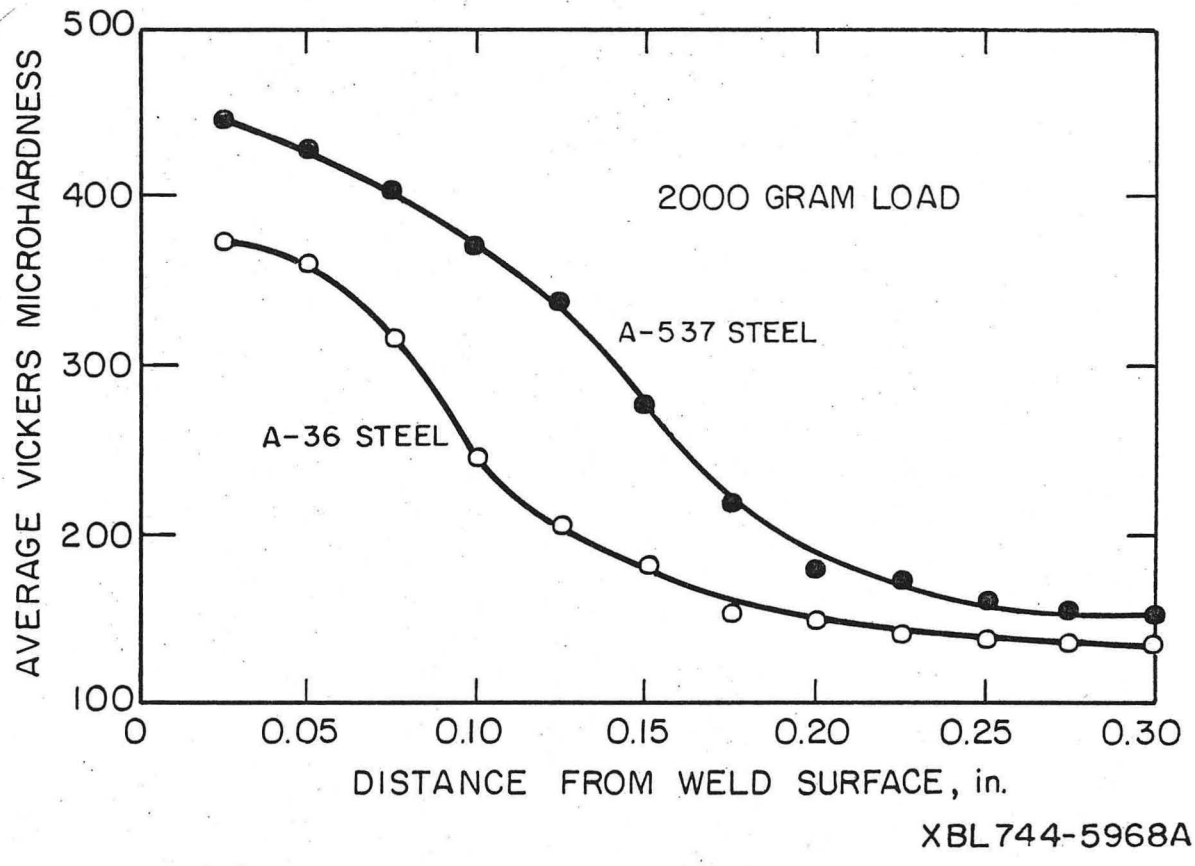
AVERAGE VICKERS MICROHARDNESS
500
400
300
200
100
0
0.05
0.10
0.15
0.20
0.25
0.30
DISTANCE FROM WELD SURFACE, in.
2000 GRAM LOAD
A-537 STEEL
A-36 STEEL
XBL744-5968A

Fig. 13

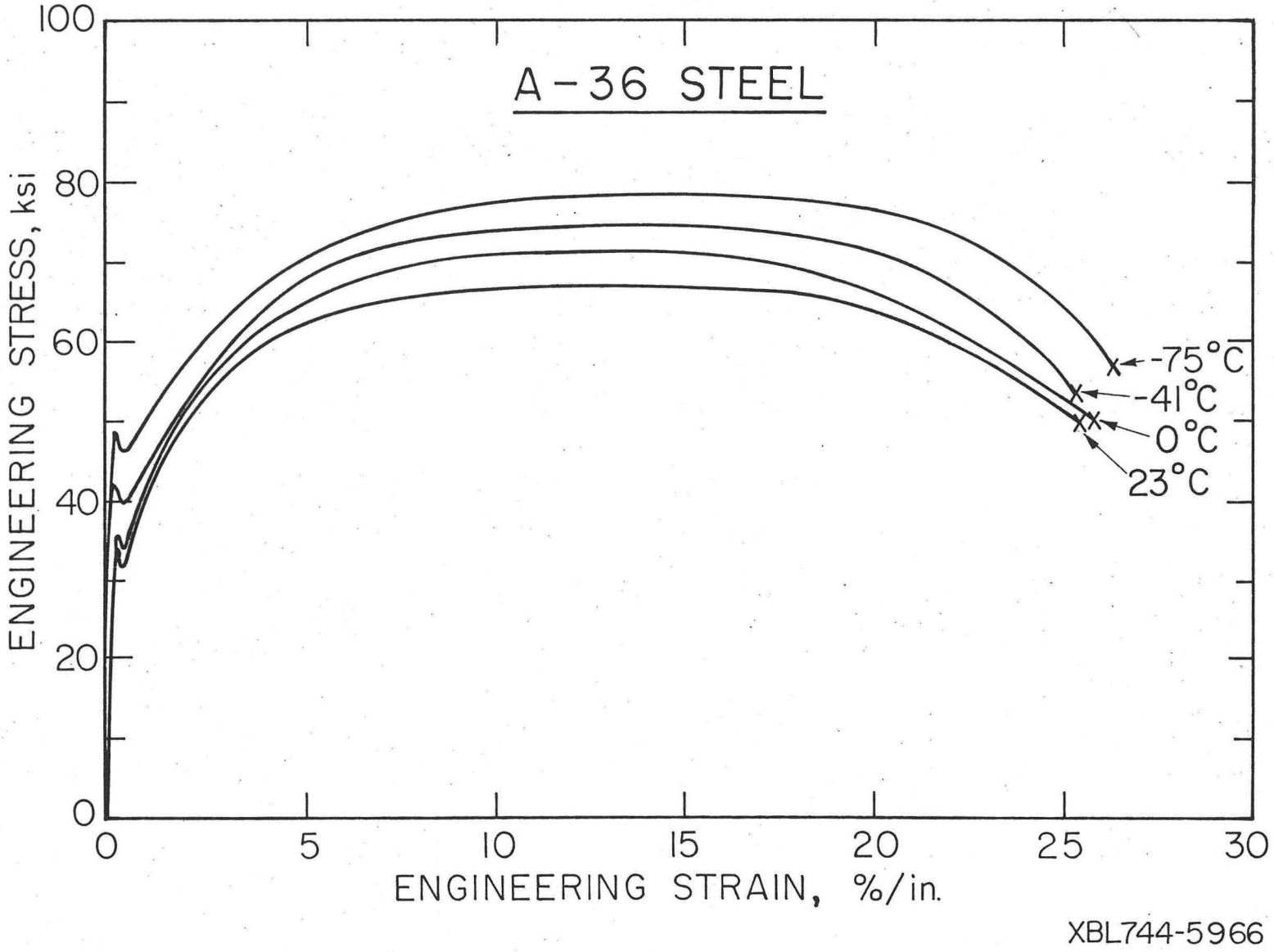
A-36 STEEL
ENGINEERING STRESS, ksi
ENGINEERING STRAIN, %/in.
100
80
60
40
20
0
0
5
10
15
20
25
30
-75°C
-41°C
0°C
23°C
XBL744-5966

Fig. 14

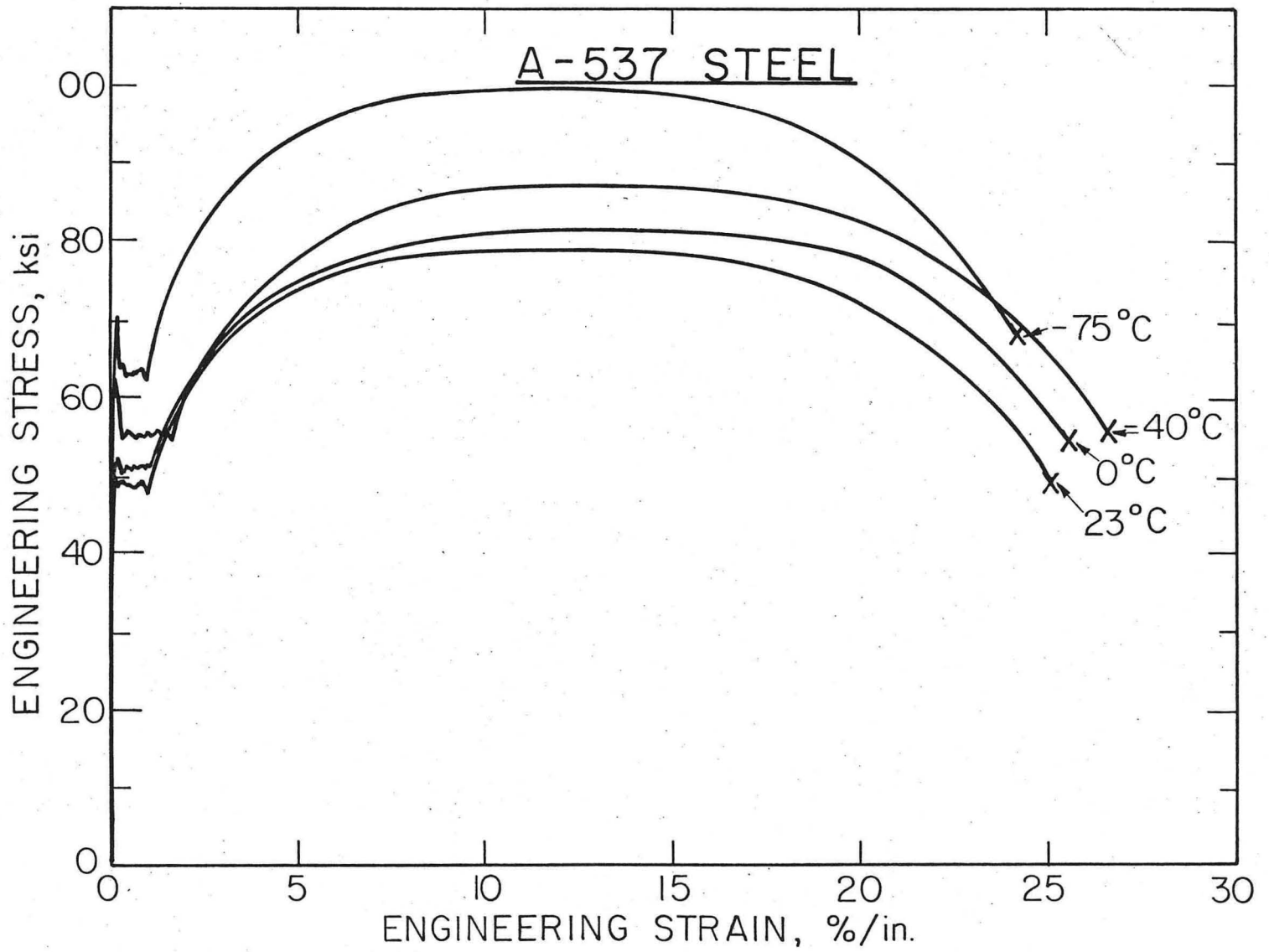


XBL 744-6192

Fig. 15

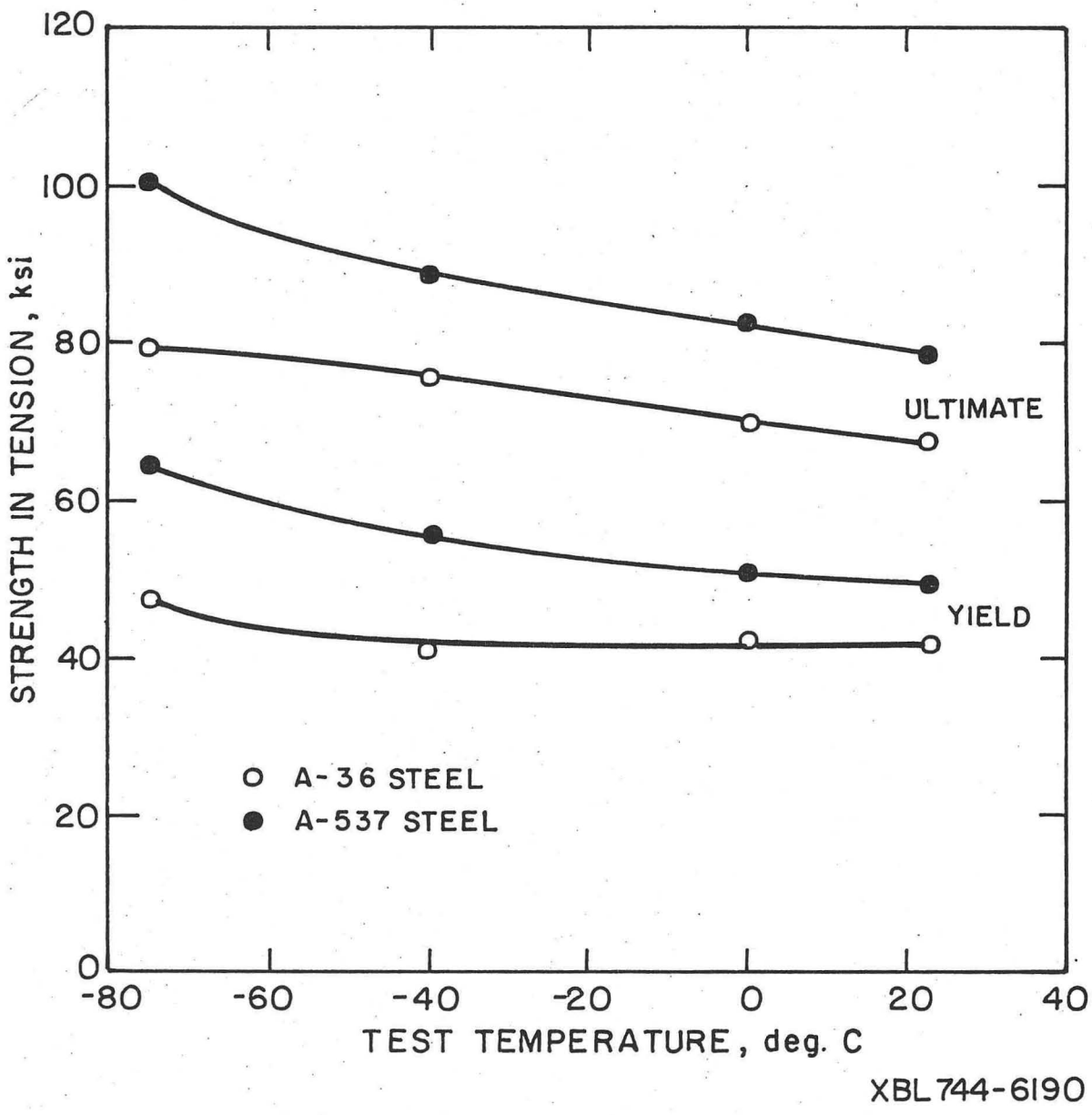
120
100
80
60
40
20
0
STRENGTH IN TENSION, ksi
ULTIMATE
YIELD
A-36 STEEL
A-537 STEEL
-80
-60
-40
-20
0
20
40
TEST TEMPERATURE, deg. C
XBL 744-6190

Fig. 16

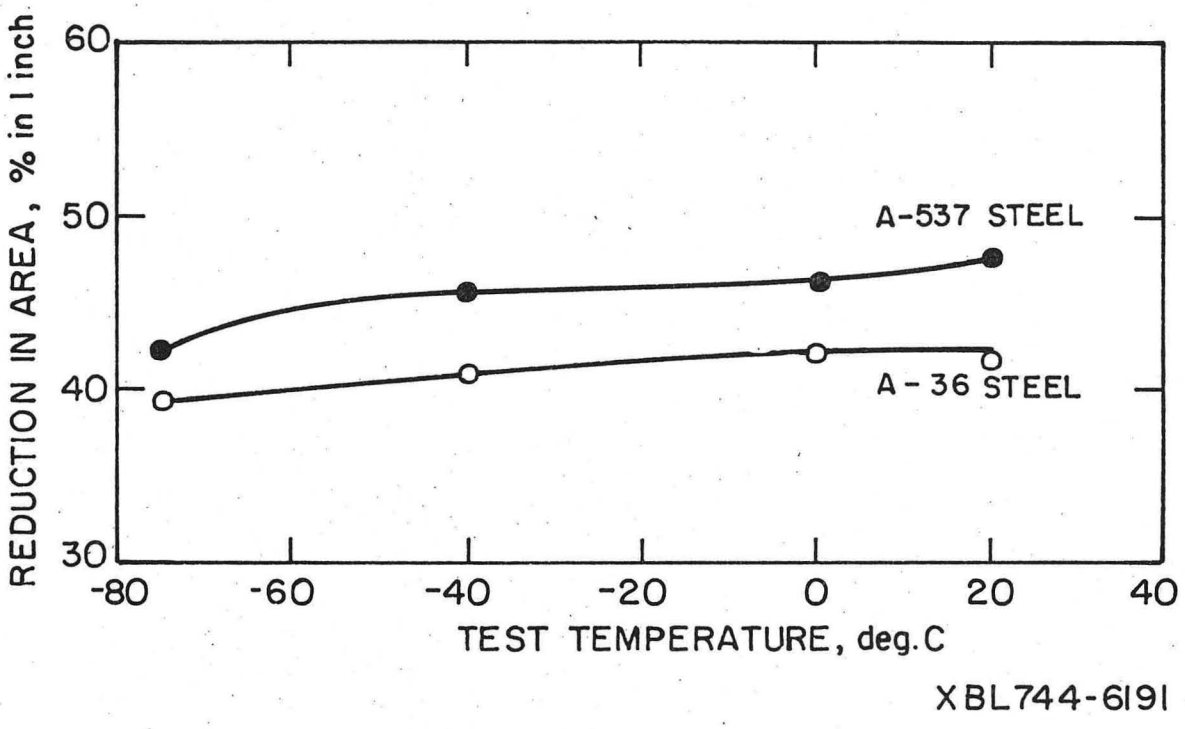
REDUCTION IN AREA, % in I inch
60
50
40
30
A-537 STEEL
A-36 STEEL
-80
-60
-40
-20
0
20
40
TEST TEMPERATURE, deg.C
XBL744-6191

Fig. 17

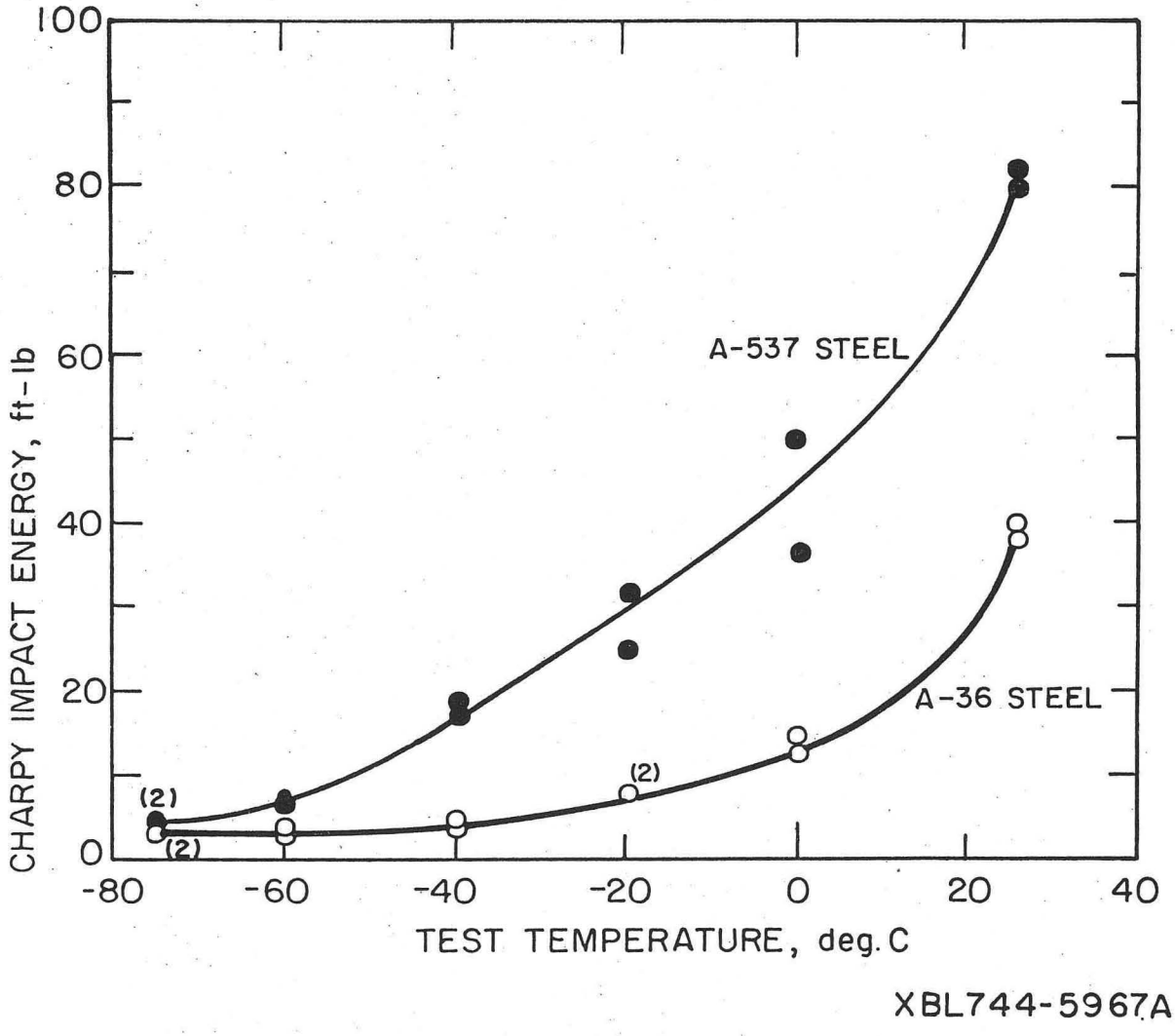
100
80
60
40
20
0
CHARPY IMPACT ENERGY, ft-lb
A-537 STEEL
A-36 STEEL
(2)
(2)
(2)
-80
-60
-40
-20
0
20
40
TEST TEMPERATURE, deg.C
XBL744-5967A

Fig. 18

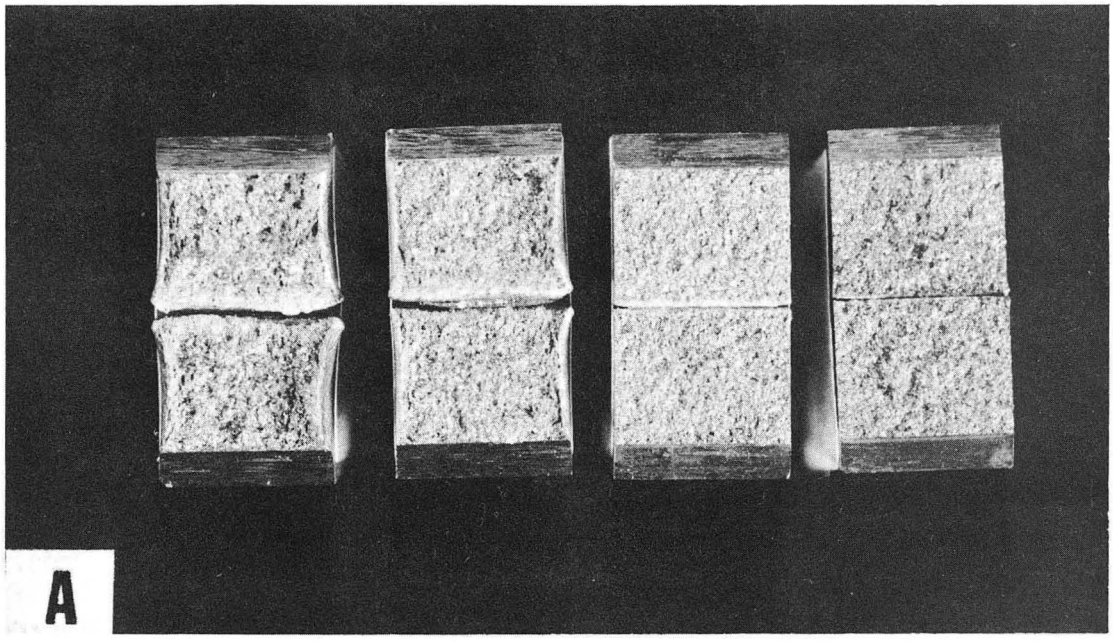


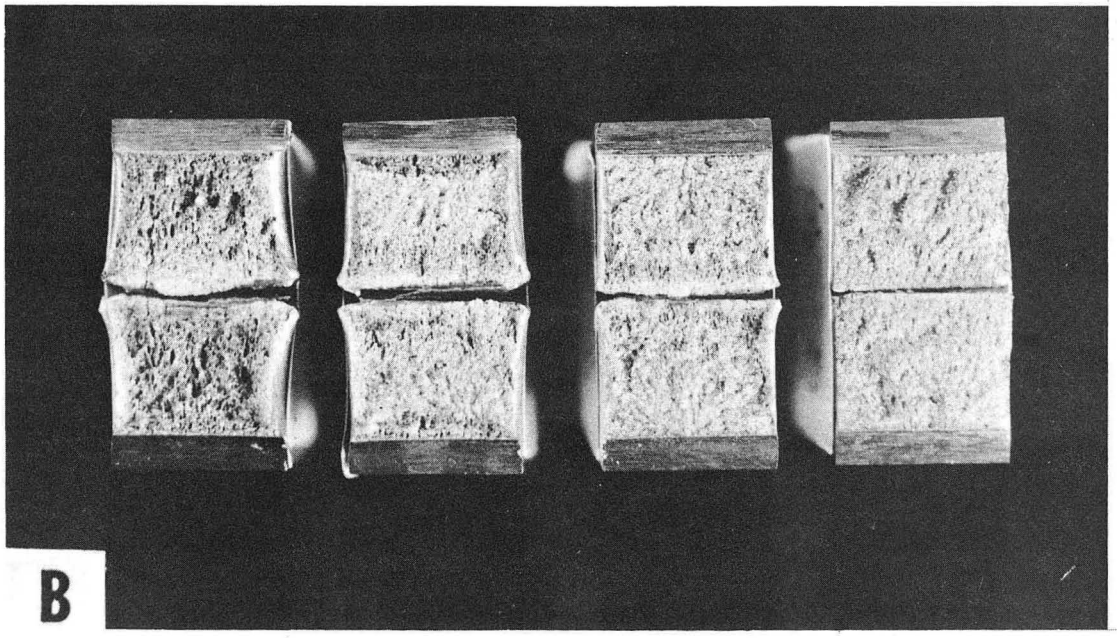


XBB 744-2292

Fig. 19

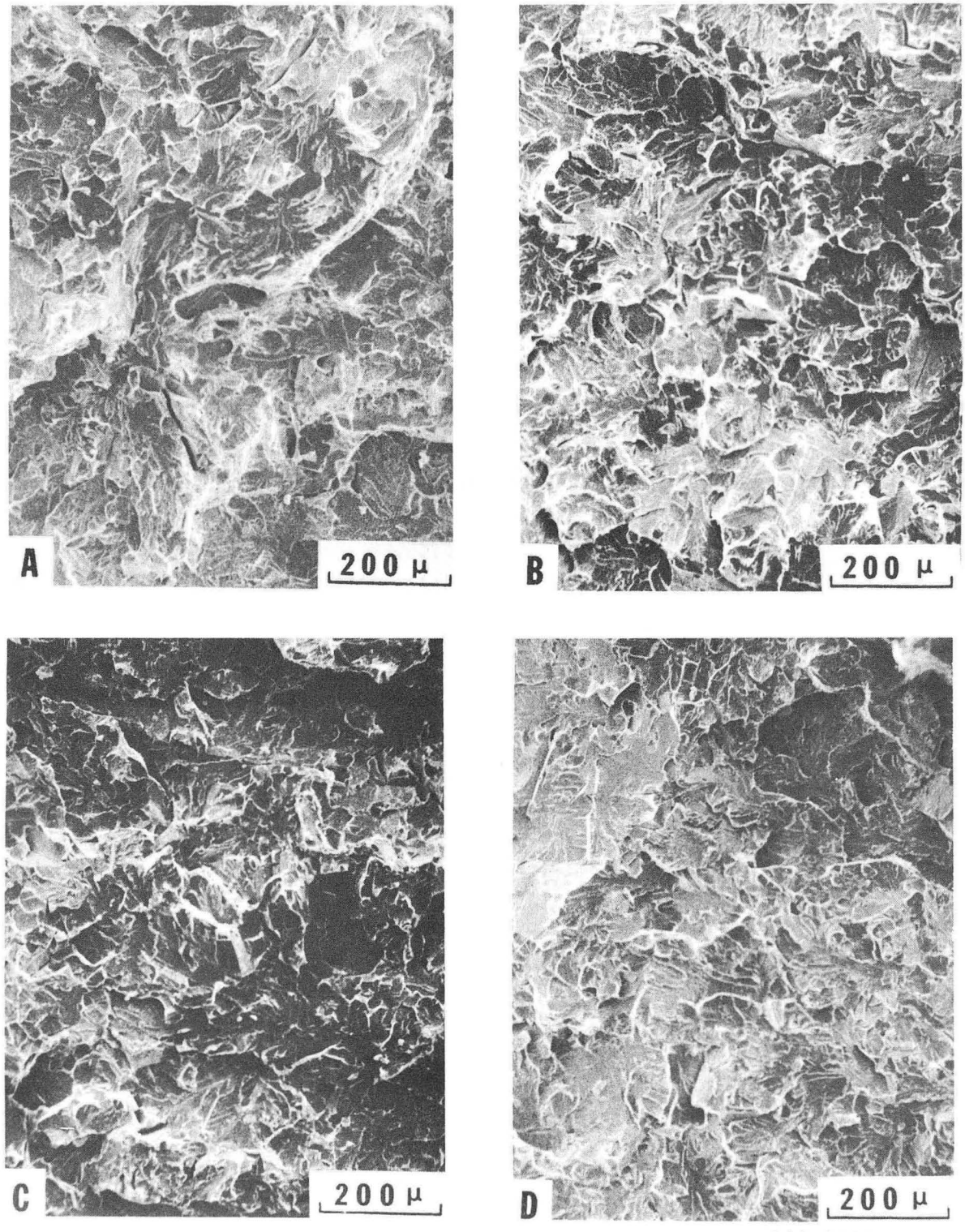


XBB 744-2301

Fig. 20

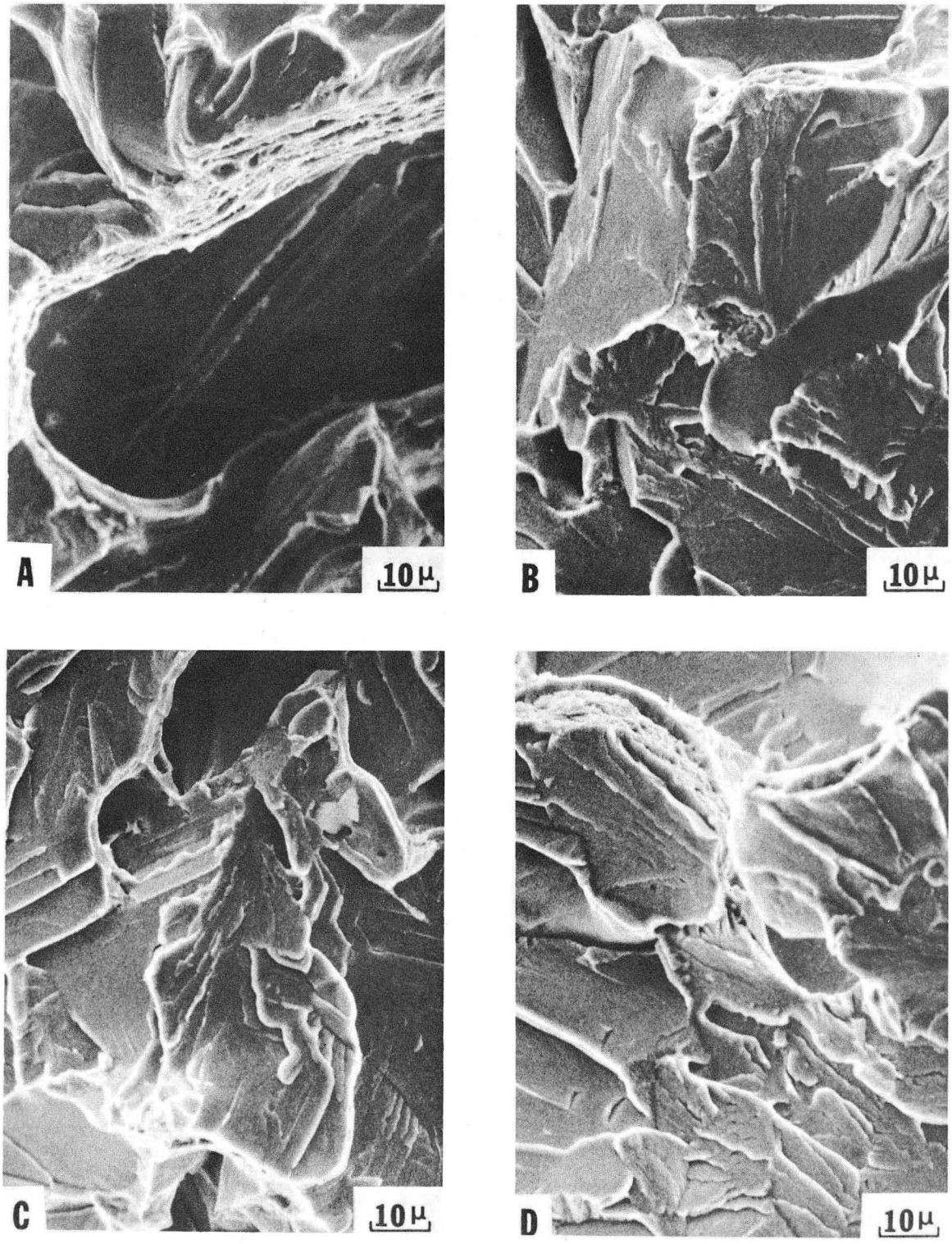


XBB 744-2300

Fig. 21

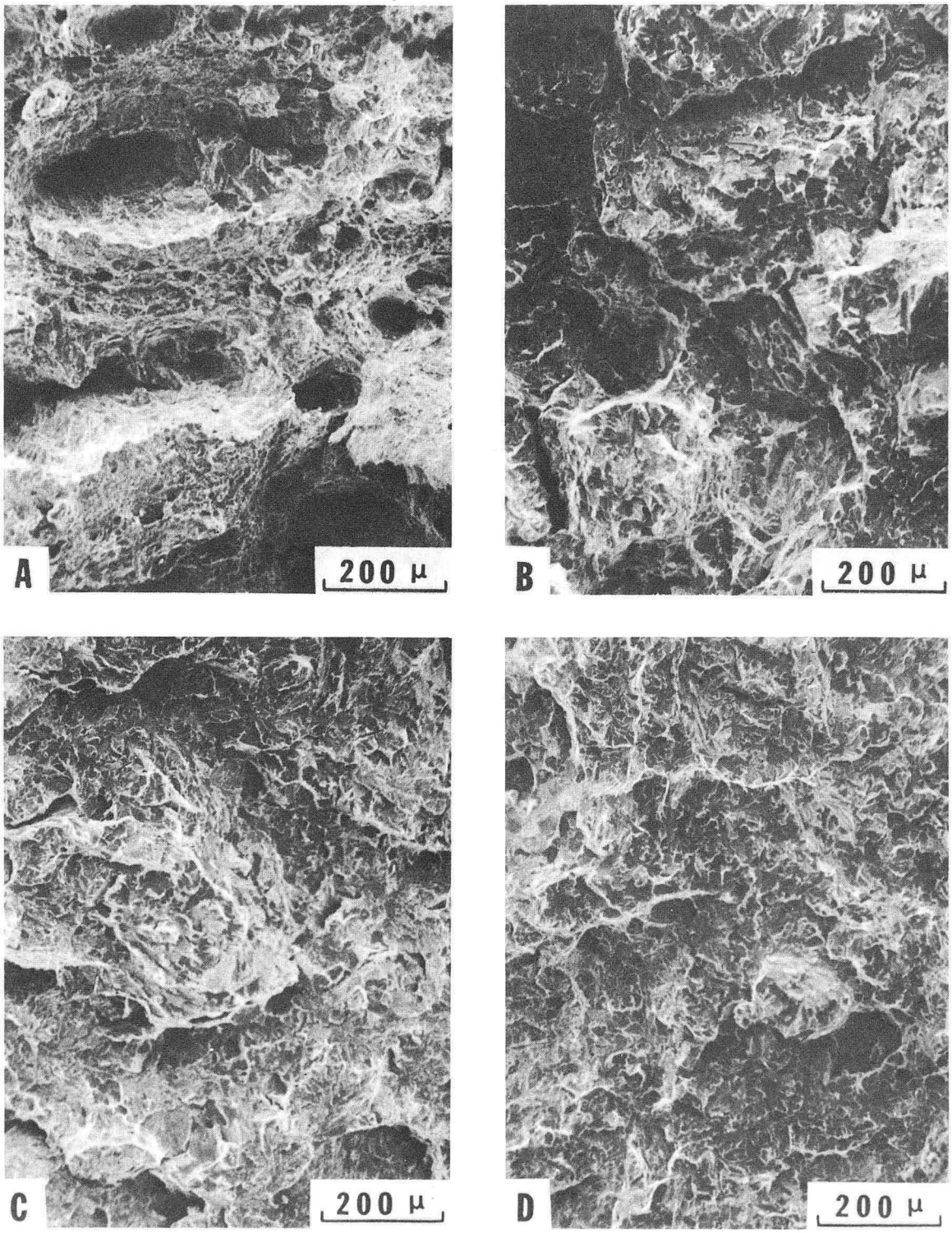


XBB 744-2299

Fig. 22

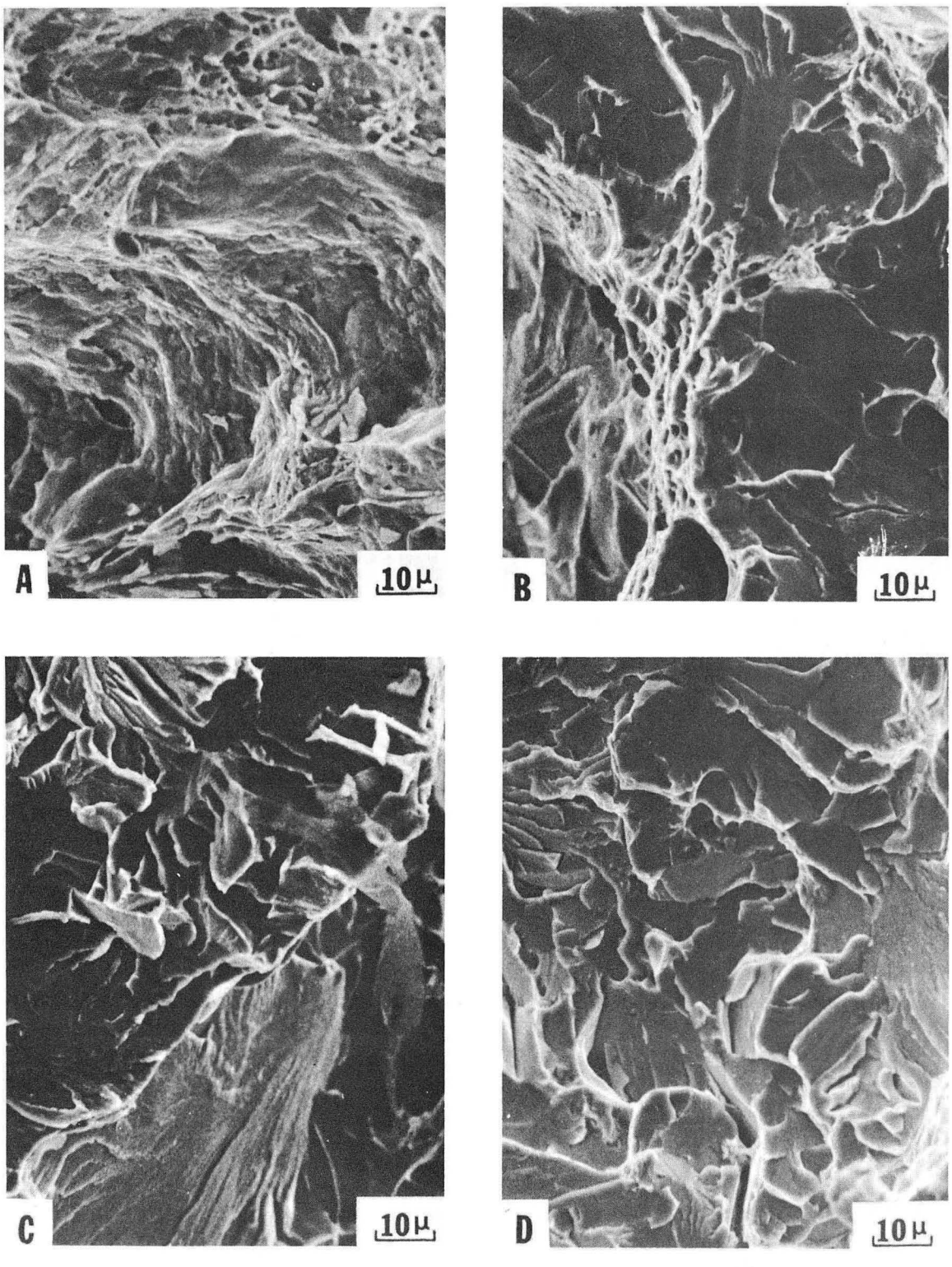


XBB 744-2296

Fig. 23

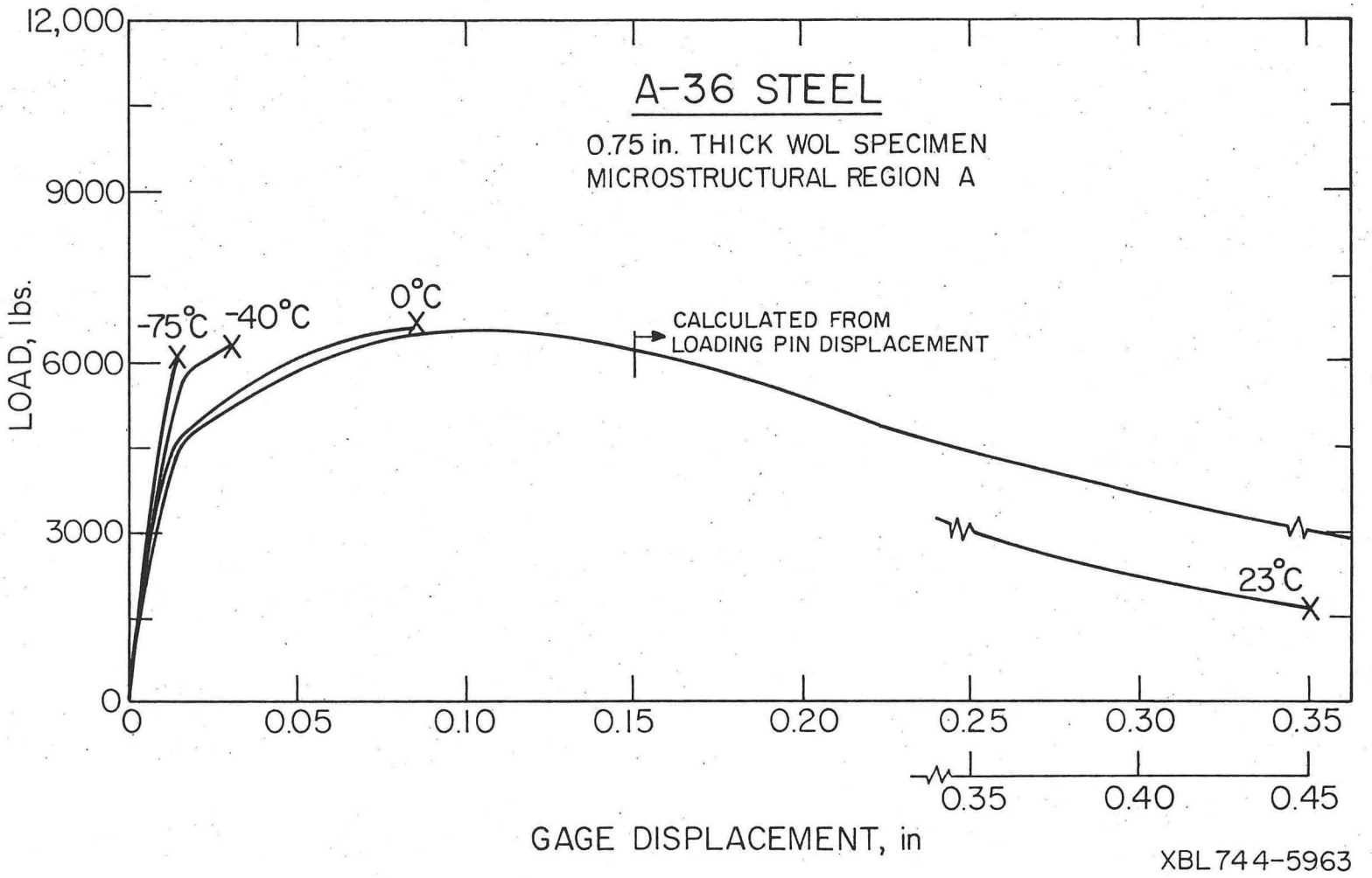
A-36 STEEL
0.75 in. THICK WOL SPECIMEN
MICROSTRUCTURAL REGION A
LOAD, lbs.
12,000
9000
6000
3000
0
-75°C
-40°C
0°C
23°C
CALCULATED FROM
LOADING PIN DISPLACEMENT
0
0.05
0.10
0.15
0.20
0.25
0.30
0.35
0.35
0.40
0.45
GAGE DISPLACEMENT, in
XBL744-5963

Fig. 24

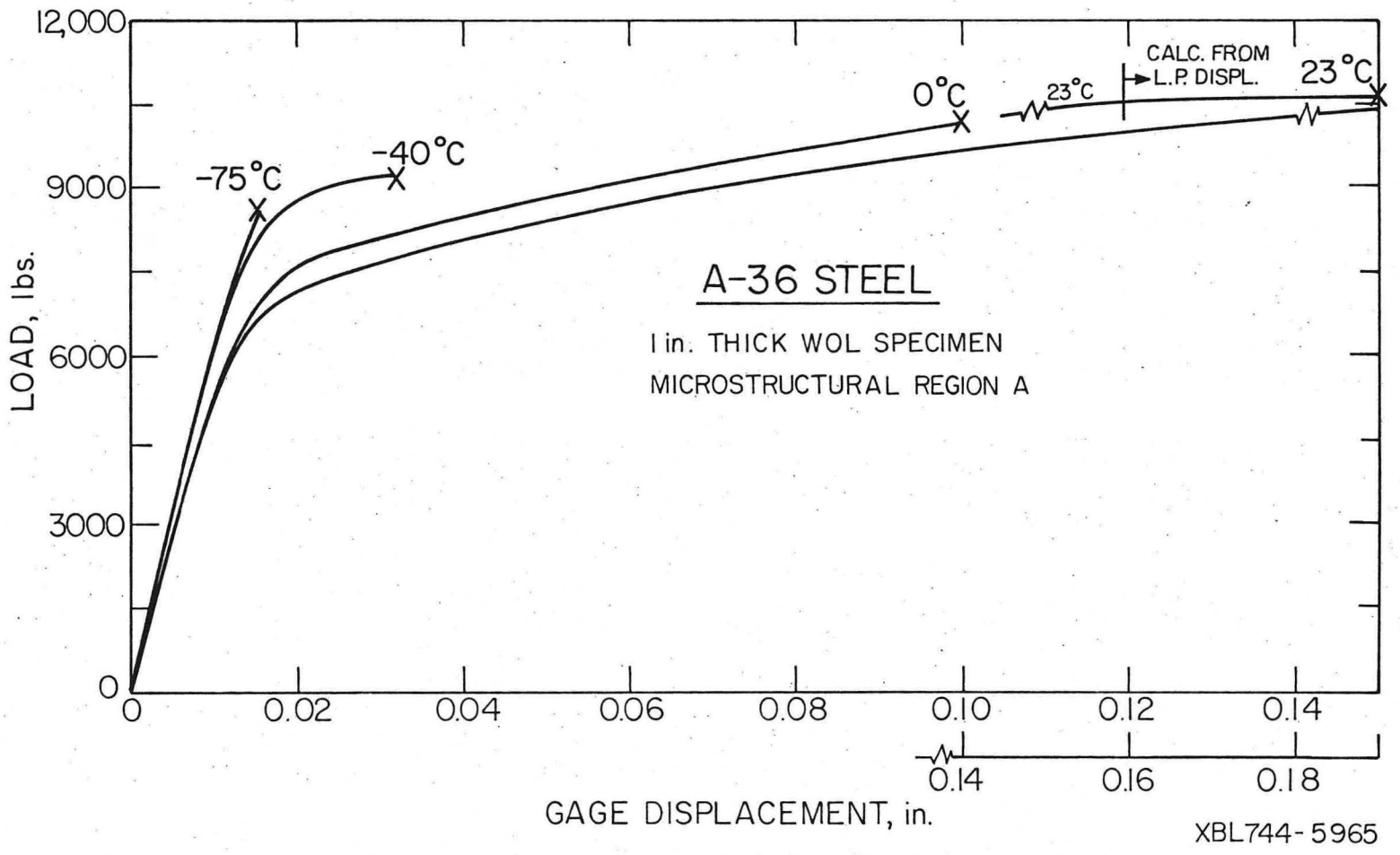
12,000
9000
6000
3000
0
LOAD, lbs.
-75°C
-40°C
0°C
23°C
CALC. FROM
L.P. DISPL.
23°C
A-36 STEEL
1 in. THICK WOL SPECIMEN
MICROSTRUCTURAL REGION A
0
0.02
0.04
0.06
0.08
0.10
0.12
0.14
0.14
0.16
0.18
GAGE DISPLACEMENT, in.
XBL744-5965

Fig. 25

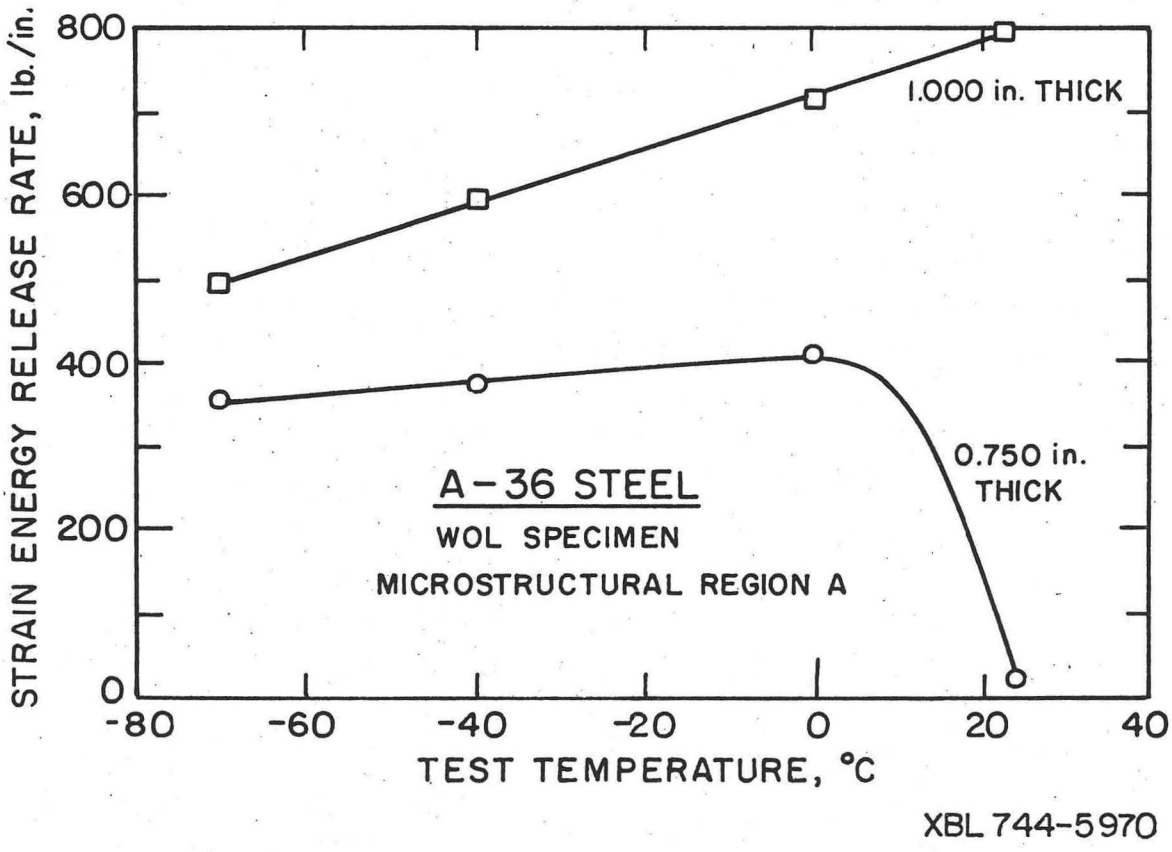
STRAIN ENERGY RELEASE RATE, lb./in.
800
600
400
200
0
-80
-60
-40
-20
0
20
40
TEST TEMPERATURE, °C
1.000 in. THICK
0.750 in.
THICK
A-36 STEEL
WOL SPECIMEN
MICROSTRUCTURAL REGION A
XBL 744-5970

Fig. 26

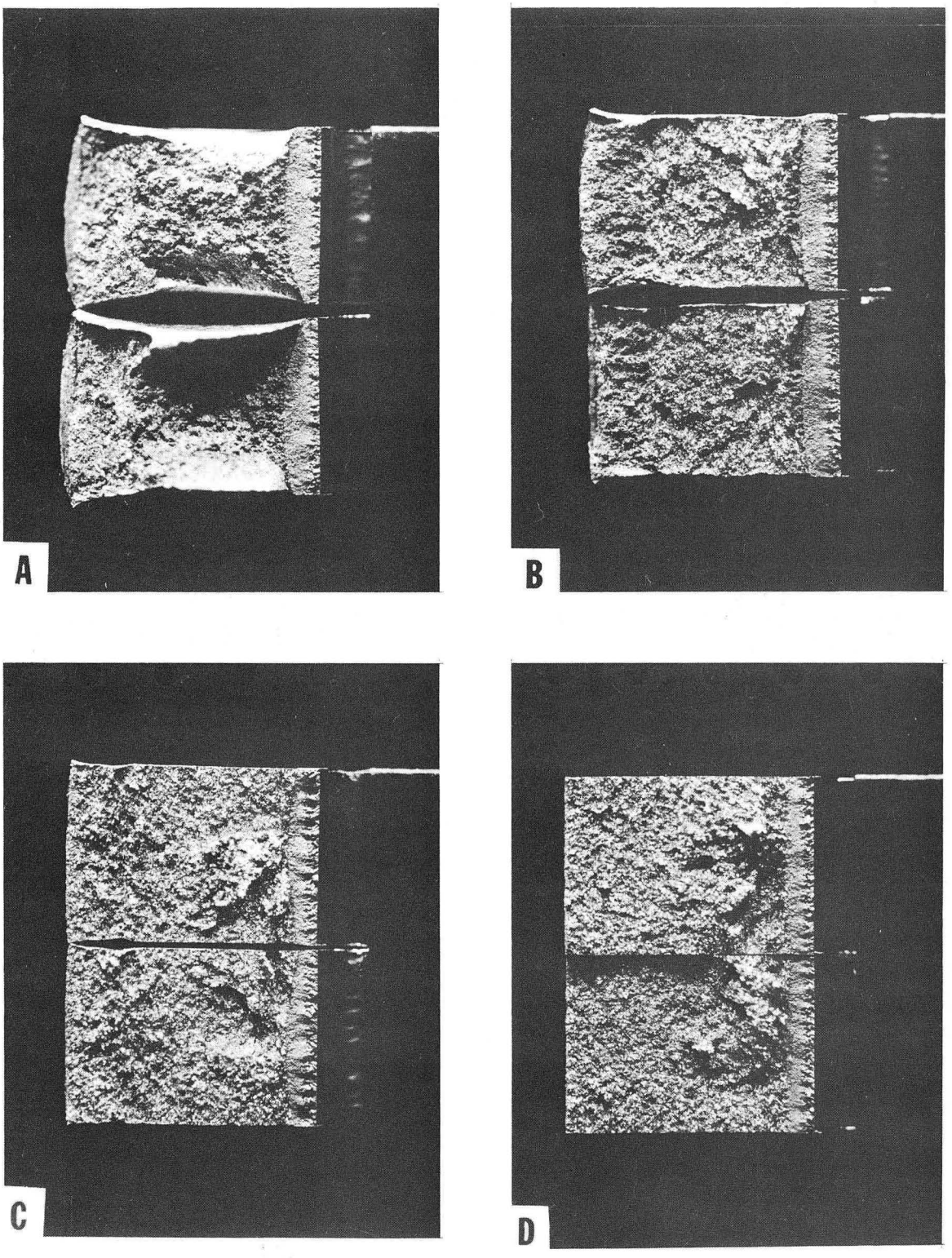


XBB 744-2304

Fig. 27

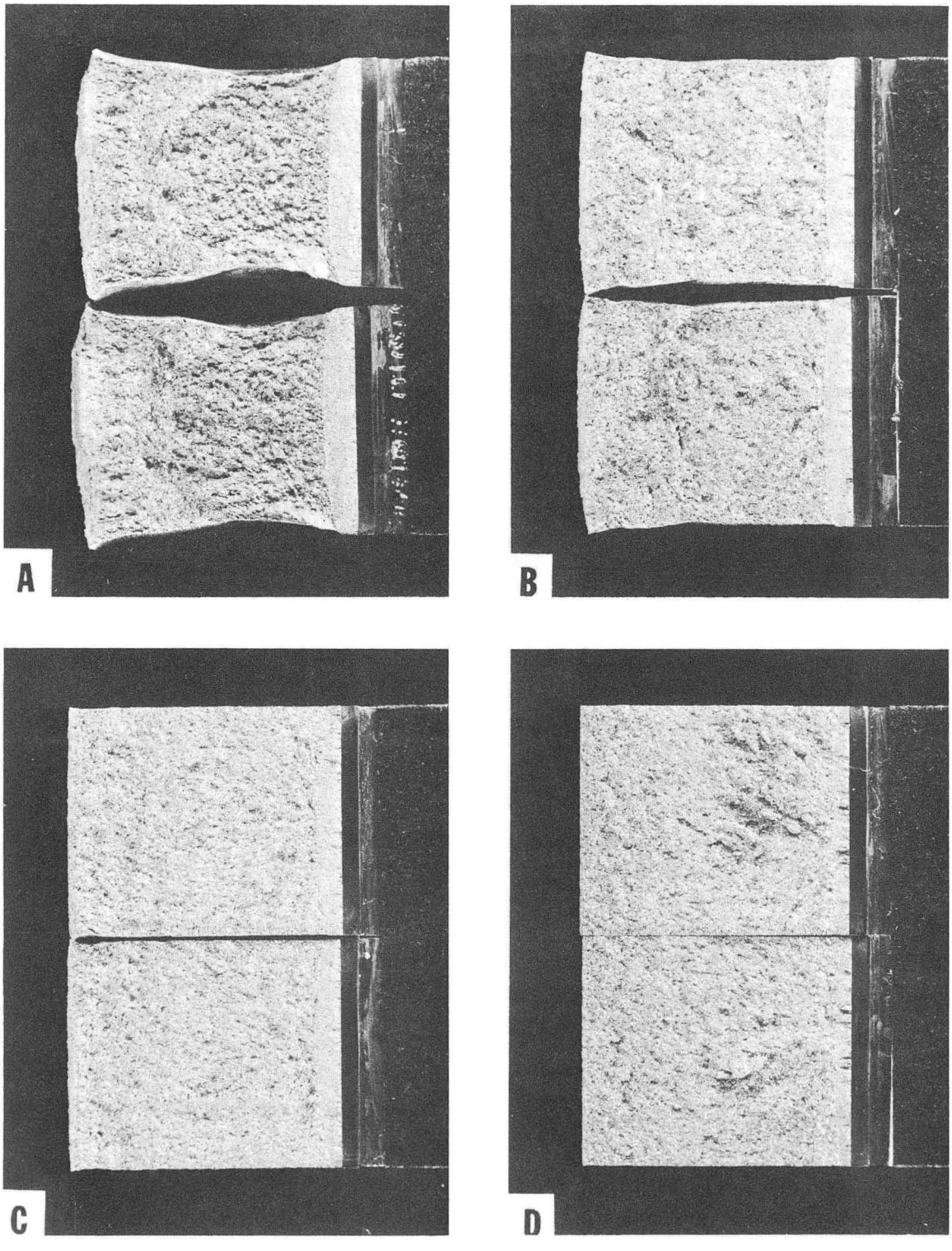


Fig. 28

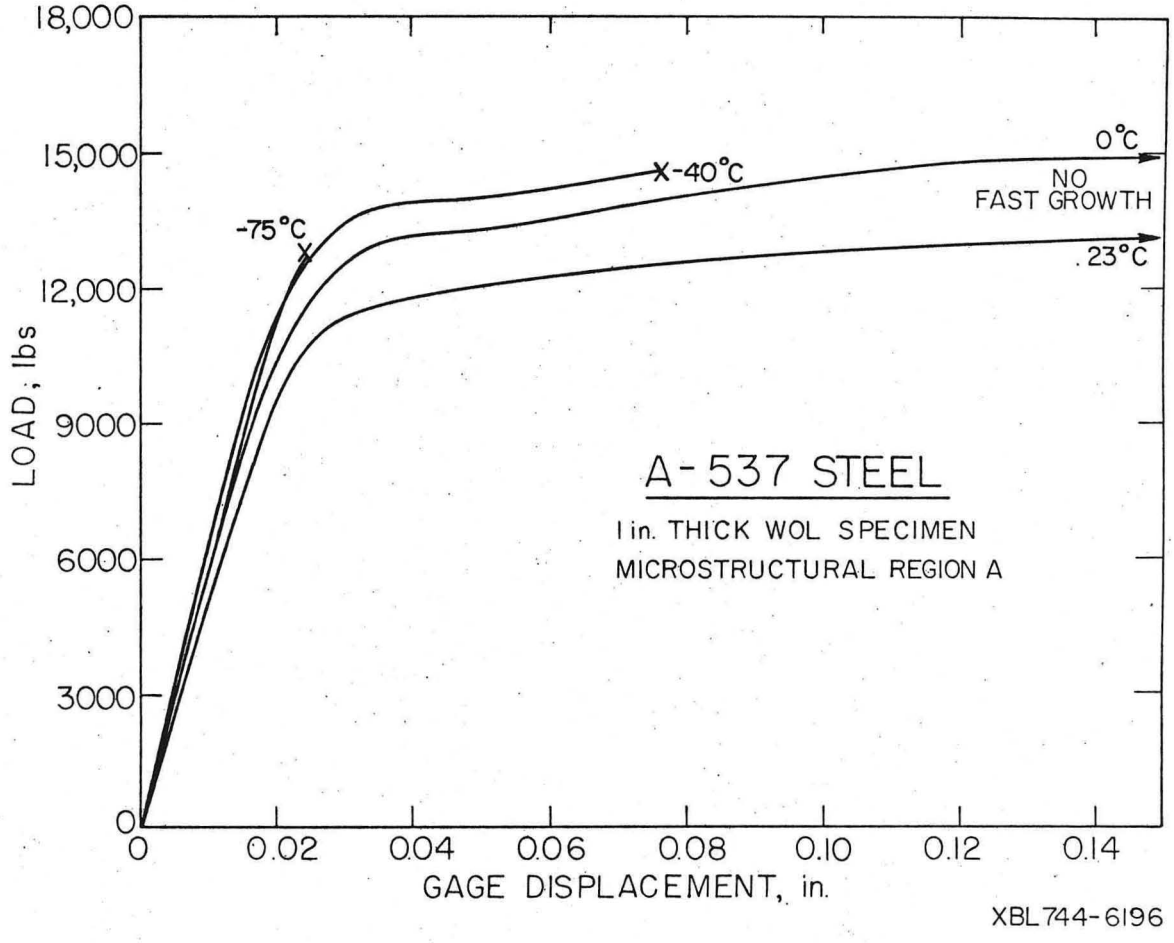
18,000
15,000
12,000
9000
6000
3000
0
LOAD; lbs
0
0.02
0.04
0.06
0.08
0.10
0.12
0.14
GAGE DISPLACEMENT, in.
0°C
NO
FAST GROWTH
-40°C
-75°C
23°C
A-537 STEEL
1 in. THICK WOL SPECIMEN
MICROSTRUCTURAL REGION A
XBL744-6196

Fig. 29

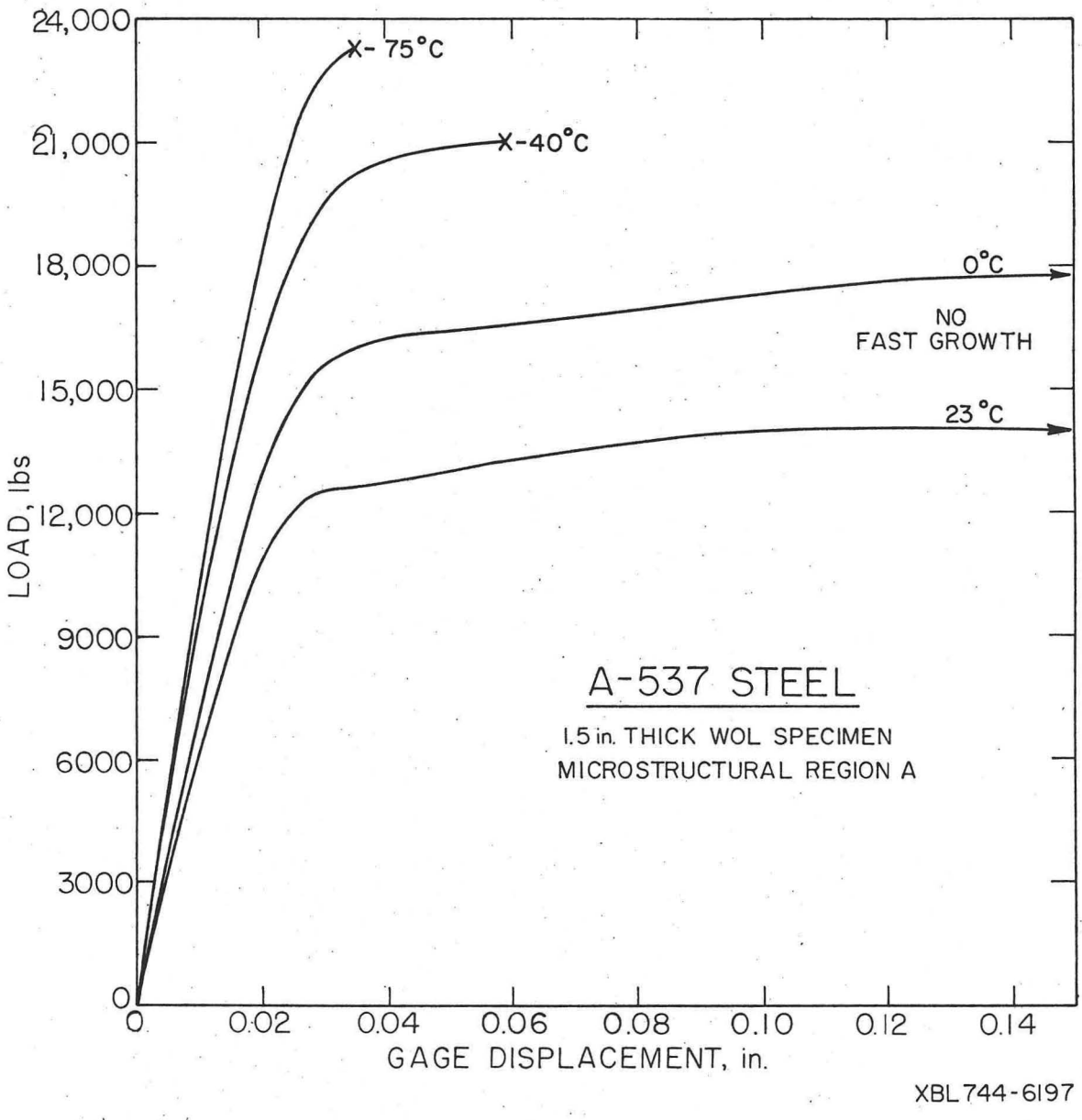
24,000
21,000
18,000
15,000
12,000
9000
6000
3000
0
LOAD, lbs
X- 75°C
X-40°C
0°C
NO
FAST GROWTH
23°C
A-537 STEEL
1.5 in. THICK WOL SPECIMEN
MICROSTRUCTURAL REGION A
0
0.02
0.04
0.06
0.08
0.10
0.12
0.14
GAGE DISPLACEMENT, in.
XBL744-6197

Fig. 30

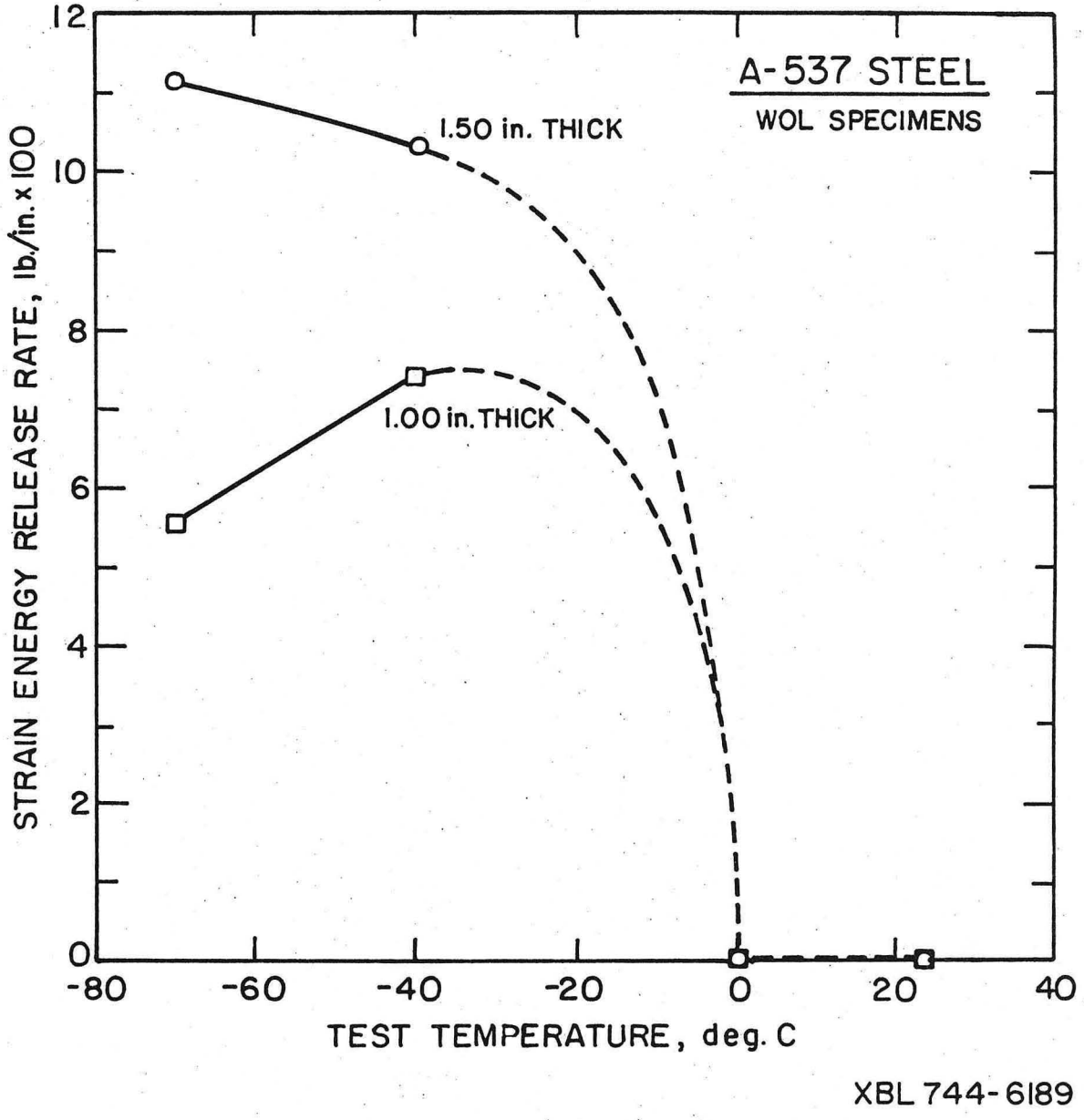
A-537 STEEL
WOL SPECIMENS
1.50 in. THICK
1.00 in. THICK
STRAIN ENERGY RELEASE RATE, lb./in. x 100
TEST TEMPERATURE, deg. C
0
2
4
6
8
10
12
-80
-60
-40
-20
0
20
40
XBL 744-6189

Fig. 31

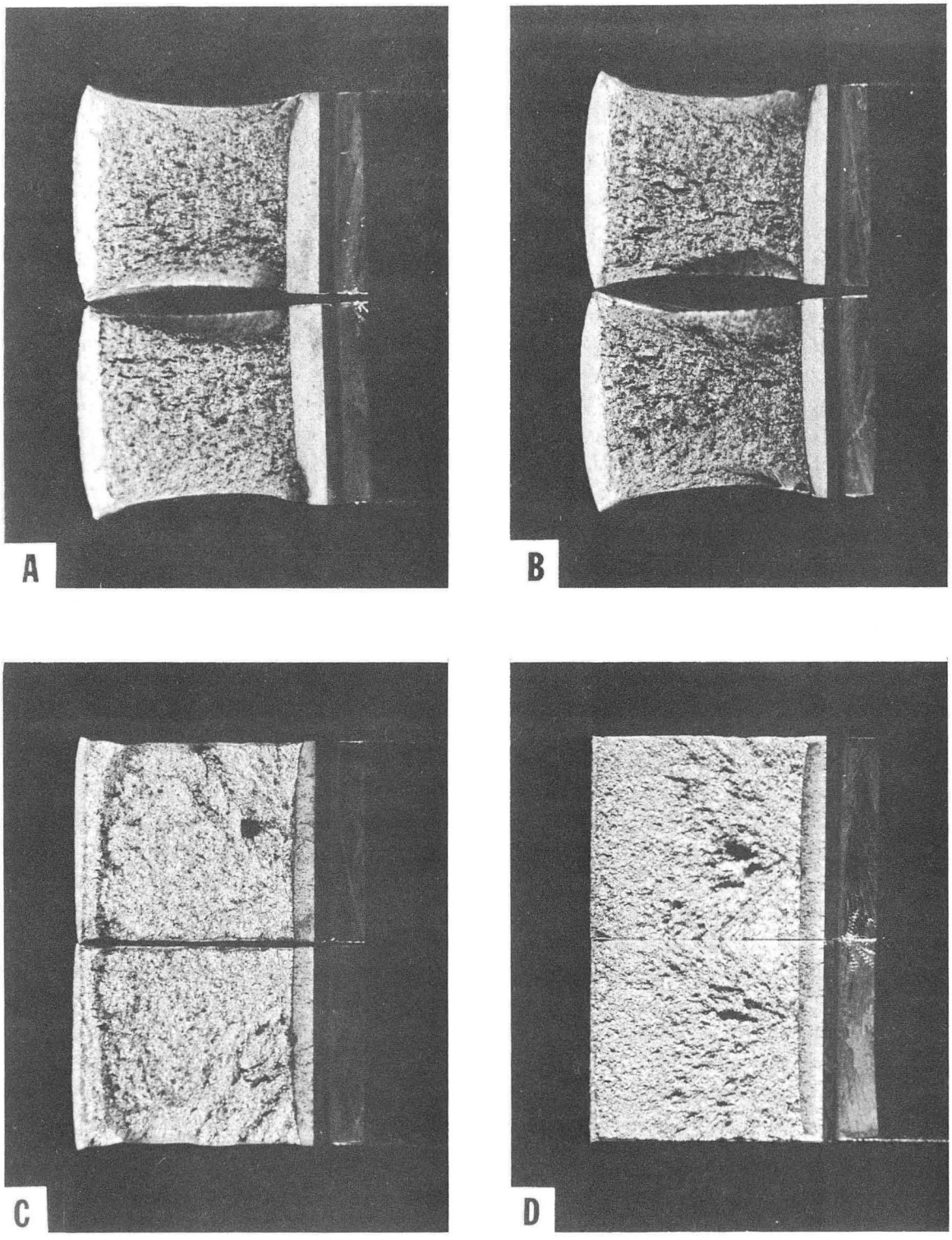


XBB 744-2587

Fig. 32

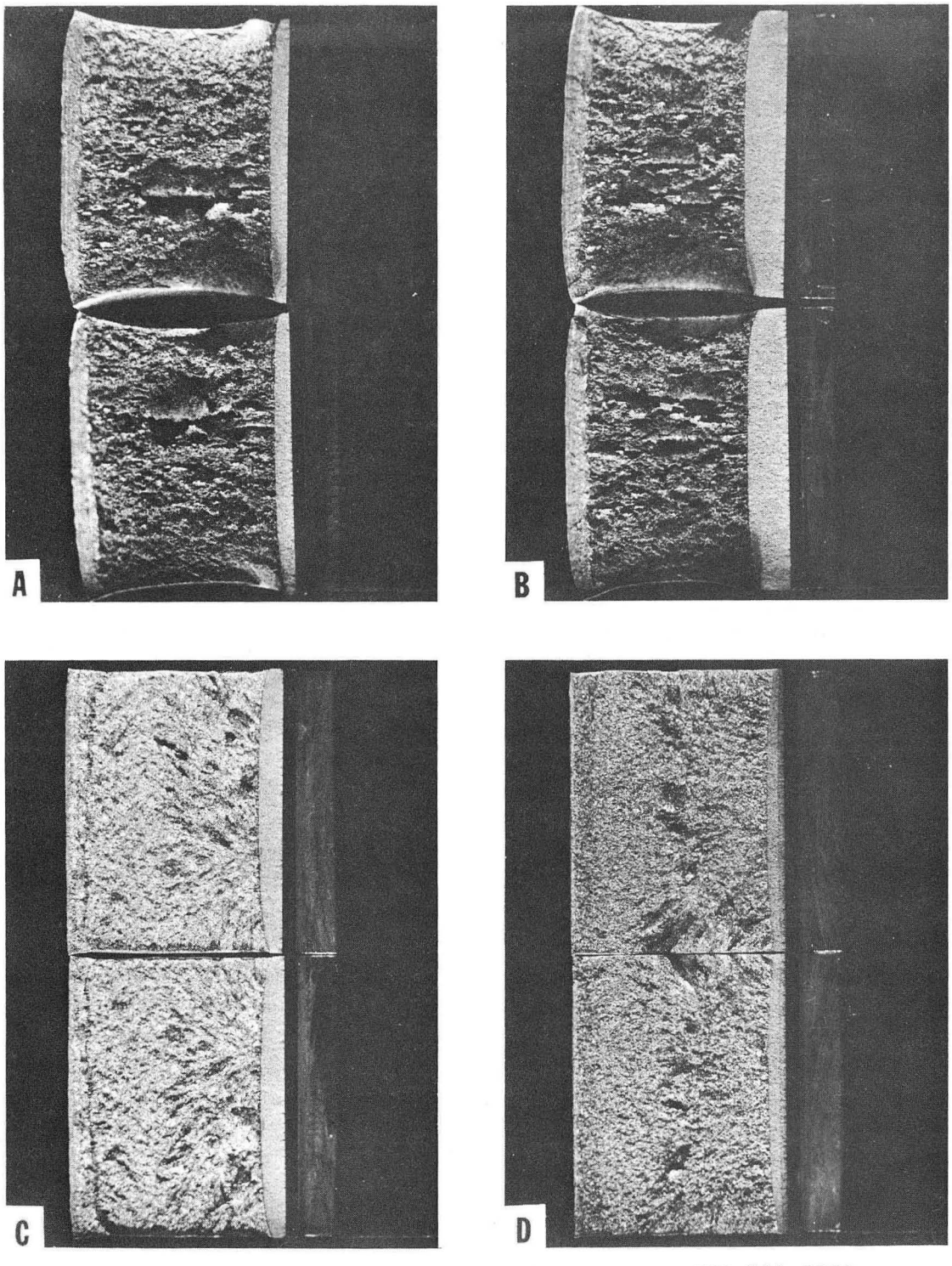


XBB 744-2588

Fig. 33

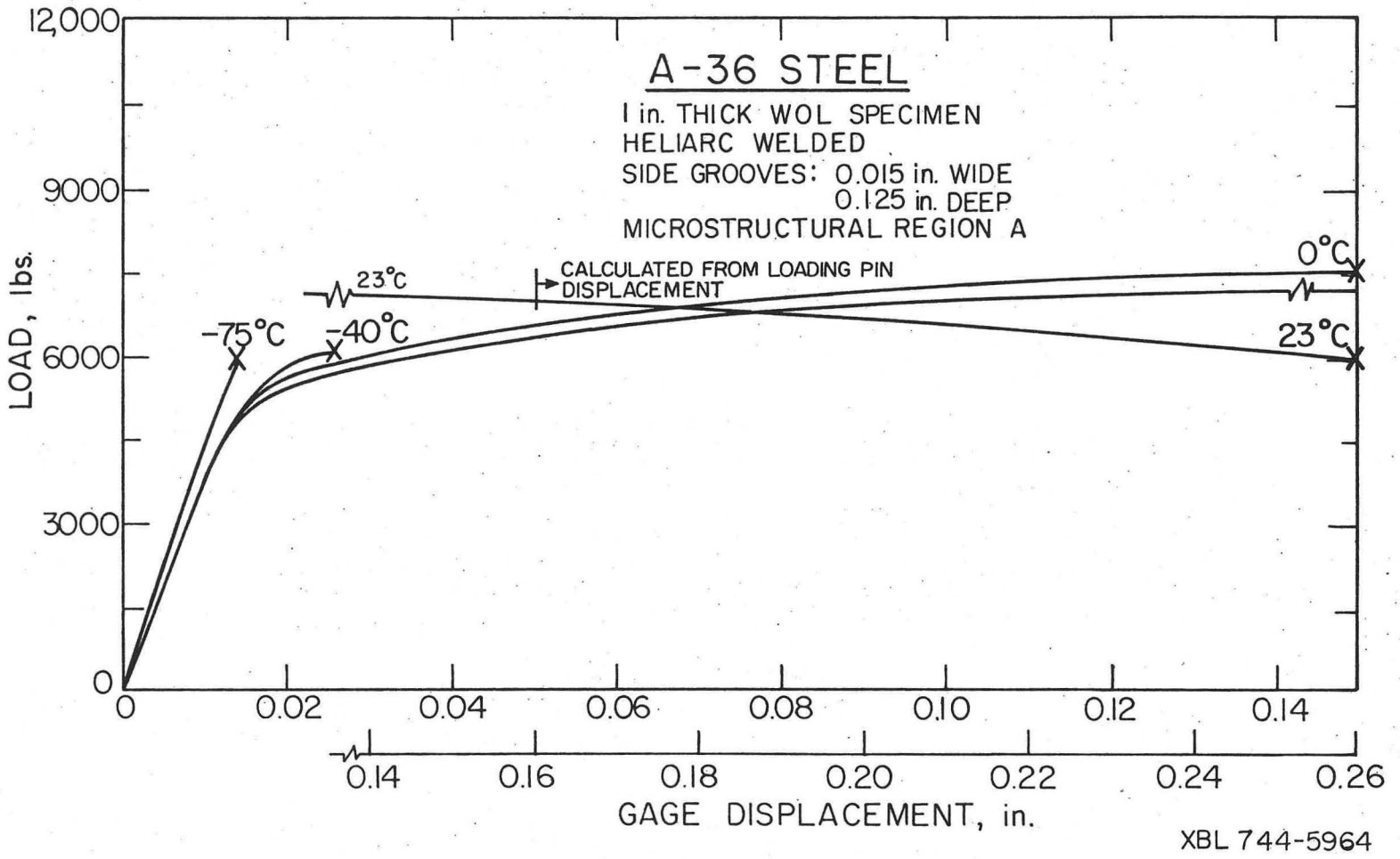
A-36 STEEL
1 in. THICK WOL SPECIMEN
HELIARC WELDED
SIDE GROOVES: 0.015 in. WIDE
0.125 in. DEEP
MICROSTRUCTURAL REGION A
CALCULATED FROM LOADING PIN DISPLACEMENT
23°C
-75°C
-40°C
0°C
23°C
LOAD, lbs.
12,000
9000
6000
3000
0
0
0.02
0.04
0.06
0.08
0.10
0.12
0.14
0.14
0.16
0.18
0.20
0.22
0.24
0.26
GAGE DISPLACEMENT, in.
XBL 744-5964

Fig. 34

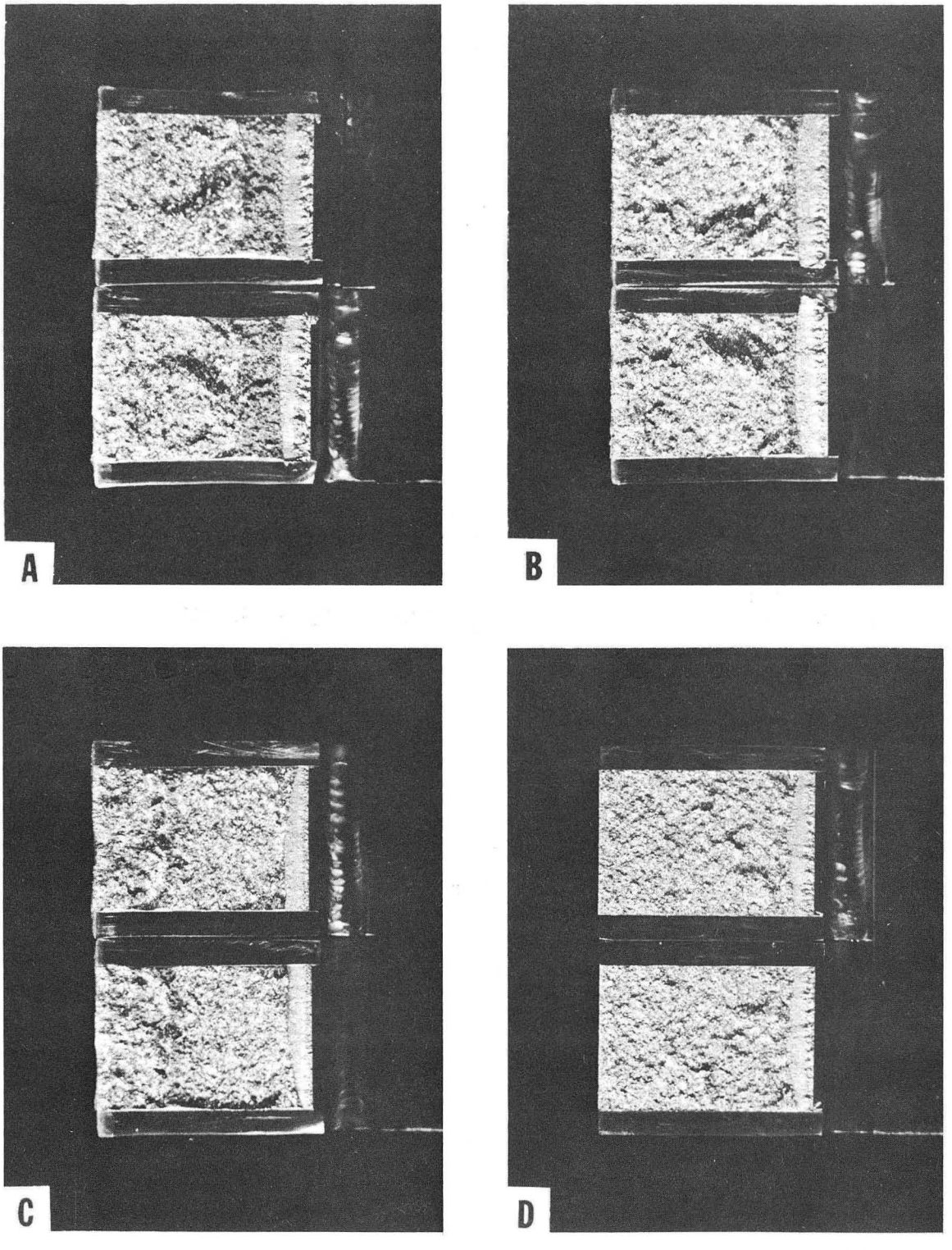


XBB 744-2586

Fig. 35

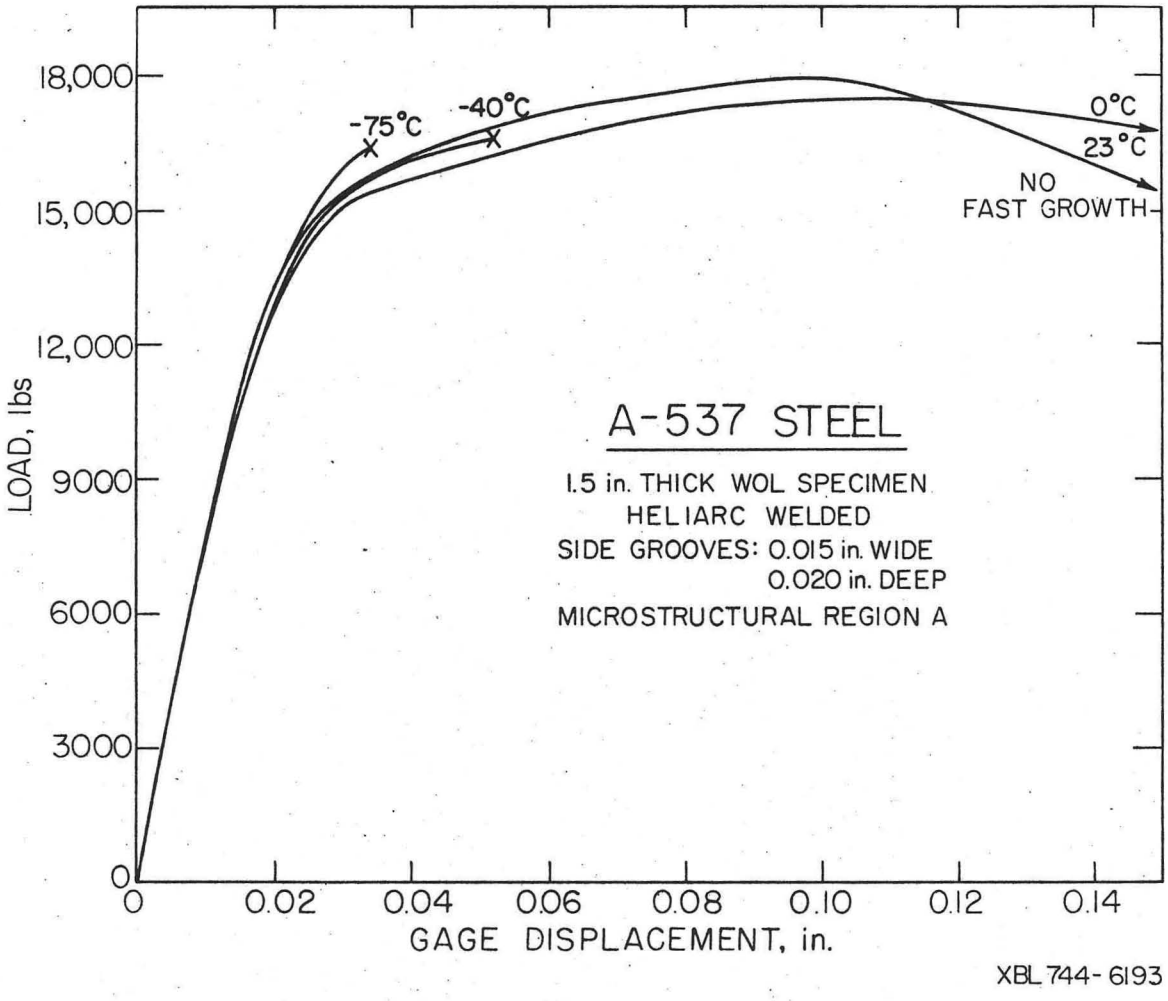
18,000
15,000
12,000
9000
6000
3000
0
LOAD, lbs
0
0.02
0.04
0.06
0.08
0.10
0.12
0.14
GAGE DISPLACEMENT, in.
-75°C
-40°C
0°C
23°C
NO
FAST GROWTH
A-537 STEEL
1.5 in. THICK WOL SPECIMEN
HELIARC WELDED
SIDE GROOVES: 0.015 in. WIDE
0.020 in. DEEP
MICROSTRUCTURAL REGION A
XBL 744-6193

Fig. 36

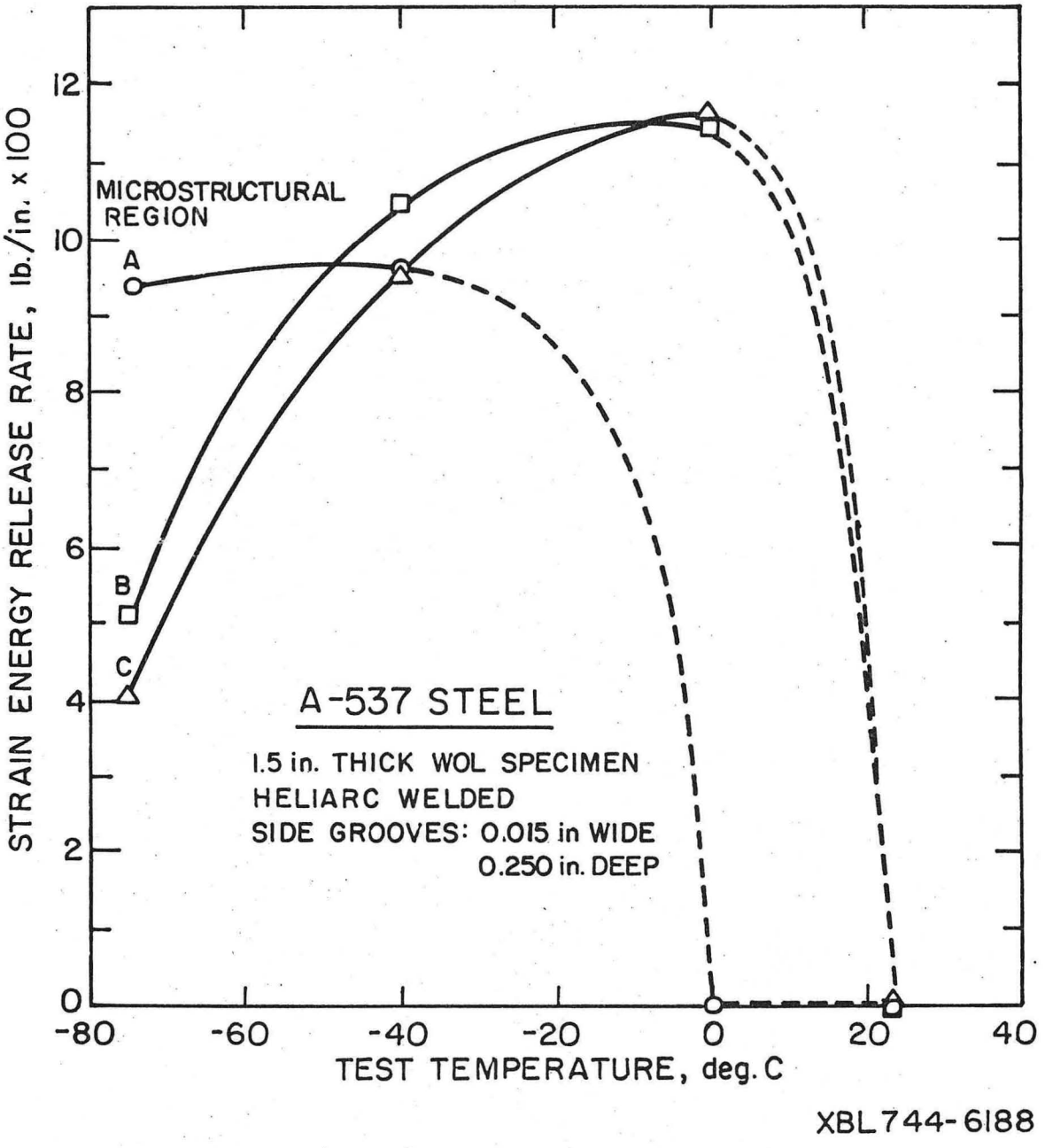
STRAIN ENERGY RELEASE RATE, lb./in. x 100
TEST TEMPERATURE, deg. C
MICROSTRUCTURAL REGION
A
B
C
A-537 STEEL
1.5 in. THICK WOL SPECIMEN
HELIARC WELDED
SIDE GROOVES: 0.015 in WIDE
0.250 in. DEEP
0
2
4
6
8
10
12
-80
-60
-40
-20
0
20
40
XBL744-6188

Fig. 37

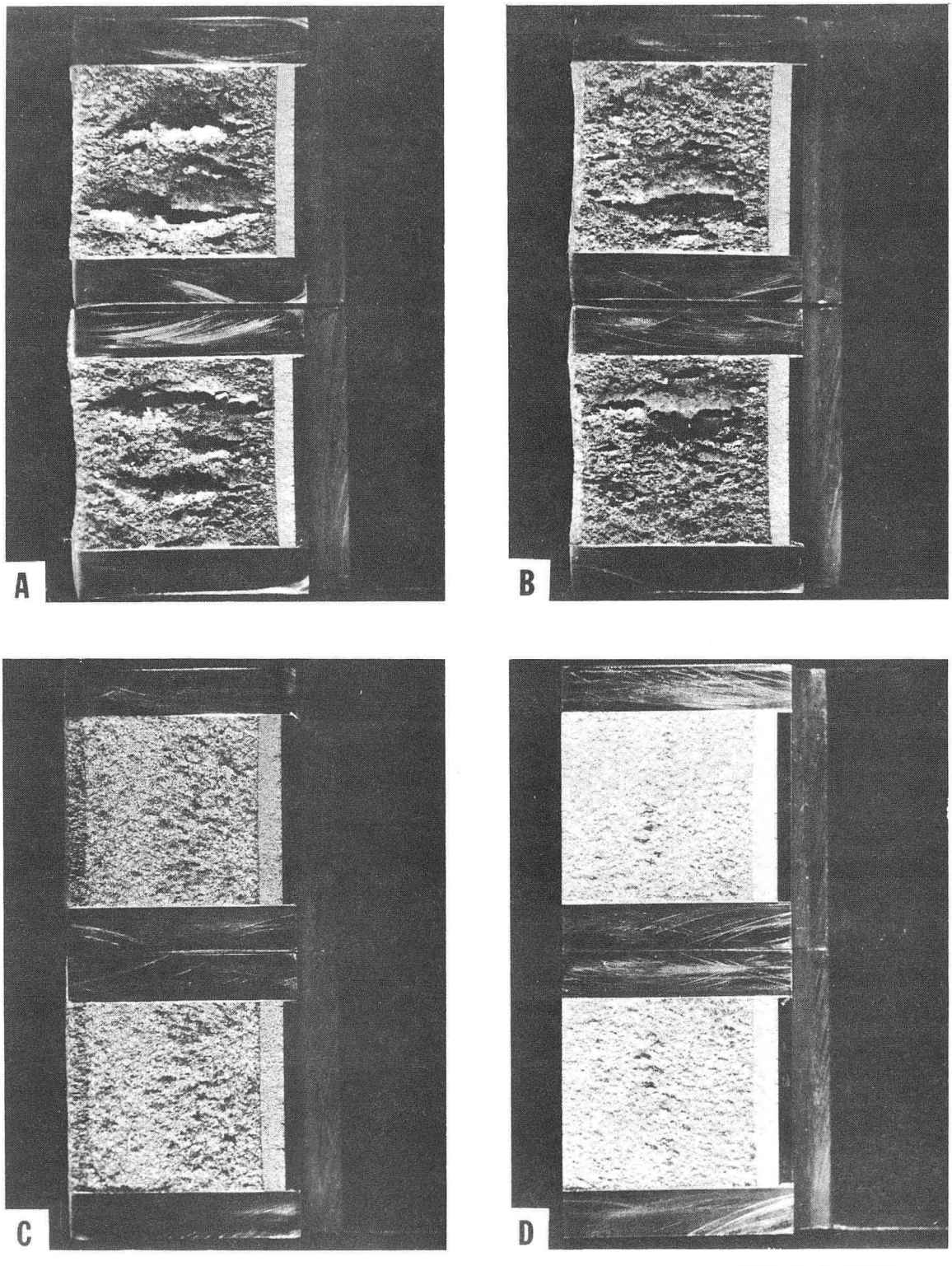


XBB 744-2583

Fig. 38

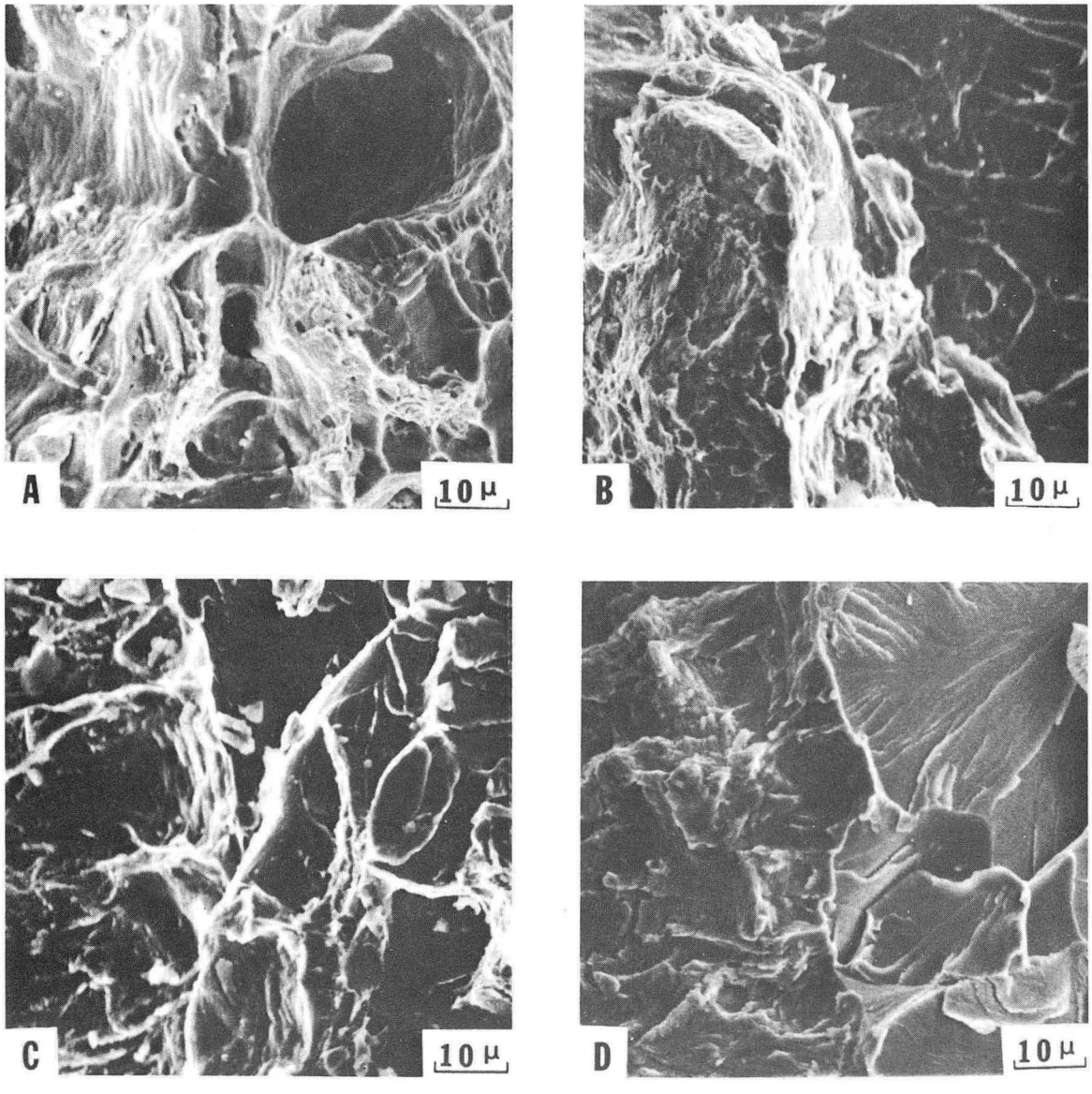


XBB 744-2589

Fig. 39

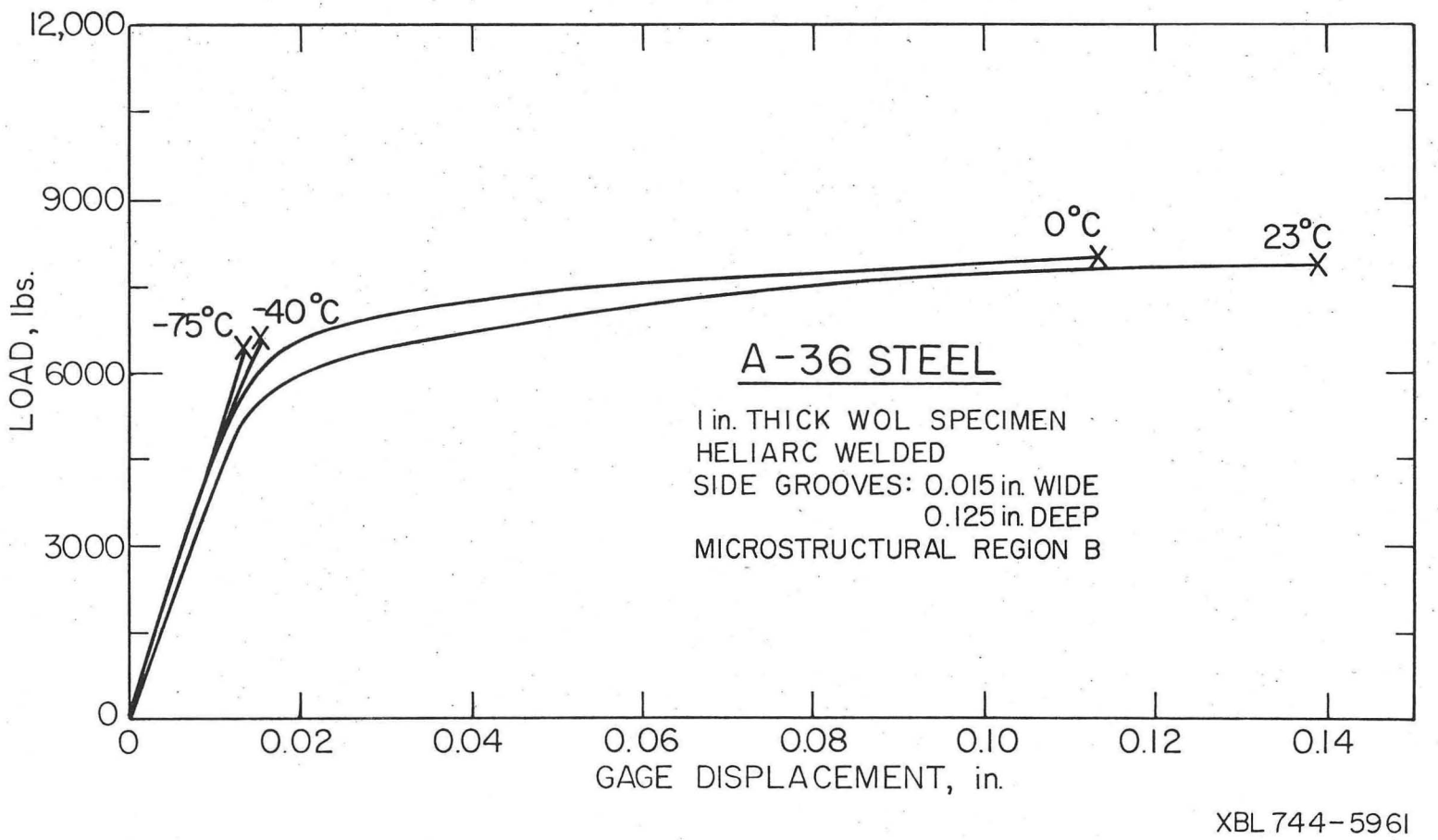
12,000
9000
6000
3000
0
LOAD, lbs.
0
0.02
0.04
0.06
0.08
0.10
0.12
0.14
GAGE DISPLACEMENT, in.
-75°C
-40°C
0°C
23°C
A-36 STEEL
1 in. THICK WOL SPECIMEN
HELIARC WELDED
SIDE GROOVES: 0.015 in. WIDE
0.125 in. DEEP
MICROSTRUCTURAL REGION B
XBL 744-5961

Fig. 40

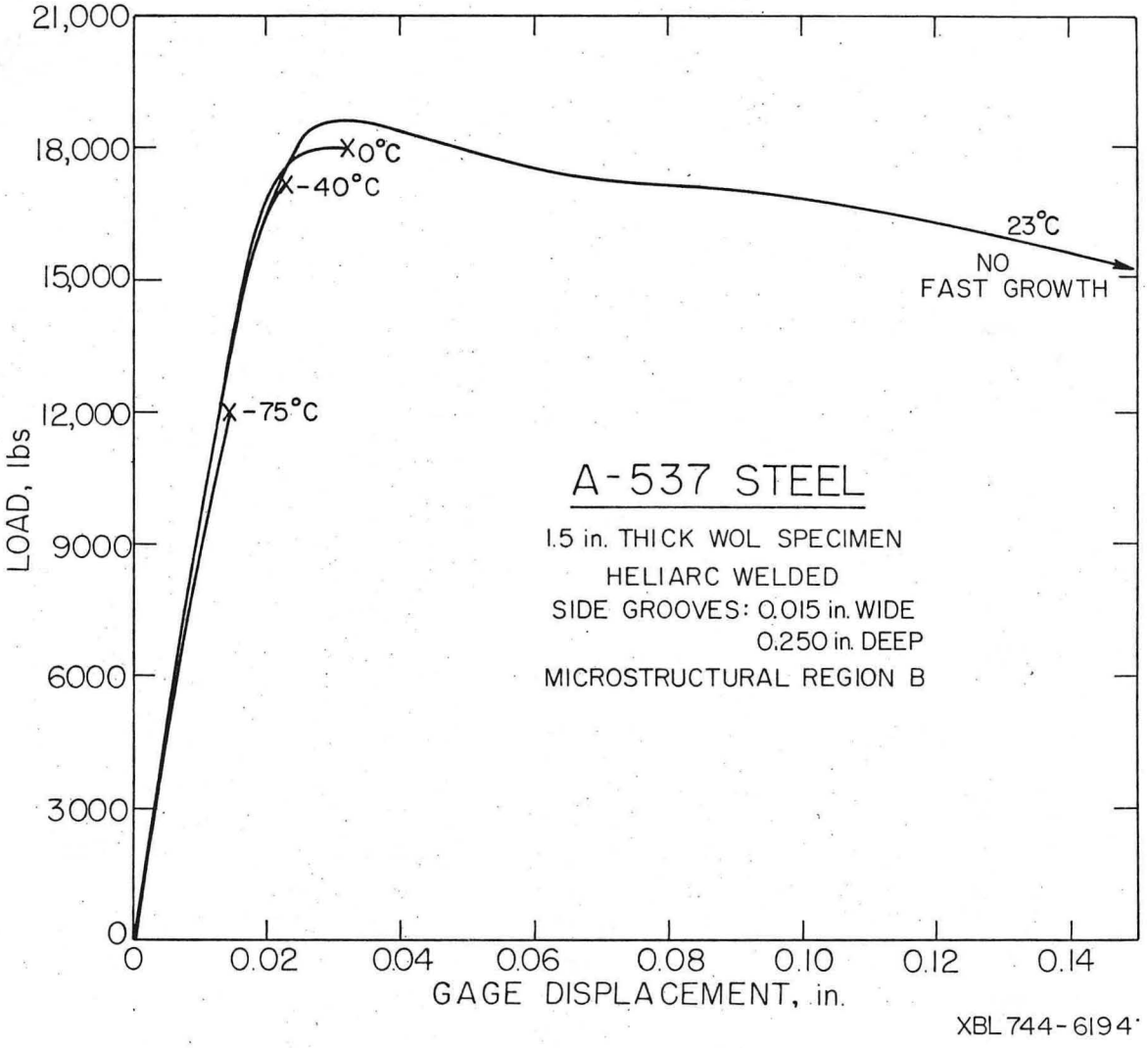
21,000
18,000
15,000
12,000
9000
6000
3000
0
LOAD, lbs
0
0.02
0.04
0.06
0.08
0.10
0.12
0.14
GAGE DISPLACEMENT, in.
0°C
-40°C
-75°C
23°C
NO
FAST GROWTH
A-537 STEEL
1.5 in. THICK WOL SPECIMEN
HELIARC WELDED
SIDE GROOVES: 0.015 in. WIDE
0.250 in. DEEP
MICROSTRUCTURAL REGION B
XBL 744-6194

Fig. 41

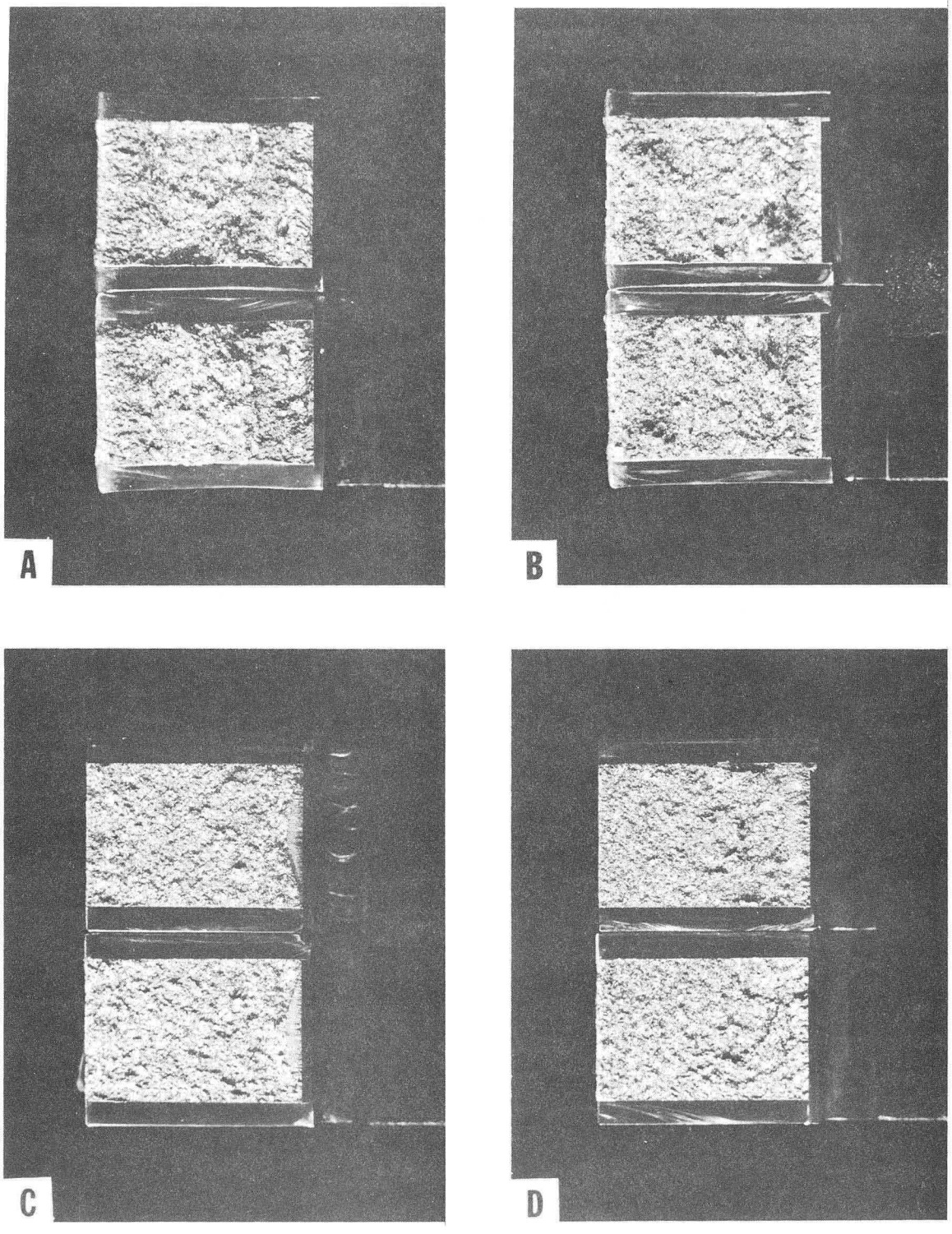


XBB 744-2581

Fig. 42

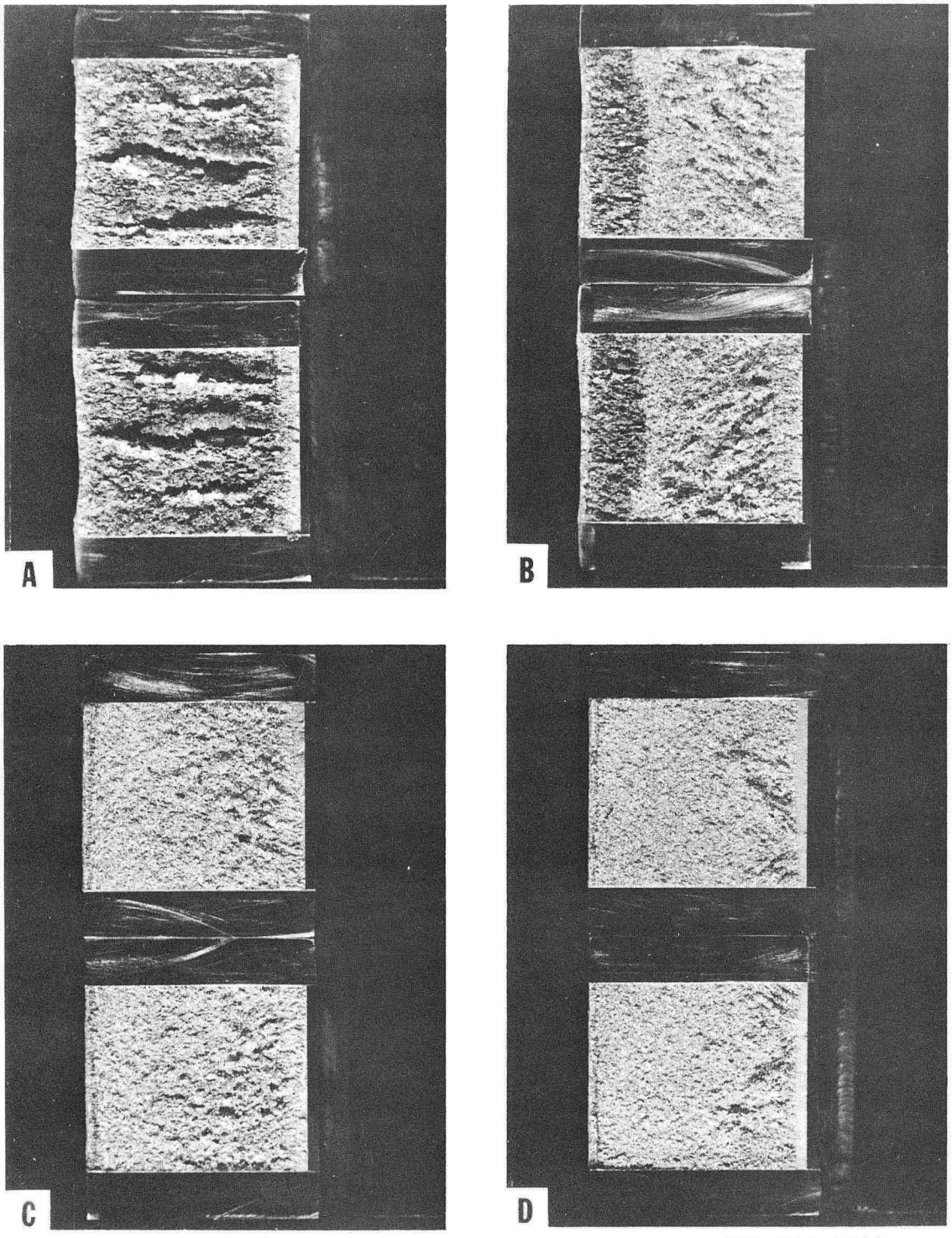


XBB 744-2582

Fig. 43

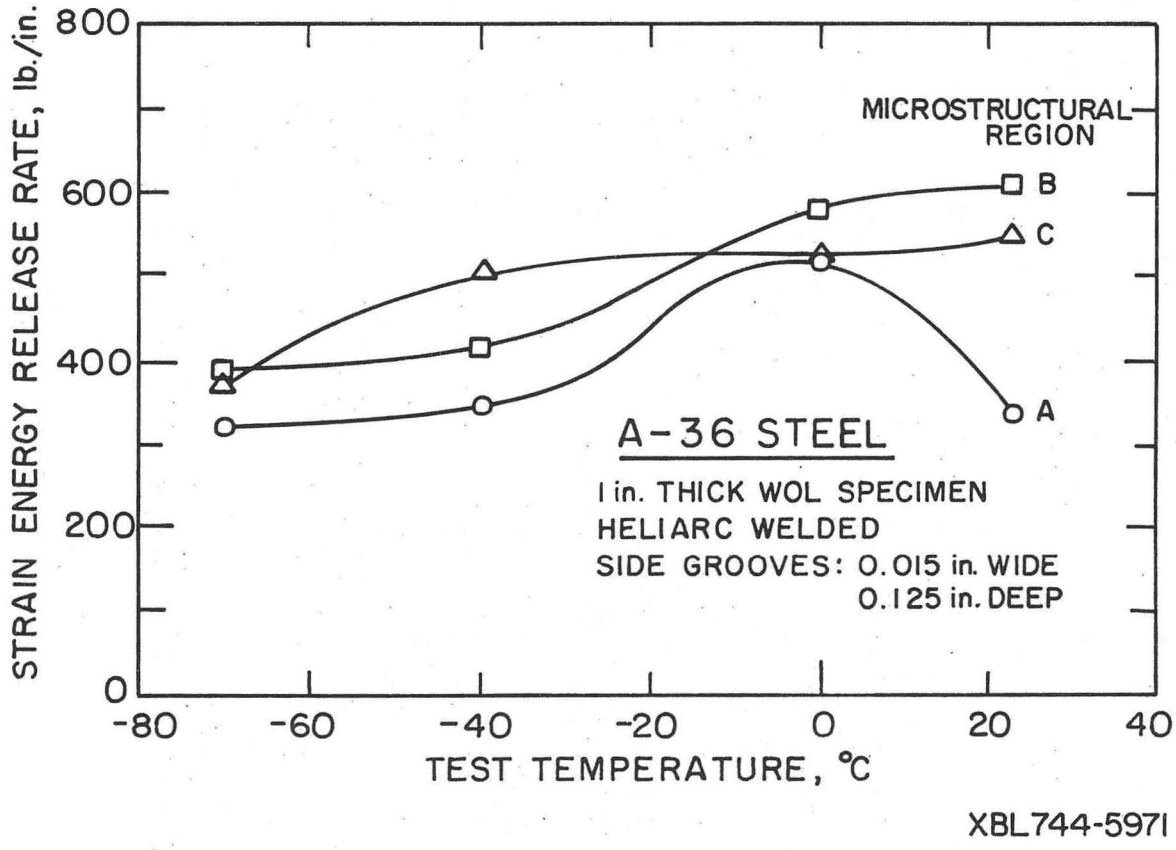
STRAIN ENERGY RELEASE RATE, lb./in.
800
600
400
200
0
-80
-60
-40
-20
0
20
40
TEST TEMPERATURE, °C
MICROSTRUCTURAL REGION
B
C
A
A-36 STEEL
1 in. THICK WOL SPECIMEN
HELIARC WELDED
SIDE GROOVES: 0.015 in. WIDE
0.125 in. DEEP
XBL744-5971

Fig. 44

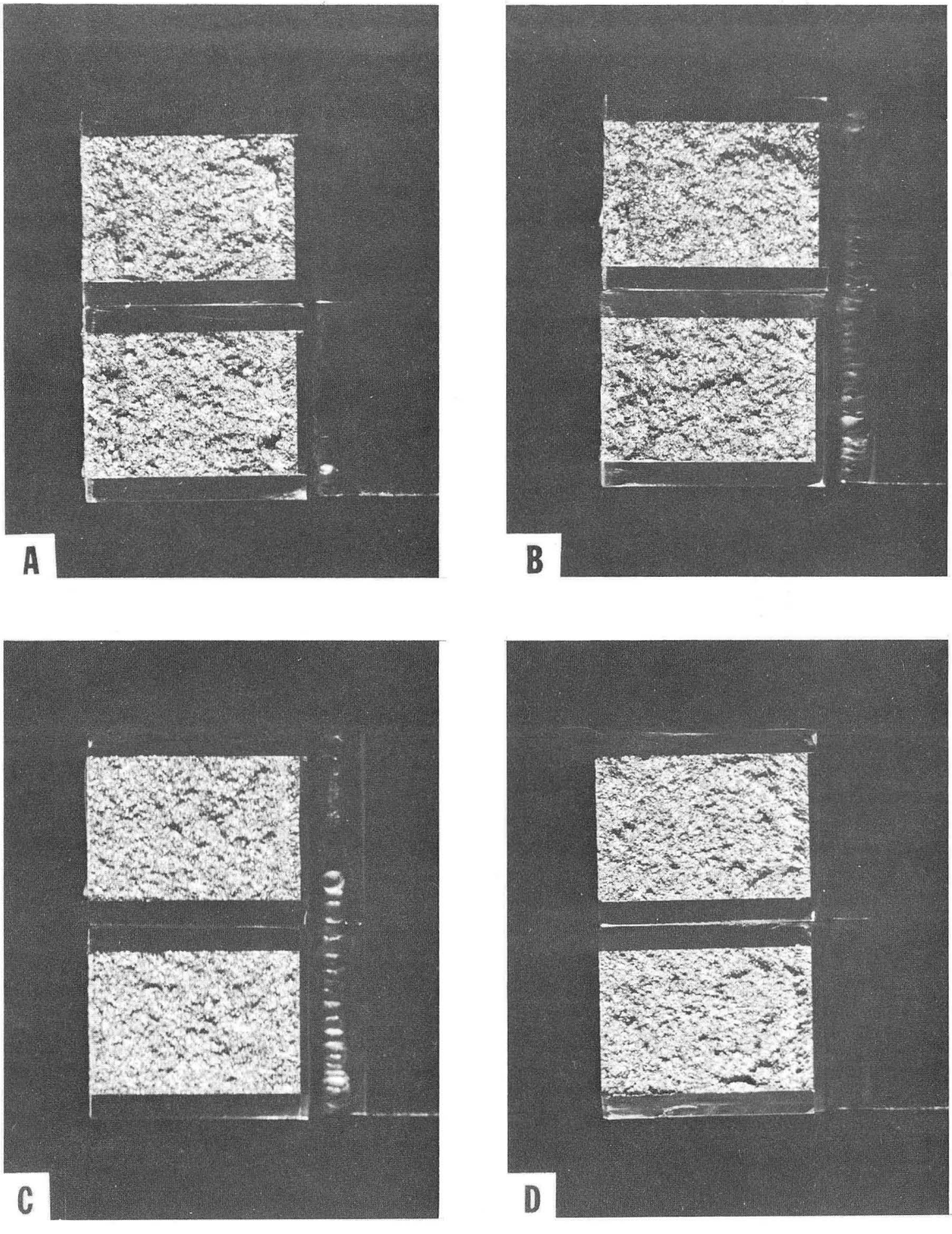


XBB 744-2584

Fig. 45

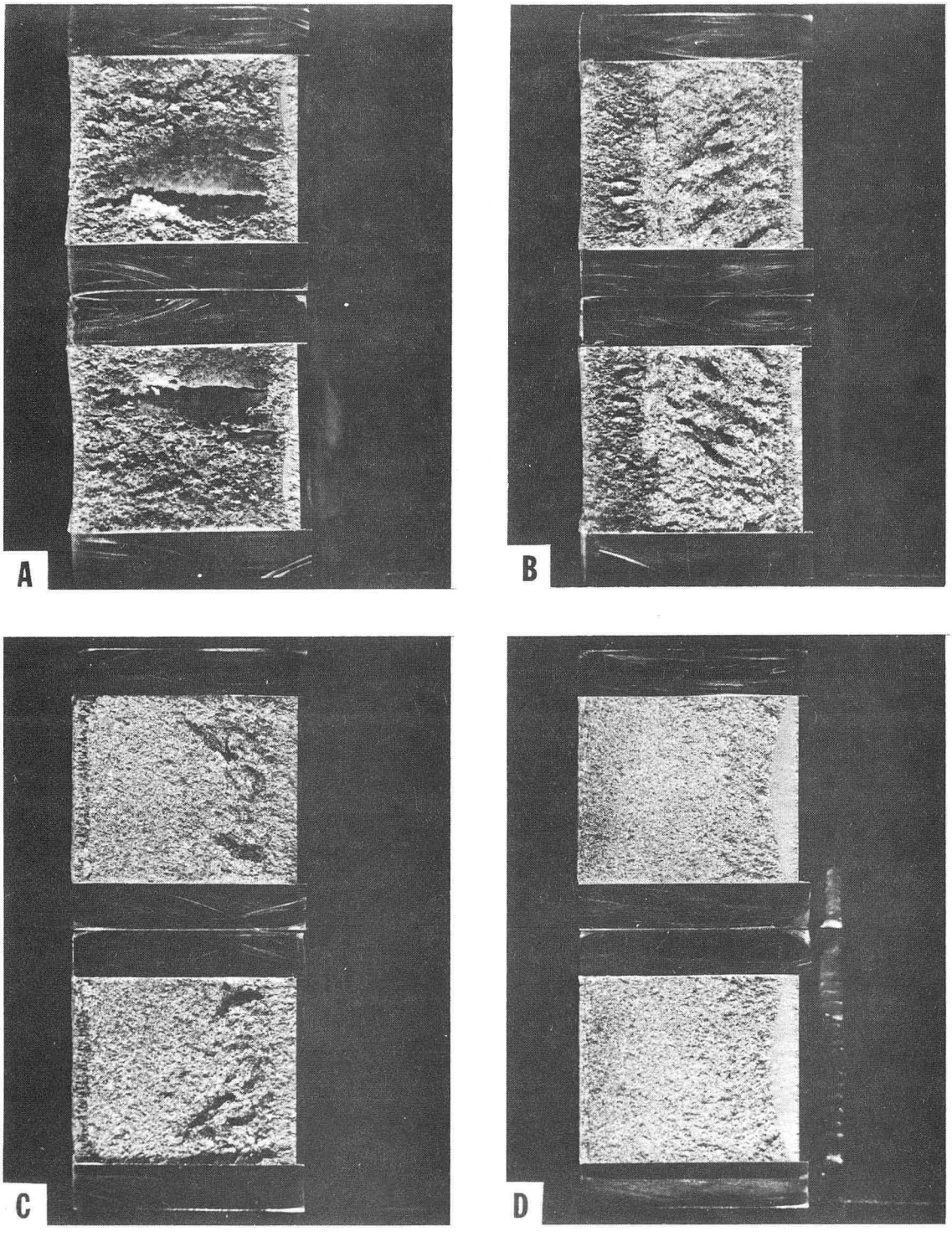


XBB 744-2585

Fig. 46

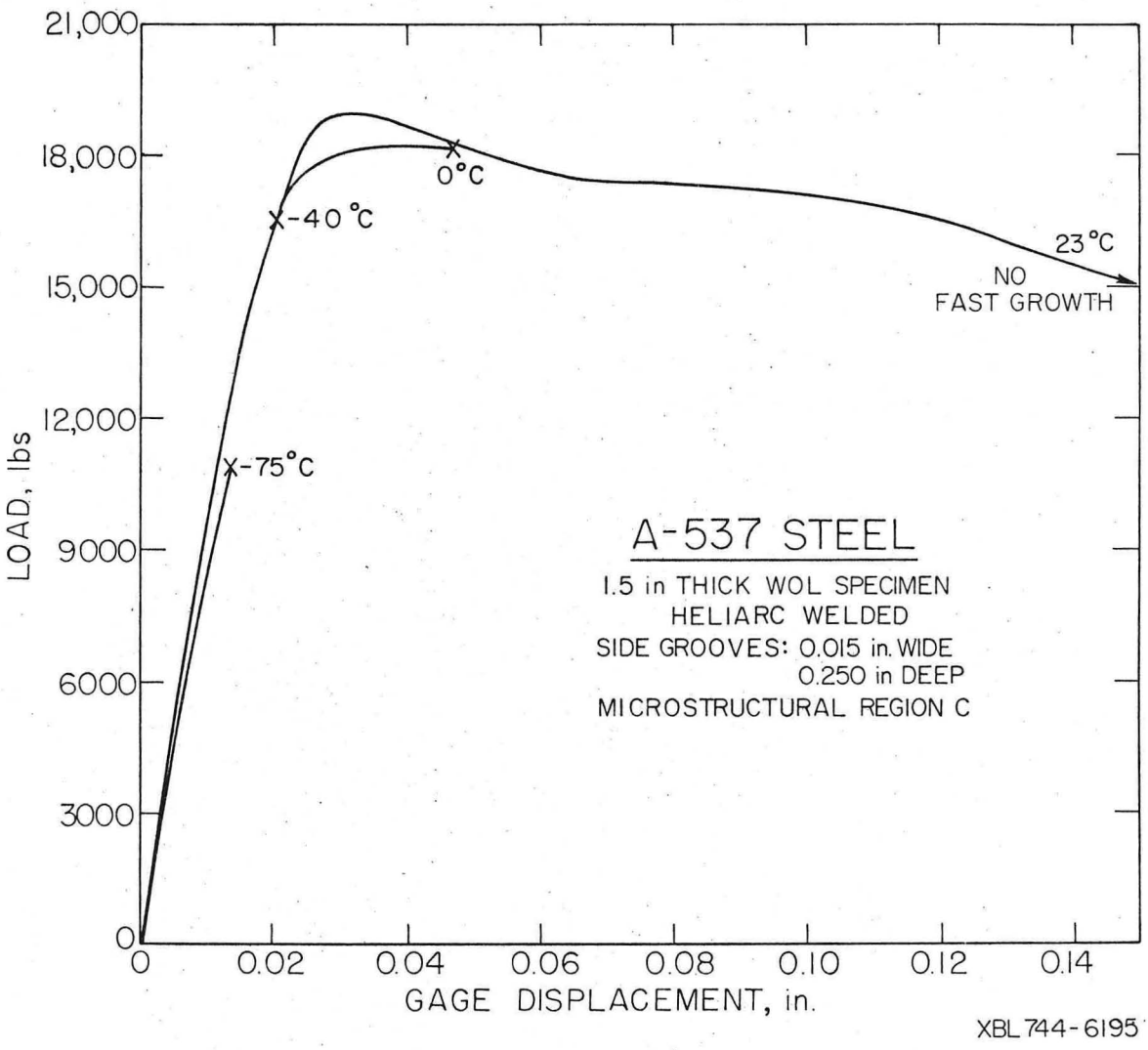
21,000
18,000
15,000
12,000
9000
6000
3000
0
LOAD, lbs
0
0.02
0.04
0.06
0.08
0.10
0.12
0.14
GAGE DISPLACEMENT, in.
-40 °C
0°C
23°C
NO
FAST GROWTH
-75°C
A-537 STEEL
1.5 in THICK WOL SPECIMEN
HELIARC WELDED
SIDE GROOVES: 0.015 in. WIDE
0.250 in DEEP
MICROSTRUCTURAL REGION C
XBL 744-6195

Fig. 47

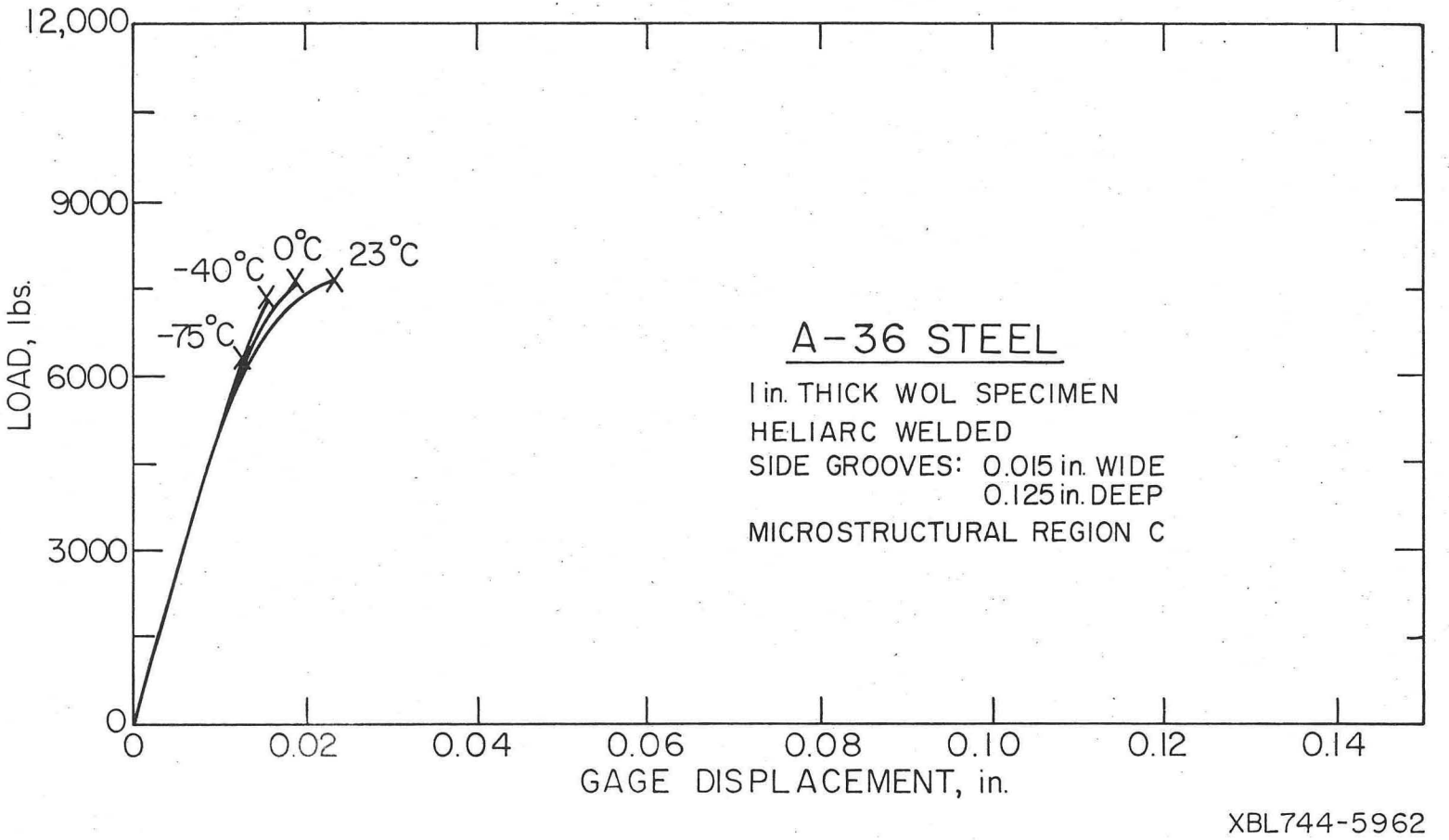
12,000
9000
6000
3000
0
LOAD, lbs.
-40°C
0°C
23°C
-75°C
A-36 STEEL
1 in. THICK WOL SPECIMEN
HELIARC WELDED
SIDE GROOVES: 0.015 in. WIDE
0.125 in. DEEP
MICROSTRUCTURAL REGION C
0
0.02
0.04
0.06
0.08
0.10
0.12
0.14
GAGE DISPLACEMENT, in.
XBL744-5962

Fig. 48

*TECHNICAL INFORMATION DIVISION*
*LAWRENCE BERKELEY LABORATORY*
*UNIVERSITY OF CALIFORNIA*
*BERKELEY, CALIFORNIA 94720*